

DESIGN OF A COMPLIANT BISTABLE LOCK MECHANISM FOR A
DISHWASHER USING FUNCTIONALLY BINARY INITIALLY CURVED
PINNED-PINNED SEGMENTS

A THESIS SUBMITTED TO
THE GRADUATE SCHOOL OF NATURAL AND APPLIED SCIENCES
OF
MIDDLE EAST TECHNICAL UNIVERSITY

BY

UYGAR ÜNVERDİ

IN PARTIAL FULFILLMENT OF THE REQUIREMENTS
FOR
THE DEGREE OF MASTER OF SCIENCE
IN
MECHANICAL ENGINEERING

JUNE 2012

Approval of the thesis:

**DESIGN OF A COMPLIANT BISTABLE LOCK MECHANISM FOR A
DISHWASHER USING FUNCTIONALLY BINARY INITIALLY
CURVED PINNED-PINNED SEGMENTS**

submitted by **UYGAR ÜNVERDİ** in partial fulfillment of the requirements
for the degree of **Master of Science in Mechanical Engineering**
Department, Middle East Technical University by,

Prof. Dr. Canan Özgen
Dean, Graduate School of **Natural and Applied Sciences**

Prof. Dr. Süha Oral
Head of Department, **Mechanical Engineering**

Prof. Dr. Eres Söylemez
Supervisor, **Mechanical Engineering Dept., METU**

Examining Committee Members:

Prof. Dr. Kemal Özgören
Mechanical Engineering Dept., METU

Prof. Dr. Eres Söylemez
Mechanical Engineering Dept., METU

Prof. Dr. Tuna Balkan
Mechanical Engineering Dept., METU

Asst. Prof. Dr. Yiğit Yazıcıoğlu
Mechanical Engineering Dept., METU

Osman Kılıç (M.S.)
R&D Engineer, Arçelik A.Ş.

Date: _____

I hereby declare that all information in this document has been obtained and presented in accordance with academic rules and ethical conduct. I also declare that, as required by these rules and conduct, I have fully cited and referenced all material and results that are not original to this work.

Name, Last name : Uygur ÜNVERDİ

Signature :

ABSTRACT

DESIGN OF A COMPLIANT BISTABLE LOCK MECHANISM FOR A DISHWASHER USING FUNCTIONALLY BINARY INITIALLY CURVED PINNED-PINNED SEGMENTS

Ünverdi, Uygur

M.Sc., Department of Mechanical Engineering

Supervisor: Prof. Dr. Eres Söylemez

June 2012, 118 pages

The aim of this study is to design a compliant lock mechanism for a dishwasher, using a systematic approach. Functionally binary pinned-pinned segment that exhibits bistable behavior is utilized. Pseudo-rigid-body model of the whole mechanism and the half segment is developed separately and the corresponding calculations are carried out. Among current solutions a different method namely “arc fitting method” is developed and it is utilized to construct the model. A software code is written to get the exact solutions, which require the evaluation of elliptic integrals. Results are compared with the analytical model and confirmed with physical prototype. Predefined tip forces are seen to provide the transition from one stable position to other. Durability, reliability and compactness characteristics are particularly considered.

Keywords: Compliant Mechanisms, Functionally Binary Pinned-Pinned Segments, Pseudo-Rigid-Body Model, Bistable, Locking Mechanisms

ÖZ

İŞLEVSEL OLARAK İKİLİ, KIVRIMLI VE PİM BAĞLANTILI KISIMLAR KULLANAN, ESNEK BİR BULAŞIK MAKİNESİ KİLİDİ TASARIMI

Ünverdi, Uygur
Yüksek Lisans, Makine Mühendisliği Bölümü
Tez yöneticisi: Prof. Dr. Eres Söylemez

Haziran 2012, 118 sayfa

Bu çalışmanın amacı, bulaşık makinesi için esnek bir kilit mekanizmasını, sistematik yöntemler kullanarak geliştirmektir. Çift denge konumu bulunan, işlevsel olarak ikili, pim bağlantılı kısımlar kullanılmıştır. Bütün ve yarım kısımlar için ayrı ayrı katımsı cisim modelleri oluşturulmuş ve gerekli hesaplamalar yapılmıştır. Mevcut çözümlerin ötesinde “çember yayı benzeştirme” isimli yeni bir yöntem geliştirilmiş ve modelleme için bu yöntem kullanılmıştır. Eliptik integral çözümü gerektiren kesin çözümün bulunması için bir bilgisayar kodu yazılmıştır. Sonuçlar analitik model ile karşılaştırılmış ve fiziksel prototip ile doğrulanmıştır. Öngörülen kuvvetlerin denge konumları arası geçişi sağladığı görülmüştür. Uzun ömür, güvenilirlik ve kompaktlık nitelikleri özellikle göz önünde bulundurulmuştur.

Anahtar kelimeler: Esnek Mekanizmalar, İşlevsel Olarak İkili Pim Bağlantılı Kısımlar, Katımsı Cisim Modeli, Çift Denge Konumlu, Kilit Mekanizmaları

*To My Supporting Family
And To My Future Wife Gizem*

ACKNOWLEDGEMENTS

First of all, I must thank to my supervisor Prof. Dr. Eres Söylemez for his invaluable supports not only during the thesis work but also during different stages of my life. I would not be the person who I am without his inspirational and instructional attitude. I must also thank to other professors of my department, even though some are challenging to be compromised, I learned a lot from them. Also to Prof. Dr. L. Larry Howell I must express my appreciations. He is the person who inspired me to choose the subject and also helped me out during my literature survey stage.

There are many friends of mine who shared the load of this study with me. Some listened to my complaints, some tried to find solutions, some supported me by just being with me... My local friends I want to say "thank you" gratefully for they were always beside me but never "hide in shadows". Also I must thank to Erdal Demir for his invaluable friendship. I am also thankful to my colleague friends Güvenç Numanoğlu, Cem Baştuji, Ferhan Erçin, Ali Egemen Uçar, Hasan Demirbağ, Osman Kılıç, İsmail Demircioğlu and many others for their technical support and companion. I have learned a lot, and hopefully will learn more, from them.

This study is a product of my efforts but sacrifice of me plus some others. "Others" may be a wrong word because they are the people who make me whole. My mother, father, brother and my fiancée are the ones I am mentioning. In my world, they are the reflections of the words sacrifice, support, happiness and love. They did not only support me or inspired me during every stage of my life but they gave the meaning of every single step I take. My appreciation to them is something impossible to express with words. I just hope that I can be as good as they deserve and let them see my gratitude.

I want to thank to ANOVA engineering (also to Dursun Öner personally) for their technical support. This study has been supported by Arçelik Dishwasher Plant, to whom I must express my sincere appreciations.

TABLE OF CONTENTS

ABSTRACT	iv
ÖZ	v
ACKNOWLEDGEMENTS	vii
TABLE OF CONTENTS.....	ix
LIST OF FIGURES	xii
LIST OF TABLES	xvi
LIST OF SYMBOLS.....	xvi
CHAPTERS	
1. INTRODUCTION.....	1
1.1 On Compliant Mechanisms.....	1
1.2 Scope of the Thesis	2
1.3 Outline of the Dissertation	3
2. LITERATURE SURVEY	5
2.1 Introduction.....	5
2.2 Compliant Mechanisms Overview	5
2.2.1 Definition and Brief History.....	5
2.2.2 Some Applications.....	8
2.2.3 Classification.....	12
2.2.4 Benefits and Challenges.....	15
2.2.5 Synthesis Methods.....	17
2.3 Failure Criteria	21
2.3.1 Introduction.....	21
2.3.2 Static Failure	22

2.3.3 Fatigue Failure.....	24
2.4 Stability	29
2.4.1 Definition	29
2.4.2 Multistability	31
2.4.3 Bistable Compliant Mechanisms	33
2.5 Compliant Locking Mechanisms (CLM) [26]	34
3. FUNCTIONALLY BINARY PINNED-PINNED (FBPP) SEGMENTS..	37
3.1 Introduction.....	37
3.2 Exact Solution [28]	39
3.3 PRBM Analysis of the FBFP Half-Model of FBPP Segment.....	48
3.4 Comparison and Evaluation of the Models.....	56
3.5 PRBM Analysis of the Whole Binary Segment.....	58
3.6 Conclusion	60
4. DESIGN OF THE LOCKING MECHANISM.....	62
4.1 Introduction.....	62
4.2 Description of the Design Space and Physical Constraints.....	62
4.3 Segment Profile Design.....	63
4.4 Replacement of the Pin Joints with Living Hinges [35]	68
4.5 Material Selection and Final Shape Design.....	72
4.6 Evaluation and Conclusion	81
5. FINITE ELEMENT MODEL (FEM) ANALYSIS AND PHYSICAL PROTOTYPE TESTING	82
5.1 Introduction.....	82
5.2 Finite Element Model (FEM) and Fatigue Life Estimation.....	82
5.2.1 Life Estimation	86
5.3 Physical Model (Prototyping).....	88
6. CONCLUSION & FUTURE WORK	91

6.1 Conclusion	91
6.2 Future Work	92
REFERENCES.....	93
APPENDICES	
A. ELLIPTIC INTEGRAL SOLUTION METHODOLOGY	97
B. VBA CODE ON ELLIPTIC INTEGRAL SOLUTION	100
C. SNAPSHOT OF NUMERICAL CALCULATIONS.....	107
D. αt^2 vs. $\Delta\theta$ PLOTS FOR DIFFERENT CURVATURE VALUES (κ_0)	108
E. ERROR VALUES FOR VARIOUS CURVATURES (κ_0) AND FIXED PIN JOINT ROTATION ($\Delta\theta_0=45^\circ$).....	113
F. MATERIAL SPECIFICATIONS OF POLYOXYMETHYLENE (POM).....	116
G. MATERIAL SPECIFICATIONS OF INNOV'PA 1550.....	117

LIST OF FIGURES

FIGURES

Figure 2-1: Bow & Arrow Analogy	7
Figure 2-2: The Greek Palintonon Weapon	8
Figure 2-3: Common Compliant Devices. A Binder Clip, Paper Clip, Backpack Latch, Lid, Eyelash Curler and Nail Clippers.	9
Figure 2-4: Bistable Medical Stent Apparatus [4]	9
Figure 2-5: A Compliant Bistable Mechanical Switch.....	10
Figure 2-6: A Micro Compliant Four-Bar Mechanism with Lumped Compliance [5]	11
Figure 2-7: Titanium Mirrors Bulk Micromachined Using Deep Etching of a Titanium Substrate	11
Figure 2-8: Classification of Compliant Mechanisms [10].....	12
Figure 2-9: Component Characteristics of a Link [11].....	14
Figure 2-10: Component Characteristics of a Segment [11]	15
Figure 2-11: Macro-scale Examples of a Monolithic (a) Stapler and (b) Windshield Wiper Developed by the Kota Group at the University of Michigan, Using Compliant Mechanisms	16
Figure 2-12: A Bistable Double-Slider Mechanism with a Pin Joint, Joining The Sliders, and a Compliant Equivalent. [16].....	19
Figure 2-13: Safe Stress Areas According to Maximum Shear Stress Theory (Tresca Yield Criterion) and Distortion Energy Theory (Von Mises Criterion).....	24

Figure 2-14: S-N Diagram Plotted from the Results of Completely Reversed Axial Fatigue Tests. Material: UNS G41300 Steel, Normalized; $S_{ut} = 110.3\text{MPa}$; Maximum $S_{ut} = 861.8\text{MPa}$. [64].....	25
Figure 2-15: Stress over Time for Fluctuating Stress State [18].....	27
Figure 2-16: Mean Stress and Stress Amplitude Diagram According to Modified Goodman Approach [19]	28
Figure 2-17: Ball on the Hill Analogy [1].....	30
Figure 2-18: A Compliant Tristable Four-Bar Mechanism and its Potential Energy Curve [24].....	32
Figure 2-19: A Bistable Compliant Four-Bar Mechanism (a), Its Pseudo-Rigid-Body Model (b) and Its Potential Energy Curve (c) [25].....	34
Figure 2-20: Compliant Locking Mechanisms for Rotational Motion [26]...	36
Figure 2-21: Compliant Locking Mechanisms for Linear Motion [26]	36
Figure 3-1: A Functionally Binary Pinned-Pinned (FBPP) Segment [27]	37
Figure 3-2: A Functionally Binary Pinned-Pinned (FBPP) Segment Whose Shape Is a Circular Arc [27]	38
Figure 3-3: FBFP Half-Model of FBPP Segment [27]	39
Figure 3-4: Deflected Shape of the FBPP Segment [27].....	40
Figure 3-5: Non-Dimensional Pin Joint Paths at Different Curvatures	48
Figure 3-6: PRBM of the FBFP Segment Constructed by Golden Section Method [28]	49
Figure 3-7: PRBM of the FBFP Segment Constructed by Arc Fitting Method	50
Figure 3-8: Force (Non-dimensionalized Load Factor [α^2]) – Deflection (Pseudo-Rigid-Body Angle Difference [$\Delta\Theta$]) Characteristics for $\kappa_0=1$ Obtained by Arc Fitting Method.....	55
Figure 3-9: Error Comparison for $\Delta\theta_0=45^\circ$ and $\kappa_0=1$	57

Figure 3-10: θ_0 Range (in degrees) for the Validity of Golden Section Method.....	58
Figure 3-11: PRBM of the Whole System: (a) 1 st Stable Position, (b) Unstable Position, (c) 2 nd Stable Position	59
Figure 4-1: Design Space for Installation	63
Figure 4-2: (a) Estimated Initial Position of Both Segments (Symmetrical), (b) Estimated Intermediate Position of the Left Segment.....	64
Figure 4-3: Illustration of the Parameters that Define Deflection Characteristics.....	65
Figure 4-4: Initial and Final Positions of the PRBM of the Half-Segment....	66
Figure 4-5: Undeformed Shape of the Living Hinge.....	68
Figure 4-6: An Example of the Wrong Designed Living Hinge without Leaving Recess.....	69
Figure 4-7: Deformed Shape of the Living Hinge.....	70
Figure 4-8: Locked (Green) and Unlocked (Blue) Positions of the Mechanism for $\Delta\theta_0=45^\circ$	73
Figure 4-9: Input Force (F_{in}), Force on Each Segment (F_{each}) and Potential Energy Variation along Deflection Path of the 1 st Mechanism (POM)	75
Figure 4-10: Input Force (F_{in}), Force on Each Segment (F_{each}) and Potential Energy Variation along Deflection Path of the 1 st Mechanism (Innov'PA) .	78
Figure 4-11: Top (a) and Isometric (b) Views of the 1st Mechanism (POM)	79
Figure 4-12: Top (a) and Isometric (b) Views of the 2 nd Mechanism (Innov'PA)	80
Figure 5-1: FEM Model of the Right Segment.....	83
Figure 5-2: Information on Mesh Element of the FEM	84
Figure 5-3: Boundary Conditions and Forcing.....	84
Figure 5-4: Stress Distribution of the Deformed Shape	85

Figure 5-5: Variation of Input Force (F_{in}) and Force on Each Segment (F_{each}) along Deflection Path (Theoretical and FEM Results)	86
Figure 5-6: S-N Diagram of Extruded (Dashed) and Molded (Intermittent) POM (Delrin) [36]	88
Figure 5-7: Experimental Setup	89
Figure 5-8: Variation of Input Force (F_{in}) along Deflection Path (Theoretical and Experimental Results)	90
Figure D-6-1: Force (Non-dimensionalized Load Factor [α_t^2]) – Deflection (Pseudo-Rigid-Body Angle Difference [$\Delta\theta$]) Characteristics for $\kappa_0=0.50$ Obtained by Golden Section and Arc Fitting Methods Respectively	108
Figure D-6-2: Force (Non-dimensionalized Load Factor [α_t^2]) – Deflection (Pseudo-Rigid-Body Angle Difference [$\Delta\theta$]) Characteristics for $\kappa_0=0.75$ Obtained by Golden Section and Arc Fitting Methods Respectively	109
Figure D-6-3: Force (Non-dimensionalized Load Factor [α_t^2]) – Deflection (Pseudo-Rigid-Body Angle Difference [$\Delta\theta$]) Characteristics for $\kappa_0=1.00$ Obtained by Golden Section and Arc Fitting Methods Respectively	110
Figure D-6-4: Force (Non-dimensionalized Load Factor [α_t^2]) – Deflection (Pseudo-Rigid-Body Angle Difference [$\Delta\theta$]) Characteristics for $\kappa_0=1.25$ Obtained by Golden Section and Arc Fitting Methods Respectively	111
Figure D-6-5: Force (Non-dimensionalized Load Factor [α_t^2]) – Deflection (Pseudo-Rigid-Body Angle Difference [$\Delta\theta$]) Characteristics for $\kappa_0=1.50$ Obtained by Golden Section and Arc Fitting Methods Respectively	112

LIST OF TABLES

TABLES

Table 3-1: Radius and the Center Coordinates of the Fitted Arc for Different Curvature Values.....	53
Table 3-2: Radius and x-Coordinate of the Arc Path Acquired by Golden Section Method [28].....	54
Table 3-3: Spring Stiffness Coefficients for the Golden Section Method.....	55
Table 3-4: Spring Stiffness Coefficients for the Arc Fitting Method	56
Table 4-1: Angle of Connection (ζ) Values for Each Curvature.....	74
Table 4-2: Design Parameters of the Mechanism (POM).....	76
Table 4-3: Design Parameters of the Mechanism (Innov'PA)	77

LIST OF SYMBOLS

SYMBOLS

τ_{\max}	Maximum Shear Stress
S_y	Yield Strength
SF	Safety Factor
σ_1, σ_2	Principle Stresses
σ'	Effective Stress
σ_x	Equivalent Stress on the x-direction
σ_y	Equivalent Stress on the y-direction
τ_{xy}	Shear Stress on x-y Plane
K_t	Concentration Factor
S_e	Endurance Limit
S_e'	Uncorrected Endurance Limit
S_{UT}	Ultimate Tensile Strength
k_a	Surface Condition Modification Factor
k_b	Size Modification Factor
k_c	Load Modification Factor
k_d	Temperature Modification Factor
k_e	Reliability Factor
k_f	Miscellaneous-Effects Modification Factor
σ_{\min}	Minimum Stress
σ_{\max}	Maximum Stress
σ_m	Mean Stress

σ_a	Alternating Stress
F_{cr}	Critical Force
F_{in}	Total Input Force
F_{each}	Individual Horizontal Component of the Input Force Applied on Each of the Half Segment
F	Horizontal Component of the Input Force
R_o	Initial Curvature
(x,y)	Local Coordinate System
(x',y')	Global Coordinate System
a	x-coordinate of the Pin Joint at the Deflected Position
b	y-coordinate of the Pin Joint at the Deflected Position
a'	Width of the Whole Segment
b'	Height of the Whole Segment
a_i	x-coordinate of the Pin Joint at Initial Position
b_i	y-coordinate of the Pin Joint at the Initial Position
s	Distance Along the Segment
θ	Angle between Segment Tangent and Horizontal
θ_0	Tip Angle between Segment Tangent and Horizontal
$M_i(s)$	Internal Moment at a Distance s along the Segment
L	Length of the Half Segment
L'	Total Length of the Whole Segment
ζ	Angle of Connection
κ	Curvature in the Deflected Position
κ_0	Non-dimensionalized Curvature at the Free End
α^2	Non-dimensionalized Load Factor
λ	Elliptic Integral Transformation Parameter
E	Young's Modulus

I	Moment of Inertia of the Cross-Section
$F(\phi,k)$	Incomplete Elliptic Integral of the First Kind
$E(\phi,k)$	Incomplete Elliptic Integral of the Second Kind
k	Modulus of the Elliptic Integral
ϕ	Amplitude of the Elliptic Integral
Θ	Pseudo-Rigid-Body (PRB) Angle
Θ_i	Initial PRB Angle
ρ	Characteristic Radius Factor
γ	Fundamental Radius Factor
(A_0, B_0)	Coordinates of the End Point of the Fixed Link on Pseudo-Rigid-Body Model
K_θ	Spring Stiffness Coefficient
h	Thickness of the Segment
p	Height of the Segment
L_{f1}	Deflected Length of the Flexure Joint
L_{f0}	Undeformed Length of the Flexure Joint
t_{f1}	Thickness of the Flexure Joint

CHAPTER 1

INTRODUCTION

1.1 On Compliant Mechanisms

Compliant mechanisms are flexible link mechanisms that gain at least some of their mobility from the deflection of flexible members [1]. Flexibility of links also provides flexibility in design stages. Keeping in mind that the deflection is a tool that may give the desired motion or force requirements, capabilities that compliant mechanisms provide are countless.

They have been utilized systematically for a few decades although their origin dates back to thousands of years ago. Since they do not depend on rigid joints in order to get mobile, quite a lot of advantages come together. In the competitive industrial market, the need for both economical and reliable designs is of high importance. Compliant mechanisms, despite of challenging theory behind them, is an opportunity to provide such designs. Hence, designing with compliance deservedly gets widespread every day, eventually research on the subject become intense nowadays. Both the improvements on the materials science and the analytical tools that are being developed accelerate the utilization of compliant mechanisms.

1.2 Scope of the Thesis

The main aim of the thesis is to design a compliant bistable locking mechanism that accomplishes the force requirements. Input force and design space are strictly specified beforehand. Coming up with a reliable and compact final working prototype is intended.

The starting point of the idea is the bistable nature of functionally binary pinned-pinned compliant segments. Among stability, due to the practical reasons such as their convenience to be designed planar and single piece, this concept is chosen. Their symmetrical nature and the mobility of the middle pinned section are also causes of the selection of initially curved functionally binary pinned-pinned segments. Different configurations will not be utilized but will be offered for future work. They are to be synthesized with similar methods that will be mentioned in the thesis.

Synthesis procedure will be carried out by using exact elliptic integral solutions but also simplifying the design stages via rigid body replacement method. The pseudo-rigid-body models (PRBM) will be constructed stage by stage and then their difference with the real case will be discussed.

Material selection and segment design procedures will be carried out. Parameters from the PRBM will be utilized and corresponding calculations will be presented. Possible living hinge replacements at the pin joint locations will be discussed.

Moreover, strength and life requirements are to be paid precise attention. Static and fatigue failure criteria will be considered and the results will be verified with a finite element software.

Experimentally measuring the output forces, the study will be finalized as soon as the requirements are met. Finally, discussions on the physical prototype measurements and the analytical results of exact calculations and pseudo-rigid-body model will be presented suitably.

1.3 Outline of the Dissertation

The outline of the dissertation is as follows:

In Chapter 2, a detailed survey on compliant mechanisms and stability is conducted. Description, classification and synthesis methods of compliant mechanisms are presented; stability, multistability and compliant bistable mechanisms are investigated in detail.

In Chapter 3, functionally binary pinned-pinned segments are defined; their pseudo-rigid-body models are constructed and evaluated. Using exact solutions and models, the tool for the design stages is built.

In Chapter 4, first, the design space to fit the mechanism in is described. Then, the segment is designed according to that design space, meeting the force and strength requirements. From segment design to mechanism construction every parameter is selected and discussed. Force and energy charts are illustrated and the finalized model screenshots are presented.

In Chapter 5, firstly, finite element model (FEM) analysis is conducted. It is shown that the critical areas are safe and the force requirements are achieved. Secondly, fatigue life analysis is conducted and the desired life requirements are proved to be satisfied. At the end of the subchapter, physical prototype and experiment setup construction is described. Experiment results are evaluated and discussed.

In the final chapter, conclusion and discussion on this study are presented and suggestions on future work are given.

CHAPTER 2

LITERATURE SURVEY

2.1 Introduction

In this chapter, a survey on compliant mechanisms is presented. A general overview is introduced and synthesis methods are explained. The description of stability concept and multi-stable behavior are presented. Two subcategories that are bistable compliant mechanisms (BSCM) and compliant locking mechanisms (CLM) are defined.

2.2 Compliant Mechanisms Overview

In this chapter, definition and classification of compliant mechanisms are given, benefits, challenges and some applications are counted.

2.2.1 Definition and Brief History

“A mechanism may be defined as a group of rigid bodies connected to each other by rigid kinematic pairs (joints) to transmit force and motion [2].” This definition excludes any deflection of links (since they are rigid) and also force and motion transmission is said to be achieved only by joints. Traditionally, designers stick to this definition and see the elastic deformation of links as a handicap. However, if the definition is extended

to include flexibility and the deflection of the flexible members can be used for the benefit of purpose, the risk may turn into an opportunity. This idea generated a new class of mechanisms called compliant mechanisms. Compliant mechanisms are flexible link mechanisms that gain at least some of their mobility from the deflection of flexible members [1]. The term compliance is referred to the quantity that is reciprocal of the spring rate. Therefore, by definition, compliant refers to the structures having the property of compliance.

Neglecting friction, a rigid link mechanism is conservative, that is the sum of potential and kinetic energy is constant over time. Compliant mechanisms however; store energy in the form of strain energy through the deflection of flexible members. That energy can then be released at a predefined state, in order to accomplish the required force or motion requirement. Hence the total amount of potential and kinetic energy plus the strain energy is conserved for this case.

For instance, the bow and arrow example (Figure 2-1) illustrates the storage of strain energy as the deflection of the bow. While the bow is pulled by the external force F , it stores strain energy until the archer releases the arrow. At that predefined moment, energy is transferred to the arrow as kinetic energy, giving the initial speed for shooting.

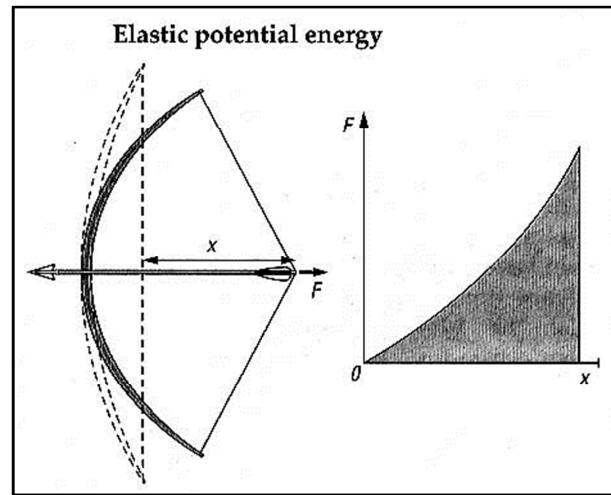


Figure 2-1: Bow & Arrow Analogy

Historically it is known that, compliance has been utilized for over 10.000 years, in the form of bows, according to cave paintings in “Les Dogues”. Subsequently, war requirements demand stronger weapons that are bigger and stronger, causing the invention of the first catapult (Figure 2-2) by Greek engineers (800 BC). After these inventions, compliant mechanism applications were limited with the war machines, until last century [3]. Recently, several examples that make use of compliance can be seen in daily life or in industrial applications.

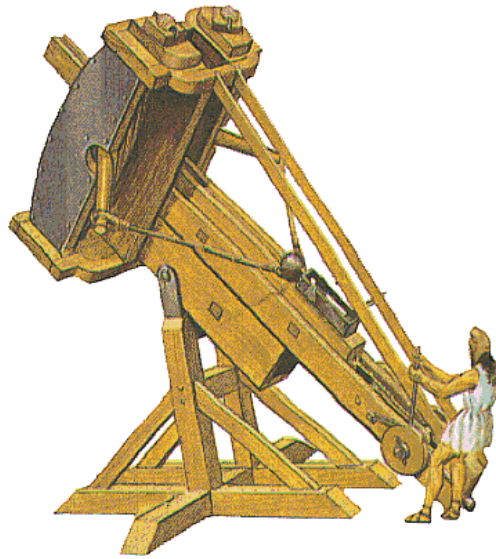


Figure 2-2: The Greek Palintonon Weapon¹

2.2.2 Some Applications

Utilization of deflection of any flexible member to fulfill force, displacement or motion requirements, can be interpreted as an application of compliant mechanisms, among them; some daily examples are illustrated in Figure 2-3.

¹<http://www.mlahanas.de/Greeks/images/Palintonon.gif>, Last accessed 05.04.2012



Figure 2-3: Common Compliant Devices. A Binder Clip, Paper Clip, Backpack Latch, Lid, Eyelash Curler and Nail Clippers.

In various disciplines, compliant mechanisms found area of application. A patented invention, compliant bistable spring to be used as a medical stent, is shown in Figure 2-4. A compliant mechanical switch that exhibits bistable behavior is also show in Figure 2-5

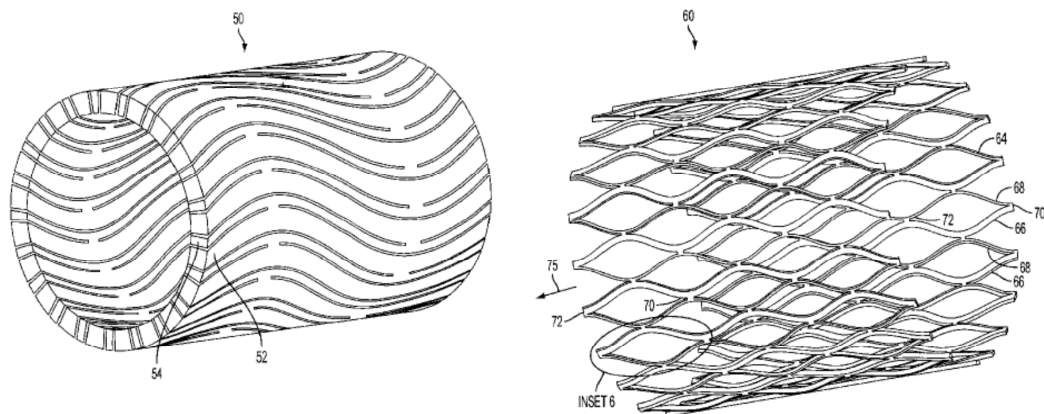


Figure 2-4: Bistable Medical Stent Apparatus [4]

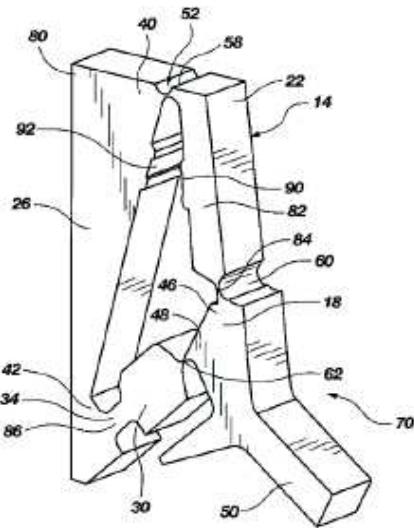


Figure 2-5: A Compliant Bistable Mechanical Switch

Although simple deformable (compliant) structures such as beams and diaphragms have performed adequately in many micro devices, more sophisticated micromechanical functions can be realized by fully exploiting the preferred uses of elastic deformation via compliant mechanisms [5].

That statement brings out the fact that the utilization of compliant theory in MEMS (microelectromechanical systems) applications is a necessity. “Examples of MEMS application are medical instruments for in-body surgery, hearing aids, air-bag sensors, micro pumps and optics and tilting mirrors for projection devices [6].” Some other applications of MEMS that are bistable have also been presented in literature ([7],[8] and [9]). Some basic examples on the field can be seen on Figure 2-6 and Figure 2-7.

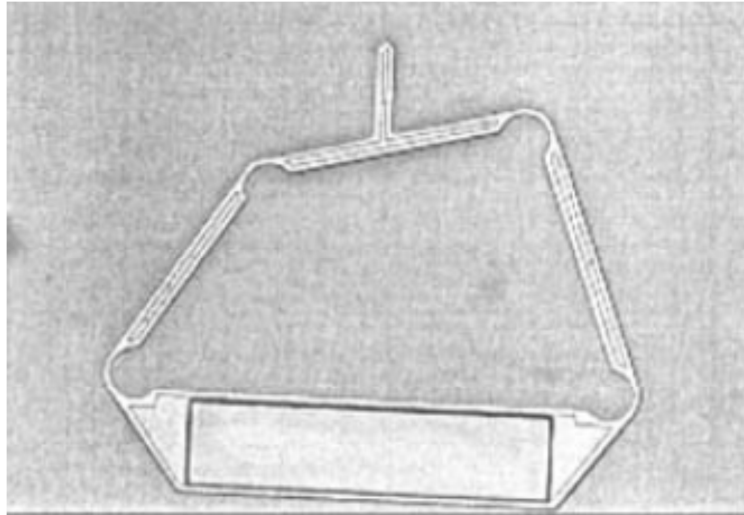


Figure 2-6: A Micro Compliant Four-Bar Mechanism with Lumped Compliance [5]



Figure 2-7: Titanium Mirrors Bulk Micromachined Using Deep Etching of a Titanium Substrate²

² <http://compliantmechanisms.byu.edu/sites/compliantmechanisms.byu.edu/files/image/fig2.jpg>, Last accessed on 19.04.2012

2.2.3 Classification

For the conventional rigid link mechanisms, link identification is quite straightforward since the kinematic pairs separate every link from each other. However for compliant mechanisms mobility is partially or fully caused by the deflection of the links, not from the joints. For example, in Figure 2-5 the mechanical switch has no joints, hence has also no links. Such mechanisms are called monolithic or fully compliant mechanisms. If it had at least one rigid-body joint, then it would be called non-monolithic, hybrid compliant or partially compliant. Monolithic compliant mechanisms are also classified as distributed and lumped compliant mechanisms, by the characteristics of motion (Figure 2-8). Motion of the lumped compliant mechanisms are mainly based on the flexures that behave like rigid-body joints, however distributed compliant mechanisms utilize most of their links to store and release energy throughout the motion.

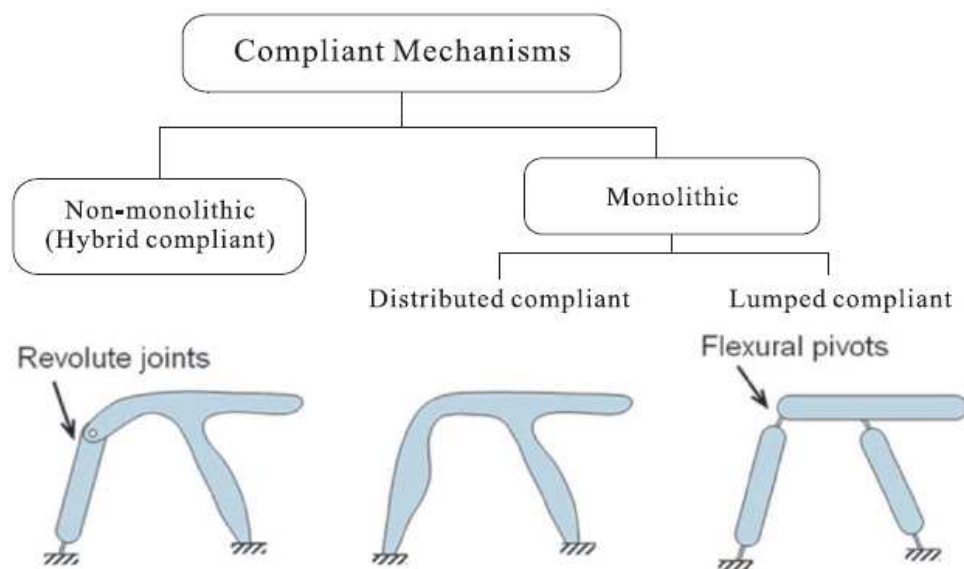


Figure 2-8: Classification of Compliant Mechanisms [10]

Link identification of compliant mechanisms is identical with the rigid-body mechanisms; rigid-body joints split each link. The structural type of the link is also the same; a link that has two rigid-body joint connections is structurally binary, a link that has three rigid-body joint connections is structurally ternary and so on... That classification only depends on the number of joints. Functional type on the other hand, can only be determined by determination of the force and motion characteristics. Since the motion of the mechanism depends on the deflection of the links, the application point of the force alters the motion characteristics. That point refers to a "pseudo-joint". The total number of rigid-body joints and pseudo-joints determines the functional type of a link. For example if a compliant link has two rigid-body joints and a force is applied on it, then the link is said to be structurally binary and functionally ternary [11].

Links can be classified into two categories as compliant and rigid links by deciding whether the deflection of the links can be neglected with respect to the rest of the mechanism. Then the compliant links can be categorized into two groups as simple and compound. The necessary and sufficient properties of a link to be simple are being initially-straight, having constant material properties and constant cross section. Links that do not have these properties are called compound links. Compound links composed of two subcategories as homogeneous and non-homogeneous. Homogeneous means that the link is either fully-rigid or fully-compliant; in this case, compound link must obviously be fully-compliant (Figure 2-9).

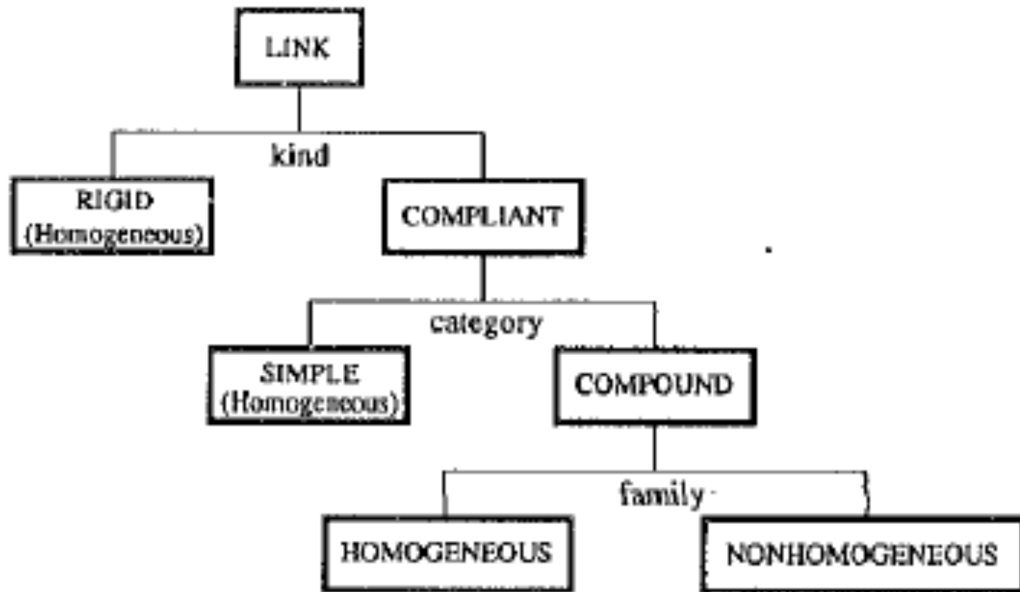


Figure 2-9: Component Characteristics of a Link [11]

For the compliant mechanisms, the shape of the link is noticeably significant in contrast with the rigid-body case. Inspecting the links, one can notice different “segments” that are combined to embody the link. The transition of the segments can be caused by the change of cross-section, material property or the force-displacement characteristics. The determination of segments within a link is generally intuitive and difficult unless it is designed in obviously separated segments. Each segment should have distinct motion characteristics and their endpoints must all be at a physical discontinuity. They can be rigid or compliant; moreover compliant segments may be simple or compound, in a similar way that is described in link classification. However compound segments must be homogeneous since the rigid and compliant sections are defined as different segments (Figure 2-10).

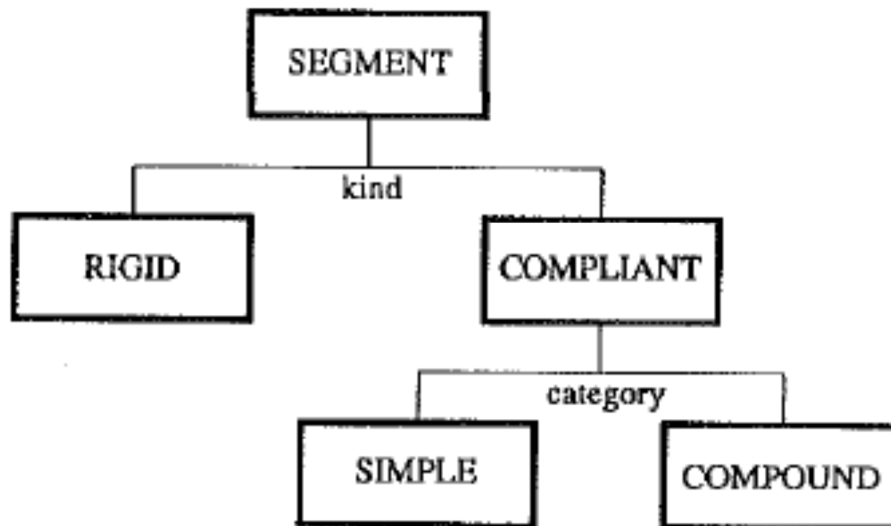


Figure 2-10: Component Characteristics of a Segment [11]

2.2.4 Benefits and Challenges

The reason for the extensive areas of applications of compliant mechanisms to take place is obviously their countless advantages.

Manufacturing of a single piece compliant mechanism is quite simple, since it can be injection molded or extruded rapidly. The post assembly process is eliminated and number of parts to perform the same task is considerably reduced (Figure 2-11). They are generally more compact compared to their non-compliant equivalents. Hence their weight and size are lower, that also leads to reduction of cost.



Figure 2-11: Macro-scale Examples of a Monolithic (a) Stapler and (b) Windshield Wiper Developed by the Kota Group at the University of Michigan, Using Compliant Mechanisms³

Since compliant mechanisms do not depend on the rigid kinematic joints in order to be mobile, wearing due to dry friction at the joints, backlash and lubrication problems are eliminated. Hence, they are more precise and reliable that is the main reason of compliant mechanisms to be used in micro-electro-mechanical systems (MEMS).

Despite their many advantages, compliant mechanisms have some challenging points in design stages and during operation period. First of all, compared to rigid-link mechanisms, synthesis steps are considerably complex and time consuming. Since the elastic deformations of linkages are considered to be design parameters in synthesis procedure, more variables must be taken into account that requires the solution of complex equations and longer periods of calculation. Secondly, compliant mechanisms are

³ http://www.flxsys.com/images/Flexsys_wiperblade.jpg, Last accessed 05.04.2010

more likely to suffer from creep and stress relaxation. Creep is defined as the increase in strain of a specimen with time under an applied stress [12]. It may occur in long periods of time due to molecular chain sliding. If the elastically-deformed part is kept in that stressed state for a long time, strain of the material will exceed an allowable value i.e it will fail. That stress relaxation phenomena is more critical in plastics, which is the common material group in compliant mechanisms. Third disadvantage comes from the basic nature of the compliant mechanism that they depend on the deformation of their flexible members. That property leads to the transformation of some of the input energy to strain energy in the flexible members; hence sum of the potential and kinetic energy is not conserved. Finally, their limited motion capability and the possibility of axis-drift are challenging risks unless the mechanism is designed accordingly.

2.2.5 Synthesis Methods

Howell [1] classifies compliant mechanism synthesis methods into two categories that are rigid body replacement synthesis and synthesis with compliance. This classification is reasonable since the two main categories accomplish the design based on dissimilar methodologies. These two kinds of methods will be described in this chapter.

First kind of methods is rigid body replacement synthesis. The methods on this category are first introduced by Midha and his associates. Some uses kinematic techniques such as graph theory [13] and Burmester theory [14], some are based on loop closure theory [15].

Basically, the idea under the rigid body replacement method, as can be understood from its title, is to convert the rigid-body mechanism satisfying the path, function or motion requirements into its compliant equivalent. The rigid-body mechanism that is to be converted is called pseudo-rigid-body model (PRBM) of the compliant mechanism. That mechanism can be synthesized by one of the many existing methods that are out of the content of the thesis.

While converting the mechanism, it must be kept in mind that only kinematic properties of the PRBM is carried to the next level, that also explains the reason of the synonym of this method: kinematic synthesis. The underlying risk that must be considered is the incompatibility of the model with the compliant equivalent. For instance, relative rotation of the links at the joints must be checked because there is a limit of maximum rotation of the flexures. Another critical point is the stress levels since the motion is somehow dependent on the deflection of the flexible members. In other words, flexures must rotate without exceeding their rotation capacity and flexible members must deflect without exceeding their yield stress level. The intersection of any link throughout the motion must also be prevented and the connection of the final mechanism to the design space must be ensured.

Any compliant mechanism can be described by various different PRBMs, one example is shown in Figure 2-12. In this example, a compliant bistable slider mechanism is modeled with a double slider with a spring attached. One must keep in mind that the spring accounts for the forcing due to the deflection and the new-slider displacement is due to the positional change

of the deflected link. Here since the only concern is to match the kinematic characteristics, spring is just placed for representative purposes.

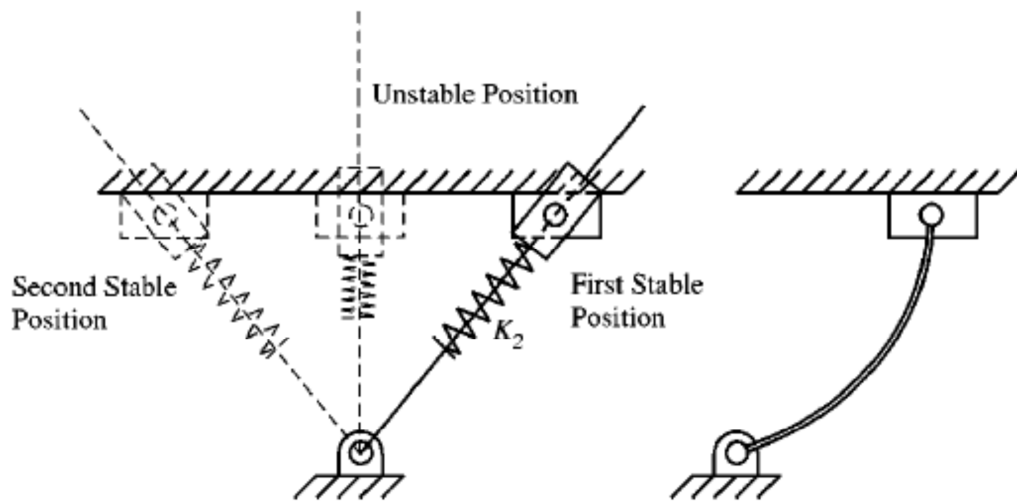


Figure 2-12: A Bistable Double-Slider Mechanism with a Pin Joint, Joining The Sliders, and a Compliant Equivalent. [16]

The second kind of synthesis methods is synthesis with compliance. This type of synthesis is basically the combination of kinematic synthesis with the energy requirements. Since the kinematic aspects of the synthesis problem is considered together with the static force requirements, these methods are also called kinetostatic synthesis methods. Energy and force considerations such as input force or torque, output force or torque, stored strain energy, total potential energy, mechanical advantage etc. are design parameters in these methods. One way to analyze the energy stored is to use virtual work method that is based on the principle that the net virtual work of all active forces is zero if the mechanism is in equilibrium. With this rather straightforward method, only the necessary forces are taken into account that simplifies the process. Another elementary way is to use pseudo-spring potential energies of PRBMs.

Some basic constraints must also be considered different than rigid body replacement synthesis. The spring constants must be positive and the thickness of the flexible beams must be reasonable. Force directions or magnitudes must be checked for validity and the final mechanism must be operable.

Coupling of the kinematic equations with the energy equations is necessary. Generally the energy equations are nonlinear and if the kinematic and energy-storage equations are coupled (they can only be solved simultaneously) the effort to solve them is highly increased. The coupling of these sets of equations must be reduced as possible in order to simplify the evaluation process. In order to ensure the “weakly coupled” condition (kinematic equations can be solved separately, after that energy-storage equations are solvable) equation (2.1) must be satisfied:

$$2m \geq n \tag{2.1}$$

Where m is the number of flexible segments and n is the number of precision points.

2.3 Failure Criteria

2.3.1 Introduction

Inspecting the all possible causes of failure, i.e. the stress types, bending stress is the most dominant one, since compliant mechanisms are composed of flexible elements that are mostly subjected to bending deformations. The effect of axial loading is usually lower but still effective. These two stresses causes the principle stresses if the mechanism is considered to be two dimensional. Shear stress is not a concern since it gets its maximum value at the middle of the cross section where bending stress is zero. Comparing these two locations, stress evaluation of the edge of the section would be much more reasonable because bending stress is at its highest level there. Torsion is another stress type that occurs in a 2-D system if only there exists out of plane forces. Neglecting these forces, torsional stresses can also be neglected.

Although it is not a requirement, generally ductile materials are more convenient then brittle ones in compliant mechanism applications, due to their elastic behavior under large deformations. Hence this is also the case for the thesis application, meaning that only the stress theories that are convenient to ductile materials will be used.

At critical points (locations where output force is applied, thin sections as flexural hinges etc.), design must be re-evaluated considering both static

failure and for fatigue failure. Convenient failure theories must be selected and utilized with a secure factor of safety.

2.3.2 Static Failure

As mentioned, for the static failure a method that is applicable to ductile materials will be chosen. Two possible theories are Maximum Shear Stress Theory and Distortion Energy Theory [17].

Maximum Shear Stress Theory also known as the Tresca Yield Criterion, assumes that the yielding will begin after the shear stress of the part exceeds the shear stress in a tensile test specimen at yield. So for the material not to yield, the necessary criterion is:

$$\tau_{max} \leq \frac{S_y}{2} \quad (2.2)$$

Here τ_{max} is the maximum shear stress that the material is exposed to and S_y is the yield strength. Considering the factor of safety, the theory can be formulized as:

$$SF = \frac{S_y}{2\tau_{max}} = \frac{S_y}{\sigma_1 - \sigma_2} \quad (2.3)$$

Safety factor (SF) can be calculated and manipulated with the preceding relation. σ_1 and σ_2 are the principal stresses on the part.

Distortion Energy Theory also known as the Von Mises Yield Criterion assumes that the strain energy is composed of two parts that are volumetric strain energy and distortion strain energy. Yielding is said to be occurred after the distortion strain energy exceeds the one in a tensile test specimen at yield. For the application, an effective stress (Von Mises Stress) is evaluated and compared with the yield strength of the material. The criterion for the material not to yield for 2-D stresses is:

$$\sigma' = \sqrt{\sigma_x^2 + \sigma_y^2 - \sigma_x\sigma_y + 3\tau_{xy}^2} \leq S_y \quad (2.4)$$

Here σ' is the effective stress. σ_x and σ_y are the equivalent stresses on the x and y directions respectively. τ_{xy} is the shear stress on x-y plane.

Both the distortion energy theory and the maximum shear stress theory are applicable to stress evaluation of the ductile materials but maximum shear stress theory is relatively more conservative (Figure 2-13). Hence during computations, its criteria will be considered.

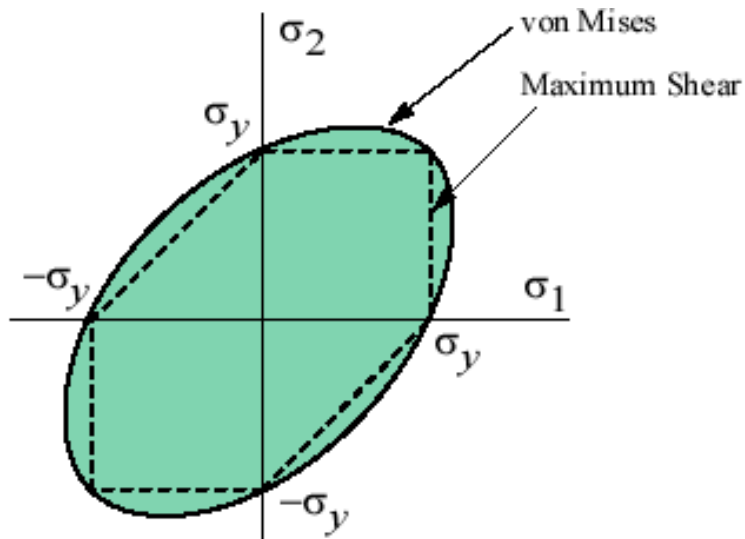


Figure 2-13: Safe Stress Areas According to Maximum Shear Stress Theory (Tresca Yield Criterion) and Distortion Energy Theory (Von Mises Criterion)

Generally, to account for the materials' property of stress increase on the sharp edges, a factor named stress concentration factor (K_t) is used. Nevertheless, ductile materials do not have that stress concentration in considerable amounts due to their nature [17], therefore it will be neglected.

2.3.3 Fatigue Failure

Due to cyclic loading of the part, a gradual decrease in the strength of the material is observed. When the strength value gets lower than the applied stress level, the fatigue failure is said to be occurred. Stress that is exerted on the material obviously decreases the life of the part. An example of that relation can be seen on Figure 2-14.

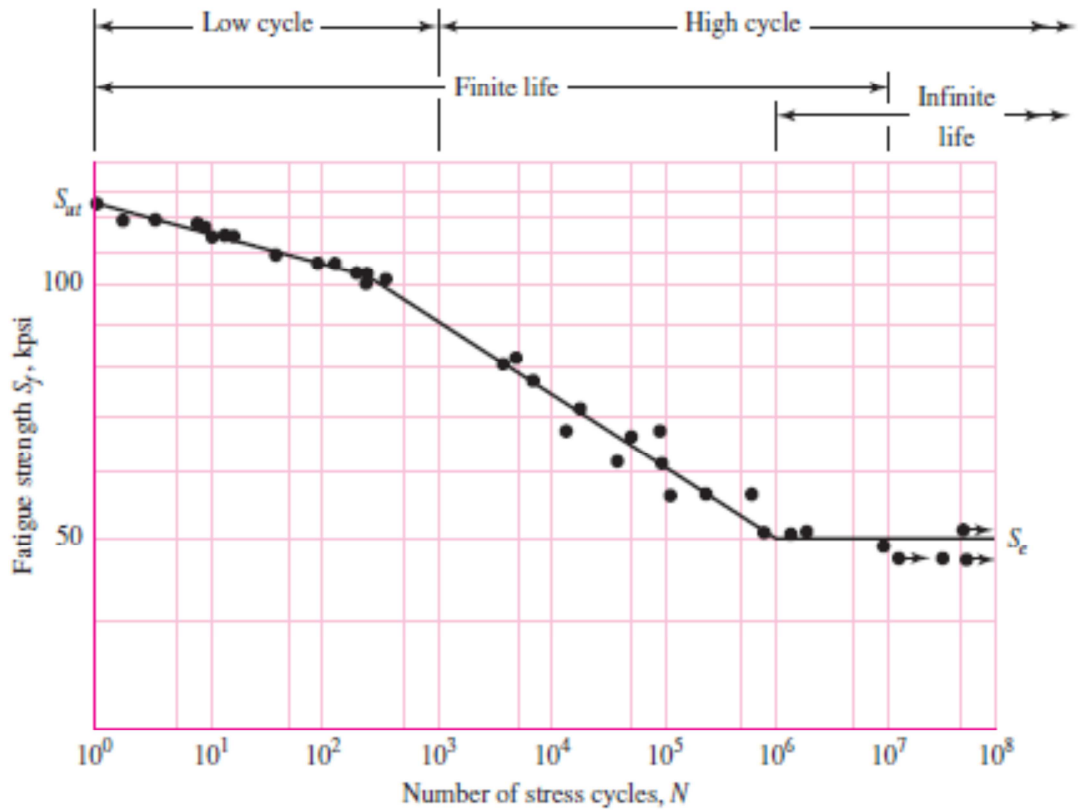


Figure 2-14: S-N Diagram Plotted from the Results of Completely Reversed Axial Fatigue Tests. Material: UNS G41300 Steel, Normalized;

$$S_{ut} = 110.3\text{MPa}; \text{ Maximum } S_{ut} = 861.8\text{MPa}.^4 [64]$$

In many applications, life of the part is considered to be a design constraint. Life expectancy differ for each application, it may even be infinite. The stress level of the material at which it has an infinite life is named the endurance limit (S_e).

⁴ Taken from NACA Technical Note 3866, December 1966

When the literature is inspected, studies are seemed to be focused on the fatigue life of metals. That is natural since the life estimation of metals is quite simpler than the polymers. Stress relaxation and creep are not much of a problem and temperature dependency of the metals is much lower. Nevertheless, a rough estimate for the endurance limit of a polymer can be made as proposed in [18] as:

$$S'_e = 0.2S_{UT} \text{ to } S'_e = 0.4S_{UT} \quad (2.5)$$

Here, S'_e is called the uncorrected endurance limit that must be multiplied by some modification factors (Marin factors) in order to come up to endurance limit. That value is found by testing the specimen on a standard rotary test. The details of the correcting factors will not be included on this study since they are explained in detail on many sources as [65],[66]. These factors are directly multiplied by the uncorrected endurance limit to give the endurance limit, as follows [18]:

$$S_e = k_a k_b k_c k_d k_e k_f S'_e \quad (2.6)$$

Where:

k_a = surface condition modification factor

k_b = size modification factor

k_c = load modification factor

k_d = temperature modification factor

k_e = reliability factor

k_f = miscellaneous-effects modification factor

The expectancy from the dynamic failure analysis, for this case, is to design the system for the specified life. Fluctuating stress state assumption (Figure 2-15) will be made and the corresponding minimum (σ_{min}) and maximum (σ_{max}) stresses will be converted into mean (σ_m) and alternating (σ_a) stresses as follows:

$$\sigma_m = \frac{\sigma_{max} + \sigma_{min}}{2} \quad (2.7)$$

$$\sigma_a = \left| \frac{\sigma_{max} - \sigma_{min}}{2} \right| \quad (2.8)$$

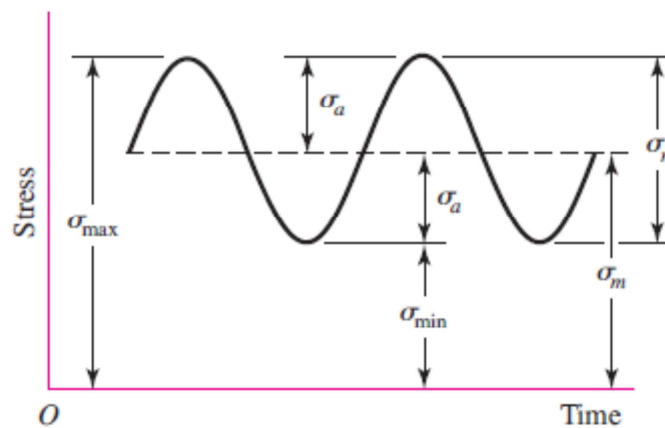


Figure 2-15: Stress over Time for Fluctuating Stress State [18]

The method that will be utilized is the quite common one, named Modified Goodman Approach. In Figure 2-16, a diagram showing the approach for estimating the factor of safety is shown. Point P is the design point, representing the current stress state. The point is in the area enclosed by the Modified Goodman line and the x-y axes, which shows that the stress level is acceptable. Out of that area, every point is either above yield point or has a finite life. Hence, the factor of safety to endurance limit can be evaluated. The theory implies that:

$$\frac{1}{SF} = \frac{\sigma_a}{S_e} + \frac{\sigma_m}{S_{ut}} \tag{2.9}$$

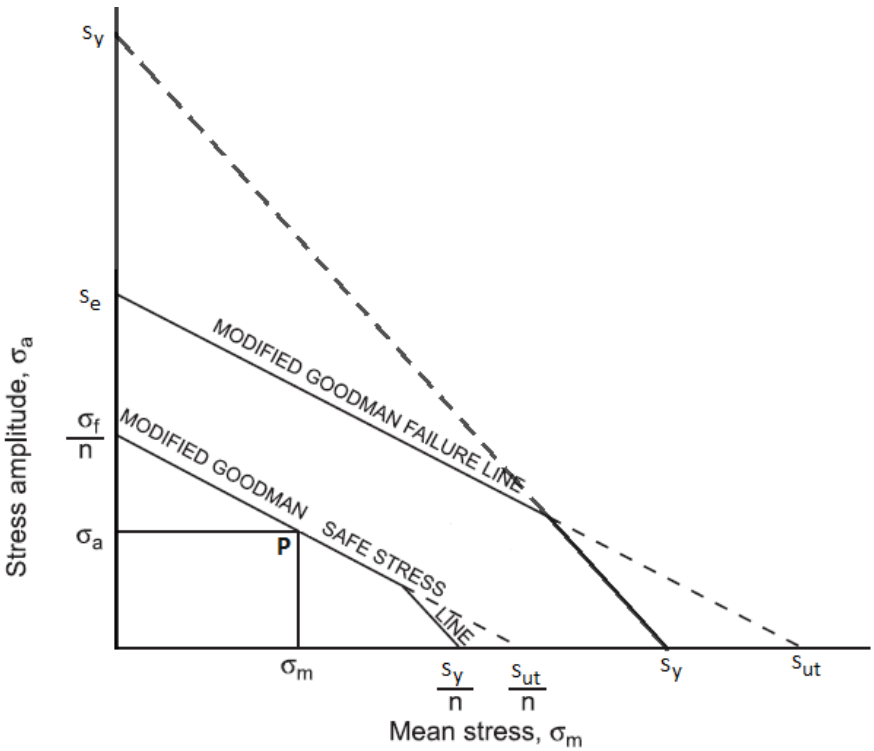


Figure 2-16: Mean Stress and Stress Amplitude Diagram According to Modified Goodman Approach [19]

2.4 Stability

Stability concept is highly beneficial in synthesis, especially in compliant mechanisms. Since a compliant mechanism is capable of storing and releasing energy throughout its motion, it is rather simple to design the mechanism as multistable, using the flexibility of the segments, in the favor of the desired energy curve.

In this subchapter, definition of stability and multistability will be made and utilization of these concepts in synthesis procedure will be explained.

2.4.1 Definition

There are various definitions of stability from different aspects, one of which is being related with the elastic stability of the structures. "If . . . 'small' external disturbances are applied and the structure reacts by simply performing oscillations about the . . . equilibrium state, the equilibrium is said to be stable [20]." Moreover, if this reaction is to diverge from the equilibrium state, then the equilibrium is called an unstable equilibrium. Although the structure reacts the disturbance if it does not diverge from but stays in the disturbed position it is a neutral equilibrium position.

Among different explanations, Lagrange-Dirichlet theorem defines the stability concept on the context of concern. It states that "when the potential energy ... has a minimum for an equilibrium position, the equilibrium position is stable [21, 22]". Thus, total potential energy curve of the mechanism describes the stability nature of that mechanism, such that, the local minima of the curve indicate the stable equilibrium positions.

To clarify the energy curve and stability correlation, an illustration is given in Figure 2-17 [1]. In the figure, different states of the system (ball on a hill in the gravitational field) can be seen. It can be thought that the form of the hill also represents the curve of the potential energy change. States A & D are stable equilibrium states, meaning that, after small disturbances the ball is effected but it reacts as an oscillation around the stable position. This is true for every small force that is under a limit, which is called critical force (F_{cr}). When a forcing beyond F_{cr} is applied, the system tends to switch to another equilibrium state. State B is unstable equilibrium position since a small disturbance causes the ball to fall (diverge from the equilibrium). E is a neutral equilibrium point. At that point, ball changes its equilibrium state to the disturbed position when exposed to a disturbance. Here a new state is seen, namely, externally constrained stable state. It can be understood by visualizing the behavior of the ball at point C. Although the form of the hill is downwards, an external obstacle causes the ball to stop, hence creating a stable state there. That is also an opportunity in the design stage of a real mechanism.

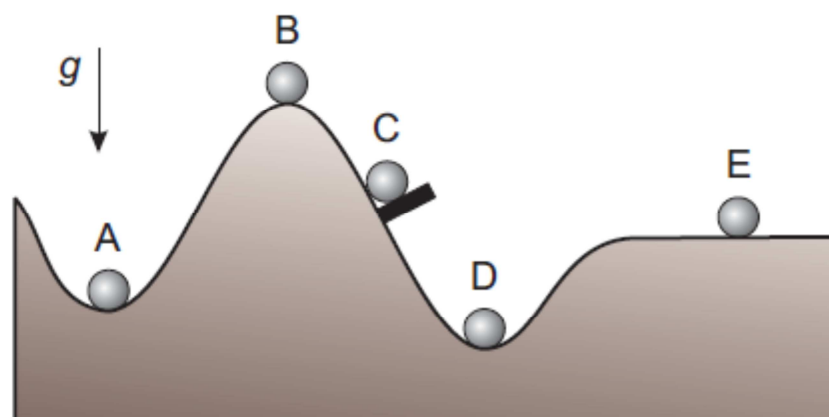


Figure 2-17: Ball on the Hill Analogy [1]

2.4.2 Multistability

As Oh clarified, definition of multistability is made in different fields as physics, dynamics, chemistry, etc [23]. Though, a common definition can be made on the mechanical point of view that, multistability of a mechanism means that the system has more than one stable position throughout its range of motion.

Rigid mechanisms cannot be multistable since the ability to store and release energy is a necessary condition to have a potential energy change thus enabling the possibility of a stable position. In order to overcome that obstacle, conventional mechanisms are designed with springs together with rigid linkages. However, compliant mechanisms contain the properties of springs within them; hence, with the proper utilization of the flexibility, one can achieve stable positions at predefined positions. An example is given on Figure 2-18, showing a compliant tristable four-bar mechanism in fully compliant and partially compliant forms. Also the energy curve with respect to the rotation of its coupler link is seen.

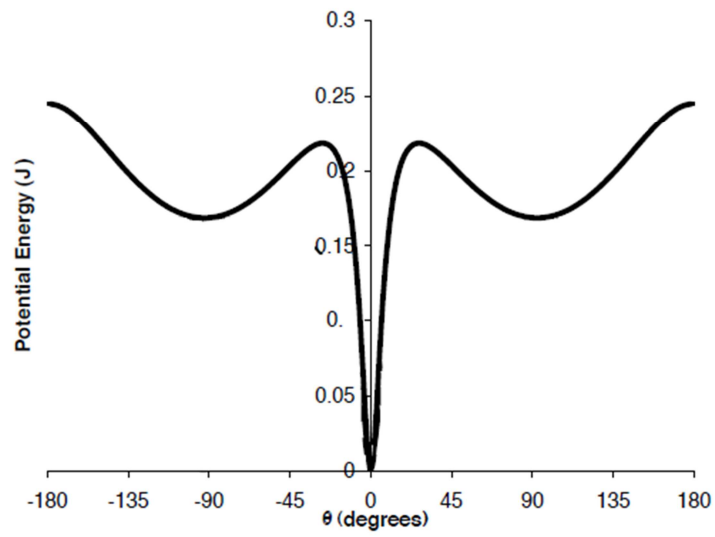
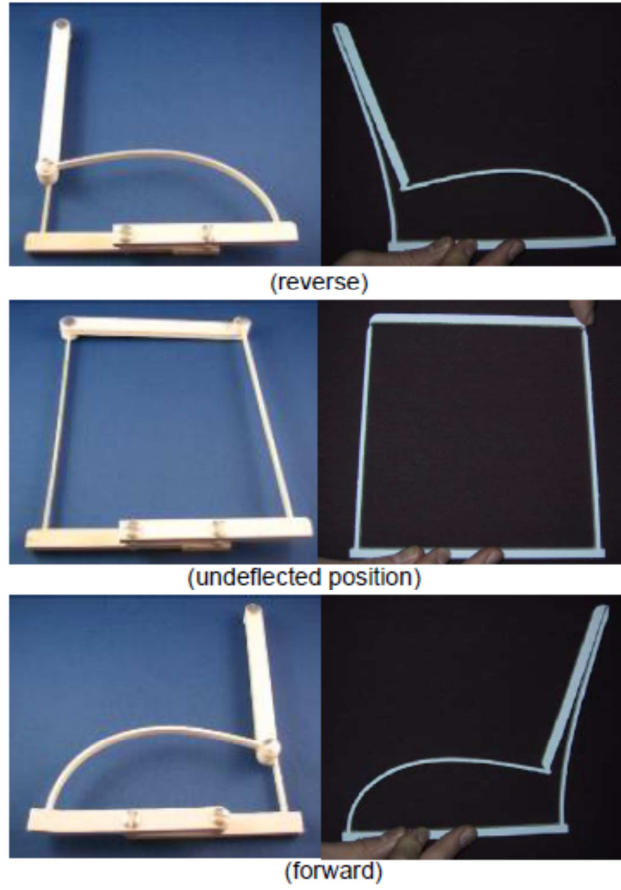


Figure 2-18: A Compliant Tristable Four-Bar Mechanism and its Potential Energy Curve [24]

2.4.3 Bistable Compliant Mechanisms

Bistable mechanisms are a subclass of multistable mechanisms that have two stable equilibrium positions. For a compliant mechanism to be bistable three conditions must be met. Firstly, the first derivative of the total potential energy of the system must be zero at three positions (equilibrium positions) at least. Secondly, second derivative of the same function must be zero at two positions (stable equilibrium positions). These two conditions are the results of the fact that the potential energy of a system is a local minimum at the stable equilibrium position. There must be one and only one unstable state between two successive stable states that makes the minimum number of equilibrium points three. Third condition is kinematic rather than kinetic; the mechanism must be movable between the equilibrium states smoothly.

A straightforward method to design a compliant bistable mechanism satisfying the stability and force requirements starts with the building of a PRBM that meets the motion requirements. After placing pseudo springs at the joints, potential energy equation for the full motion is derived parametrically in terms of geometric parameters and stiffness values. Equations then can be solved in order to satisfy the positions of the stable positions and/or the critical force requirements. One application of the method can be found in [25]. An example from that study is shown in Figure 2-19.

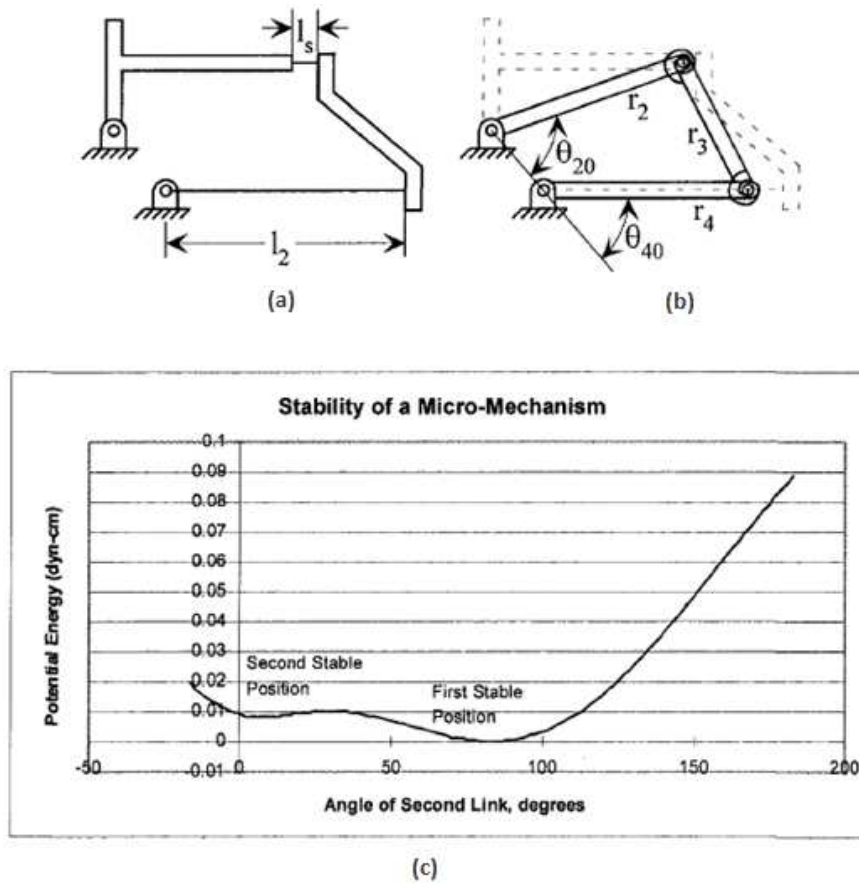


Figure 2-19: A Bistable Compliant Four-Bar Mechanism (a), Its Pseudo-Rigid-Body Model (b) and Its Potential Energy Curve (c) [25]

2.5 Compliant Locking Mechanisms (CLM) [26]

The task of the compliant locking mechanisms (CLM) is to prevent the mobility of an element at a specified position, in one-way or two-ways temporarily. They can be classified functionally as automatic, semi-automatic and commanded mechanisms. Automatic CLMs lock and release the part when a specific forcing is exceeded. Locking and releasing forces (or torques) and displacements can be manipulated separately as desired and the mechanism is functional once it is installed. Commanded CLMs, on

the other hand, need another command to lock or unlock the part. An external positive contact or friction is applied on the locking element. The actuation force can be provided in various ways as; mechanically, magnetically, electrically, chemically, thermally, etc. Semi-automatic CLMs exhibit automatic behavior during locking or unlocking and commanded at the reverse motion.

CLMs are capable of restraining linear or rotational motion. Some examples of CLMs for rotational motion and linear motion are shown in Figure 2-20 and Figure 2-21 respectively. There are some labels on the figures showing the parts of the mechanisms:

- 1 : Anchor
- 2 : Latch
- 3 : Profiled Blocked Element

The mechanism shown in Figure 2-21-k, is a good example of the utilization of FBPP sections in locking mechanisms.

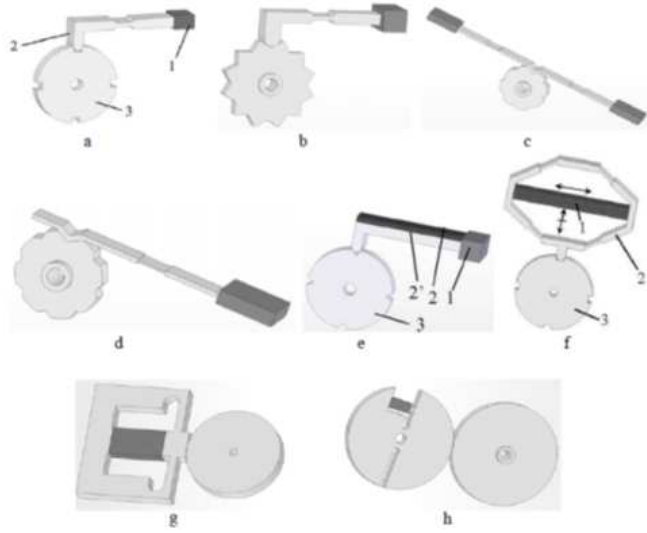


Figure 2-20: Compliant Locking Mechanisms for Rotational Motion [26]

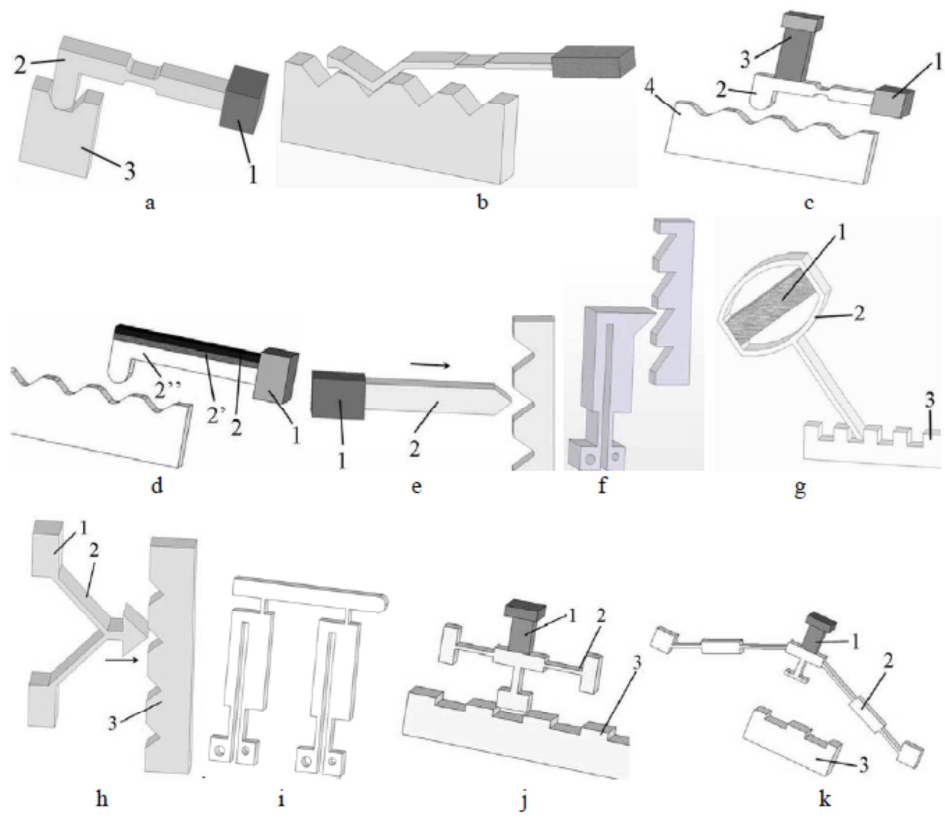


Figure 2-21: Compliant Locking Mechanisms for Linear Motion [26]

CHAPTER 3

FUNCTIONALLY BINARY PINNED-PINNED (FBPP) SEGMENTS

3.1 Introduction

As explained, compliant mechanisms are composed of segments, one kind of which is being functionally binary pinned-pinned (FBPP) segments (Figure 3-1). This kind of segment is being utilized widely in compliant mechanism design. Both ends of this segment are connected with pin joints, thus the only possible way to deflect the segment is to apply a force whose direction is intersected with the joints. Except that force, every force and moment causes the rigid-body motion (rotation) of the segment. Hence; if the force-deflection characteristics are specified, the segment can be employed as a nonlinear spring.



Figure 3-1: A Functionally Binary Pinned-Pinned (FBPP) Segment [27]

In order to evaluate and formulate the force-deflection characteristics practically, the initial shape of the FBPP segment is chosen to be circular (Figure 3-2). Pseudo-rigid-body model of the segment will be constructed and the force deflection behavior will be formulated accordingly.

On Figure 3-2, the segment is plotted on the global coordinate system (x' , y'). Initial curvature (R_0), total length (L'), width (a') and height (b') of the whole segment are illustrated. Horizontal force that is the only force that causes the segment to deflect is shown with F .

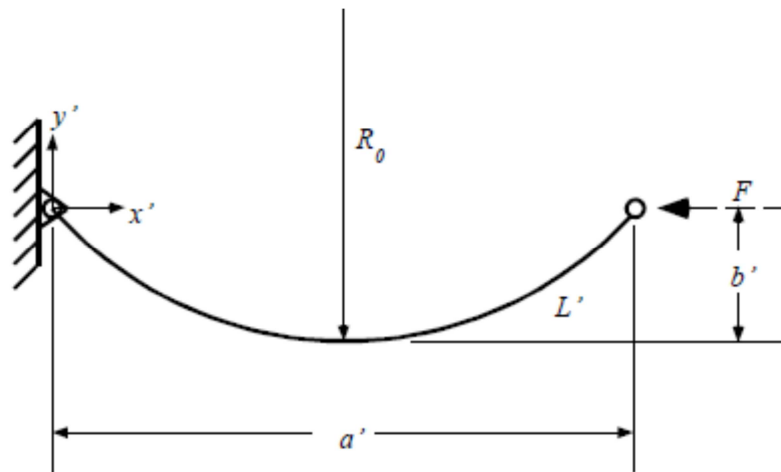


Figure 3-2: A Functionally Binary Pinned-Pinned (FBPP) Segment Whose Shape Is a Circular Arc [27]

“... the problem can be simplified by realizing that the segment is symmetric about a vertical line through its center. This symmetry can be used to divide the complete FBPP segment into two equivalent half-segments [28].” (Figure 3-3). A local coordinate system (x, y) is used and some parameters

such as the horizontal force (F) and initial curvature (R_0) remains the same. Obviously, vertical component of the pin joint (b) is equal to height of the whole segment (b') and horizontal component of the pin joint is half the width of the whole segment. Length of the half segment (L) is also half of the length of the whole segment (L').

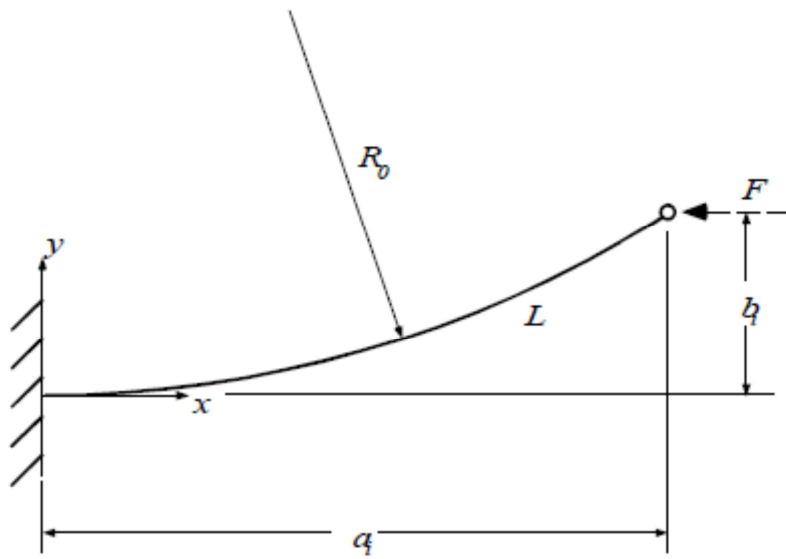


Figure 3-3: FBFP Half-Model of FBPP Segment [27]

This half-segment will be analyzed with elliptic integrals (exact solution) and with rigid body replacement method (the pseudo-rigid-body model). Results will be compared and evaluated.

3.2 Exact Solution [28]

According to Bernoulli-Euler equation the curvature in the deflected position is as follows:

$$\kappa = \frac{d\theta}{ds} = \frac{1}{R_0} + \frac{M_f(s)}{EI} = \frac{\frac{d^2y}{dx^2}}{\left[1 + \left(\frac{dy}{dx}\right)^2\right]^{3/2}} \quad (3.1)$$

Where, on this equation, θ is the angle of the curve tangent with respect to horizontal axis. s is the distance along the segment and $M_f(s)$ is the internal moment at the distance s . That moment can then be computed as:

$$M_f(s) = F(b - y) \quad (3.2)$$

where b is the vertical distance of the pin joint at the deflected position (Figure 3-4). a is similarly the horizontal distance.

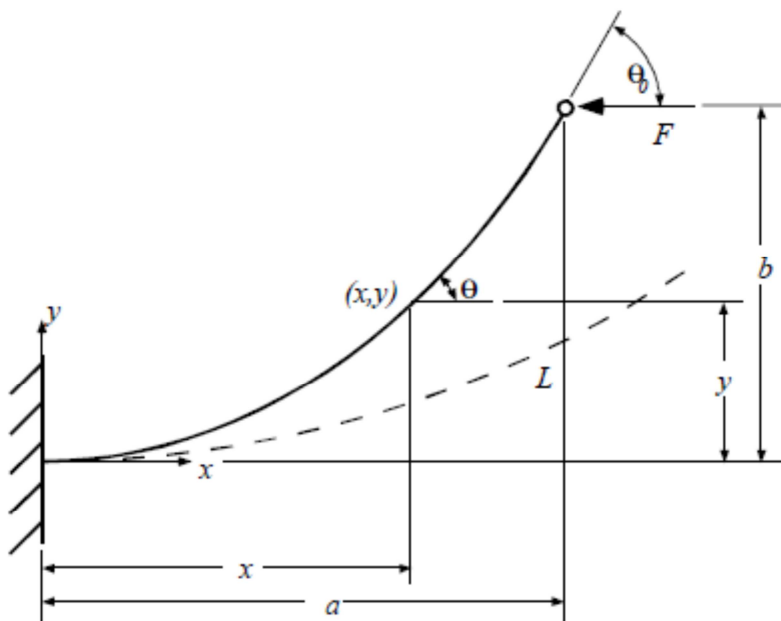


Figure 3-4: Deflected Shape of the FBPP Segment [27]

Inserting equation (3.2) into equation (3.1) and differentiating, one can get:

$$\frac{d^2\theta}{ds^2} = -\frac{F}{EI} \frac{dy}{ds} \quad (3.3)$$

Left hand side of the equation (3.3) can be manipulated by the chain rule in order change the parameter s to κ .

$$\frac{d^2\theta}{ds^2} = \frac{d}{d\theta} \left(\frac{d\theta}{ds} \right) \frac{d\theta}{ds} = \frac{d\kappa}{d\theta} \kappa = \frac{d}{d\theta} \left(\frac{\kappa^2}{2} \right) \quad (3.4)$$

Following two equations (3.5) and (3.6) hold true by definition of differentiation, since the distance ds is infinitesimal.

$$\frac{dx}{ds} = \cos \theta \quad (3.5)$$

$$\frac{dy}{ds} = \sin \theta \quad (3.6)$$

Inserting equations (3.4) and (3.6) into the left and right hand sides of the equation (3.3) respectively, one can get:

$$\frac{d}{d\theta} \left(\frac{\kappa^2}{2} \right) = -\frac{F}{EI} \sin \theta \quad (3.7)$$

By separating the variables and integrating with respect to θ , equation becomes:

$$\frac{\kappa^2}{2} = \frac{F}{EI} \cos \theta + C \quad (3.8)$$

Integration constant C can then be evaluated by using the boundary condition at the end, i.e. at the pinned connection there is no internal moment. Using this condition, equation (3.1) can be rewritten as:

$$\kappa_{\theta=\theta_0} = \frac{1}{R_0} \quad (3.9)$$

Inserting this condition into equation (3.8), integration constant C can be evaluated as in equation (3.10). Using equation (3.10), in equation (3.8), the relation that gives the curvature κ , can be obtained as in equation (3.11).

$$C = \frac{1}{2R_0^2} - \frac{F}{EI} \cos \theta_0 \quad (3.10)$$

$$\kappa = \frac{d\theta}{ds} = \sqrt{\frac{2F}{EI} (\cos \theta - \cos \theta_0) + \frac{1}{R_0^2}} \quad (3.11)$$

For the equation (3.11) to be solved, substitution of some parameters is necessary. Following three equations, (3.12) to (3.14) give the corresponding relations.

$$\kappa_0 = \frac{L}{R_0} \quad (3.12)$$

$$\alpha^2 = \frac{FL^2}{EI} \quad (3.13)$$

$$\lambda = \frac{\kappa_0^2}{2\alpha^2} - \cos \theta_0 \quad (3.14)$$

Where κ_0 is the non-dimensionalized curvature at the free end and α^2 is the non-dimensionalized load factor. λ is a parameter in order to transform accordingly. Changing the parameters as described in the previous three equations, equation (3.11) becomes:

$$\frac{d\theta}{ds} = \frac{\sqrt{2}\alpha}{L} \sqrt{\lambda + \cos \theta} \quad (3.15)$$

Separating the variables and integrating, one can get:

$$\alpha = \frac{1}{\sqrt{2}} \int_0^{\theta_0} \frac{d\theta}{\sqrt{\lambda + \cos \theta}} \quad (3.16)$$

Equation (3.16) resembles the form of an elliptic integral. Incomplete elliptic integral of the first kind is defined as the following:

$$F(\varphi, k) = \int_0^{\varphi} \frac{d\theta}{\sqrt{1 - k^2 \sin^2 \theta}} \quad (3.17)$$

Where ϕ is defined as the amplitude and k is the modulus of the integral.

One more time, some change of parameters is necessary. Following four equations, (3.18) to (3.21) are the required relations for the substitutions.

$$\beta = \frac{\theta_0}{2} \quad (3.18)$$

$$t = \frac{2}{\sqrt{\lambda+1}} \quad (3.19)$$

$$\Psi = a \sin \sqrt{\frac{1-\cos\theta_0}{\lambda+1}} \quad (3.20)$$

$$r = a \sin \sqrt{\frac{\lambda+1}{2}} \quad (3.21)$$

Substituting the aforementioned intermediate parameters, following relations can be written for α :

$$\alpha = \begin{cases} tF(\beta, t) & \text{for } \lambda > 1 \\ F(\Psi, r) & \text{for } |\lambda| < 1 \end{cases} \quad (3.22)$$

Following two constrains are required for each interval, in order to ensure the validity of equation (3.22).

$$0 < \theta_0 < \pi \quad \text{for } \lambda > 1 \quad (3.23)$$

$$0 < \theta_0 < \arccos(-\lambda) \quad \text{for } |\lambda| < 1 \quad (3.24)$$

Although not straightforward, a solution for the load factor becomes available. It requires the evaluation of the corresponding elliptic integrals. A numerical process named “Landen Scale of Increasing Amplitudes”, that converges to the solution rather quickly, is described in Appendix-A. Also in Appendix-B, a VBA code is presented to solve for the integrals using that method.

Now that α is known, calculations will be directed to solve for a and b. Inserting equation (3.5) into equation (3.1), one can get:

$$\kappa = \frac{d\theta}{ds} = \frac{d\theta}{dx} \frac{dx}{ds} = \frac{d\theta}{dx} \cos \theta \quad (3.25)$$

Now using the previous equation in equation (3.15), it can be written that:

$$\frac{d\theta}{dx} \cos \theta = \frac{\sqrt{2}}{L} \sqrt{\lambda + \cos \theta} \quad (3.26)$$

Separating the variables and integrating result in the following relation of the horizontal distance of the pin joint, a:

$$\frac{a}{L} = \frac{1}{\sqrt{2}\alpha} \int_0^{\theta_0} \frac{\cos \theta d\theta}{\sqrt{\lambda + \cos \theta}} \quad (3.27)$$

Equation (3.27) does not have an elementary solution hence it must be converted into another form. It involves two types of elliptic integrals that are; “Incomplete Elliptic Integral of the First Kind” that is shown in equation (3.17) and “Incomplete Elliptic Integral of the Second Kind” that is described as follows:

$$E(\varphi, k) = \int_0^\varphi \sqrt{1 - k^2 \sin^2 \theta} \quad (3.28)$$

Using the described elliptic integrals, equation (3.27) can be manipulated to get a form that is possible to evaluate:

$$\frac{a}{L} = \begin{cases} \frac{1}{\alpha t} [(t^2 - 2) F(\beta, t) + 2E(\beta, t)] & \text{for } \lambda > 1 \\ 2E(\Psi, r) - F(\Psi, r) & \text{for } |\lambda| < 1 \end{cases} \quad (3.29)$$

For equation (3.29) to be valid, following four constraints, that are the equations (3.30) to (3.33), must be satisfied.

$$\alpha \neq 0 \quad (3.30)$$

$$\lambda > -1 \quad (3.31)$$

$$0 < \theta_0 < \pi \quad \text{for } \lambda > 1 \quad (3.32)$$

$$0 < \theta_0 < \text{acos}(-\lambda) \quad \text{for } |\lambda| < 1 \quad (3.33)$$

Evaluation of b , vertical component of the pin joint, is rather simple. It begins by inserting equation (3.6) into equation (3.1) and manipulating:

$$\kappa = \frac{d\theta}{ds} = \frac{d\theta}{dy} \frac{dy}{ds} = \frac{d\theta}{dy} \sin \theta \quad (3.34)$$

Equating the right hand side of the equation (3.34) with the left hand side of the equation (3.15), it is possible to write:

$$\frac{d\theta}{dy} \sin \theta = \frac{\sqrt{2}\alpha}{L} \sqrt{\lambda + \cos \theta} \quad (3.35)$$

Separating the variables and integrating result in the following relation:

$$\frac{b}{L} = \frac{1}{\sqrt{2}\alpha} \int_0^{\theta_0} \frac{\sin \theta d\theta}{\sqrt{\lambda + \cos \theta}} \quad (3.36)$$

Following equation can be obtained by using integration by substitution.

$$\frac{b}{L} = \frac{\sqrt{2}}{\alpha} \sqrt{(\lambda + 1)} - \sqrt{(\lambda + \cos \theta_0)} \quad (3.37)$$

Again some conditions must be satisfied in order to ensure the validity of equation (3.37). These constrains are defined by the following two equations, (3.38) and (3.39).

$$\alpha \neq 0 \quad (3.38)$$

$$\lambda > -\cos \theta_0 \quad (3.39)$$

Using equations (3.29) and (3.37) the path of the pin joint at the tip, can be sketched for different κ_0 values (Figure 3-5). This path illustrates the deflection characteristics of any FBPP segment clearly.

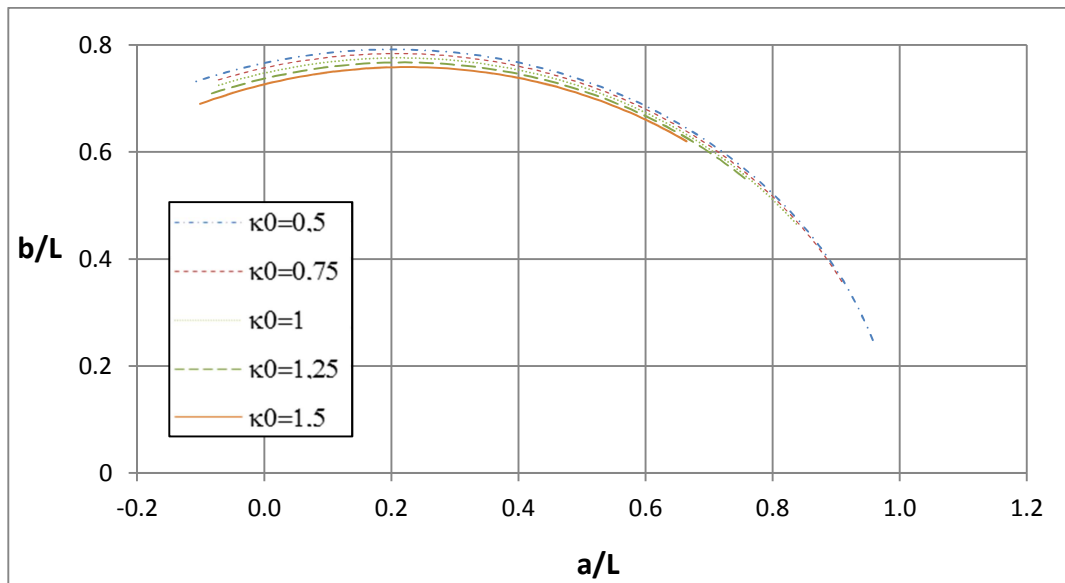


Figure 3-5: Non-Dimensional Pin Joint Paths at Different Curvatures

3.3 PRBM Analysis of the FBFP Half-Model of FBPP Segment

Complicated calculations for determining the pin joint path throughout the deflection can be eliminated by modeling the segment as its pseudo rigid body model (PRBM). One can notice that the shape of the path given in

Figure 3-5 resembles a circular arc; that is the starting point of building the model.

Edwards et al. modeled the segment as two rigid links connected with a torsional spring between them (Figure 3-6). Fixed link is forced to be directed through the x-axis and the second link is subjected to rotate with the applied force at the tip. To evaluate the link lengths they used an optimization procedure. Golden Section Method is carried out for the maximization of the allowable rotation amount of the second link, subjected to a predefined maximum relative error constraint [28].

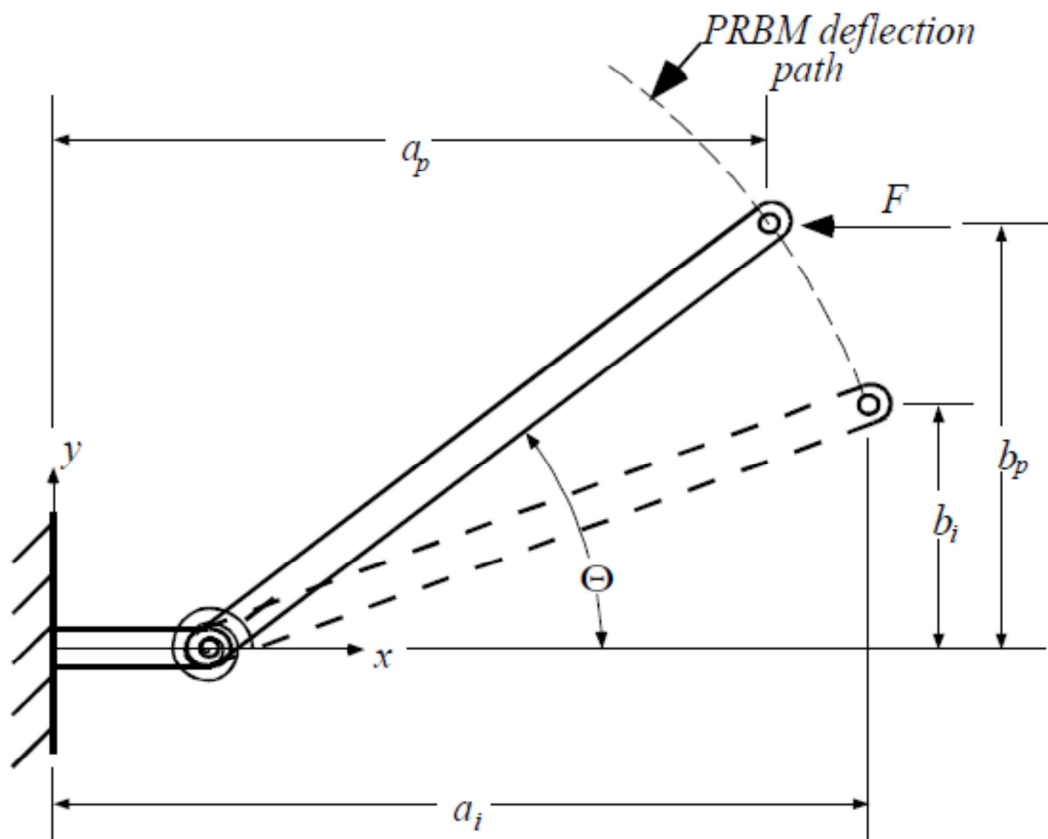


Figure 3-6: PRBM of the FBFP Segment Constructed by Golden Section Method [28]

A new method is proposed for the link length determination. The idea is based on relaxing the constraint that the fixed link must be on the x-axis and determining the link lengths by fitting a circular arc to the path of the pin joint. Resulting PRBM resembles the current one but a little bit different (Figure 3-7).

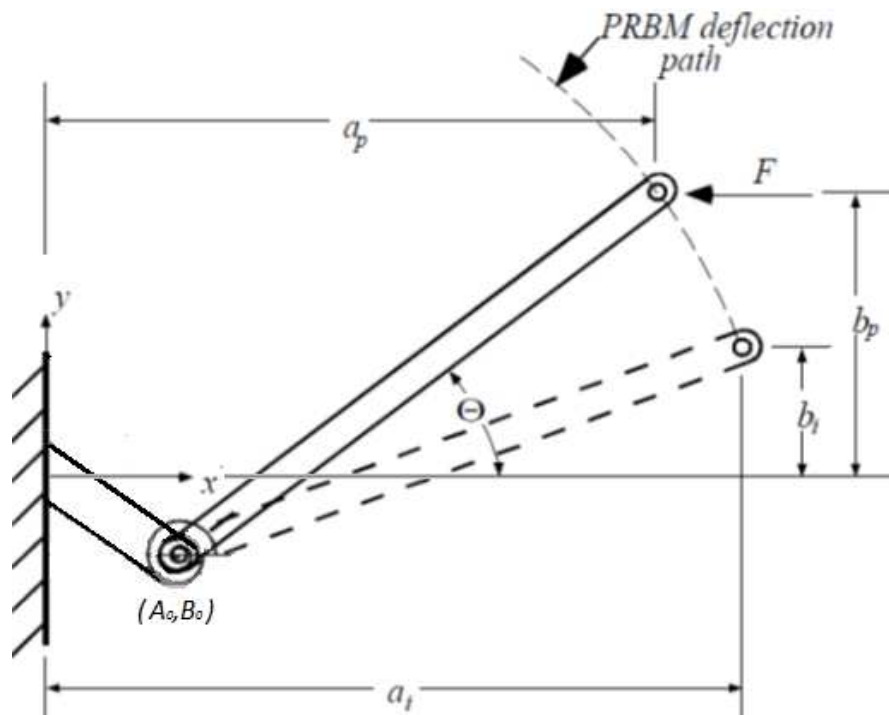


Figure 3-7: PRBM of the FBFP Segment Constructed by Arc Fitting Method

The PRB angle (Θ) and its initial value can then be computed from following relations:

$$\Theta = \tan^{-1} \left(\frac{\frac{b - B_0}{L} - \frac{L}{a - A_0}}{\frac{L}{L} - \frac{L}{L}} \right) \quad (3.40)$$

$$\Theta_i = \tan^{-1} \left(\frac{\frac{b_i - B_0}{L} - \frac{L}{L}}{\frac{a_i - A_0}{L} - \frac{L}{L}} \right) \quad (3.41)$$

Before starting the arc fitting method, the path of the pin joint is located from the exact elliptic integral solution. Thus as long as the center point (A_0, B_0) and the radius (R) of the arc is evaluated, the process will be accomplished. For the evaluation, least squares method will be utilized over the function F , such that:

$$F = \sum_{i=1}^n d_i^2 \quad (3.42)$$

Where F is the objective function to be minimized and d_i is the geometric distance from the data point to the hypothetical arc. d_i can then be evaluated as such:

$$d_i = \sqrt{(x_i - A_0)^2 + (y_i - B_0)^2} - R \quad (3.43)$$

Where x_i and y_i are horizontal and vertical coordinates of the data points and A_0 and B_0 are the horizontal and vertical coordinates of the hypothetical arc, respectively. R is the radius of the same arc.

In order to reduce the number of variables in the objective function, R must be eliminated from the expression. This step is necessary in order to decrease the calculation time in numerical evaluation process and increase

the possibility of convergence. Also the examination of the function behavior is rather easy since it has two variables which can be sketched on a 3-D plot [29]. To eliminate R, it will be written in a form that suggests R is the arithmetic mean of all the individual radii corresponding to each data point.

$$R = \frac{1}{n} \sum_{i=1}^n \sqrt{(x_i - A_o)^2 + (y_i - B_o)^2} \quad (3.44)$$

Hence, by inserting equation (3.42) into equation (3.41) and plug the result into equation (3.40) the objective function will be as follows:

$$F = \left\{ \sqrt{(x_i - A_o)^2 + (y_i - B_o)^2} - \frac{1}{n} \sum_{j=1}^n \sqrt{(x_j - A_o)^2 + (y_j - B_o)^2} \right\}^2 \quad (3.45)$$

Now the minimization of the objective function will be taken care of. To accomplish the process three most successful and common methods will be evaluated [30]:

- ✓ Levenberg-Marquardt method [31]
- ✓ Landau algorithm [32]
- ✓ Späth algorithm [33, 34]

Levenberg-Marquardt method is known to be stable, reliable and rapidly converging. Landau algorithm is very stable but converging rather slow.

Theoretically Späth algorithm is converging to the solution certainly but it also has a slow rate of convergence.

As a result, Levenberg-Marquardt method will be utilized during iterative calculations. A software program (MATHCAD 14 ®) that is capable of using that method for iterative processes is used. Plugging in the coordinates of the data points (elliptic integral solution outputs for the end pin joint coordinates) the result is taken as the center point coordinates (A_0, B_0) and the radius (R) of the arc. Related software snapshot samples are provided in Appendix-C.

According to comparative analysis of the results a table summarizing the related values is presented in Table 3-1. Corresponding values acquired by the method described in [28] is also given in Table 3-2. The data ranges are directly taken from Table-1 of [28] in order to eliminate the mismatch resulting from calculation interval.

Table 3-1: Radius and the Center Coordinates of the Fitted Arc for Different Curvature Values

κ_0	ρ	A_0	B_0
0.50	0.79784	0.20152	-0.00554
0.75	0.79132	0.20670	-0.00696
1.00	0.78639	0.21121	-0.01015
1.25	0.78163	0.21614	-0.01390
1.50	0.77745	0.22171	-0.01862

Table 3-2: Radius and x-Coordinate of the Arc Path Acquired by Golden Section Method [28]

κ_0	ρ	γ	A_0
0.50	0.79076	0.79305	0.20695
0.75	0.78289	0.78753	0.21248
1.00	0.77559	0.78320	0.21680
1.25	0.76781	0.77888	0.22113
1.50	0.75960	0.77455	0.22545

Since the link lengths of the PRBM of the segment are known, the remaining work is to determine the spring constant of the torsional spring between two links. The procedure is straightforward; relation between the PRB angle difference ($\Delta\Theta$) and tangential non-dimensionalized load factor (α_t^2) will be evaluated. These terms are defined as:

$$\Delta\Theta = \Theta - \Theta_i \quad (3.46)$$

$$\alpha_t^2 = \alpha^2 \sin\Theta \quad (3.47)$$

Tangential non-dimensionalized load factor (α_t^2) stands for the only force that crates moment on the torsional spring hence its value is that matters. The related values are evaluated and the relations are interpreted to be appropriate to be approximated by a polynomial of the 2nd degree as described on equation (3.46) as:

$$\alpha_t^2 = K_{\Theta 1} \Delta\Theta + K_{\Theta 2} (\Delta\Theta)^2 \quad (3.48)$$

The values of the coefficients that describe the spring stiffness are tabulated on Table 3-3 and Table 3-4 for both methods. The graphs of the related force-deflection characteristics are given in Appendix-D and one of them that is obtained by arc fitting method, with $\kappa_0=1$, is given as an example on Figure 3-8.

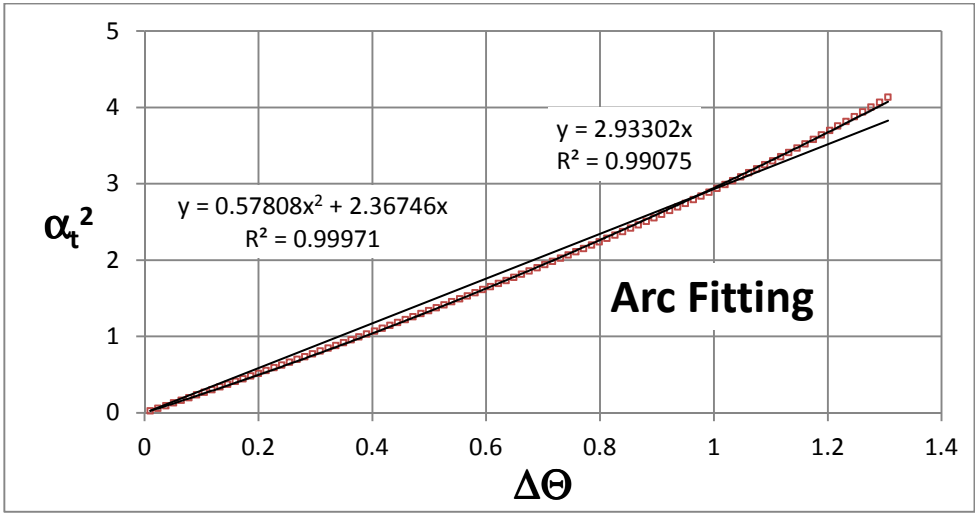


Figure 3-8: Force (Non-dimensionalized Load Factor [α_t^2]) – Deflection (Pseudo-Rigid-Body Angle Difference [$\Delta\Theta$]) Characteristics for $\kappa_0=1$ Obtained by Arc Fitting Method

Table 3-3: Spring Stiffness Coefficients for the Golden Section Method

$K_{\theta 1}$	$K_{\theta 2}$	r^2
2,24	0,45	0,99999
2,30	0,48	0,99977
2,34	0,55	0,99980
2,40	0,63	0,99984
2,48	0,72	0,99987

Table 3-4: Spring Stiffness Coefficients for the Arc Fitting Method

$K_{\theta 1}$	$K_{\theta 2}$	r^2
2,25	0,47	0,99949
2,32	0,50	0,99969
2,37	0,58	0,99971
2,44	0,67	0,99975
2,53	0,79	0,99979

Correlation coefficients (r^2) of the preceding tables imply that 2nd order polynomial fitting is quite accurate and applicable.

3.4 Comparison and Evaluation of the Models

The motivation behind the study of a new method to describe the deflection characteristics of FBPP segments is based on this specific application. The current model developed by Edwards et al. is quite suitable for the practical applications where the purpose is to analyze an available mechanism or to design the mechanism in the provided interval of motion. As the $\Delta\theta$ value increases, error introduced is also increased. The purpose is to provide a method that optimizes the path approximation for a fixed tip angle rotation ($\Delta\theta_0$). If $\Delta\theta_0$ is constant over the design phase then the arc fitting method provides the optimum PRBM giving the opportunity to ignore the error caused by neglecting the complex deflection characteristics. For instance, in this application $\Delta\theta_0$ is kept on the value of 45° . Corresponding error values for $\kappa_0=1$ is given as an example on Figure 3-9. For remaining curvature values corresponding error distributions are provided in Appendix-E.

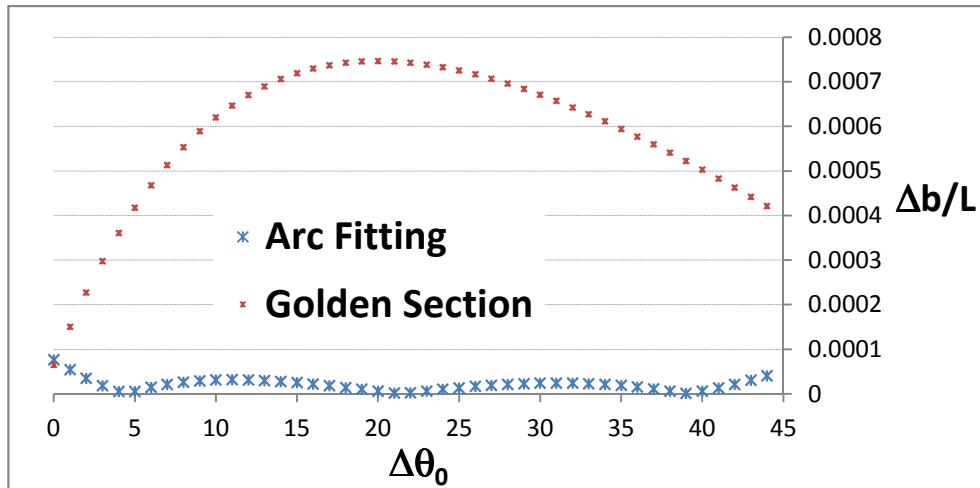


Figure 3-9: Error Comparison for $\Delta\theta_0=45^\circ$ and $\kappa_0=1$

Golden section method introduces an application range that may or may not be suitable for a specific application. As the required rotation amount gets far (lower or higher) away from provided, error of the model gets much more increased. The application ranges are illustrated on Figure 3-10. For arc fitting method on the other hand, if the design requirement on the tip rotation is known, the optimum path approximation can be achieved. One must go through the exact calculation steps for once, and then utilize the coefficients obtained, on further design stages. The disadvantage is obviously the need for the exact solution to be carried out for one time that is considered to be a necessary effort if the error minimization is critical.

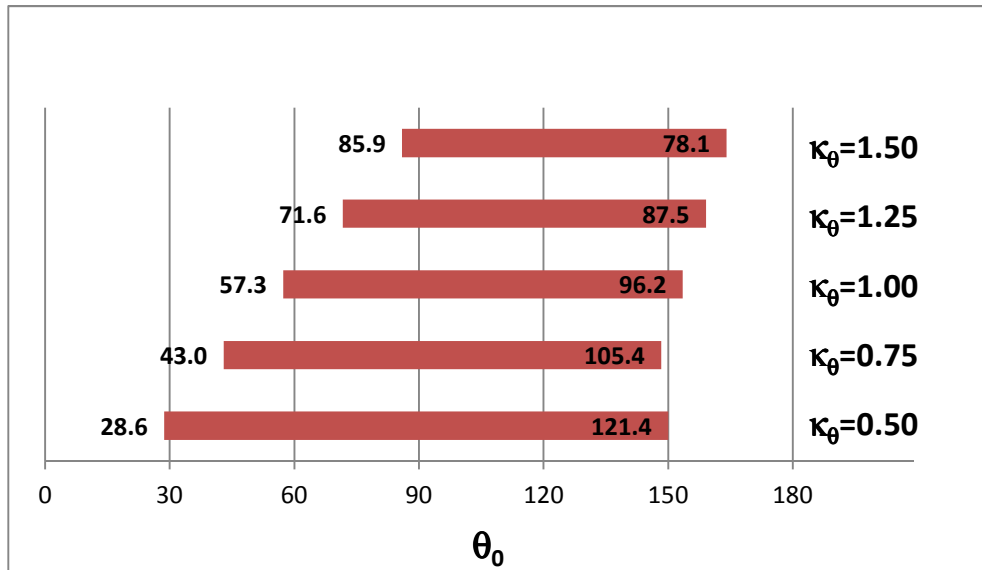


Figure 3-10: θ_0 Range (in degrees) for the Validity of Golden Section Method

3.5 PRBM Analysis of the Whole Binary Segment

The designed full mechanism is composed of two segments, each having two half segments. These half segments are modeled as two-linked parts which are interconnected with torsional springs. Each segment is joined to the other and to ground by pin joints. The pin joint at the middle is the area where the input force is applied. It will be locking or unlocking force depending on the situation. Mentioned full model can be seen on Figure 3-11 as a sketch.

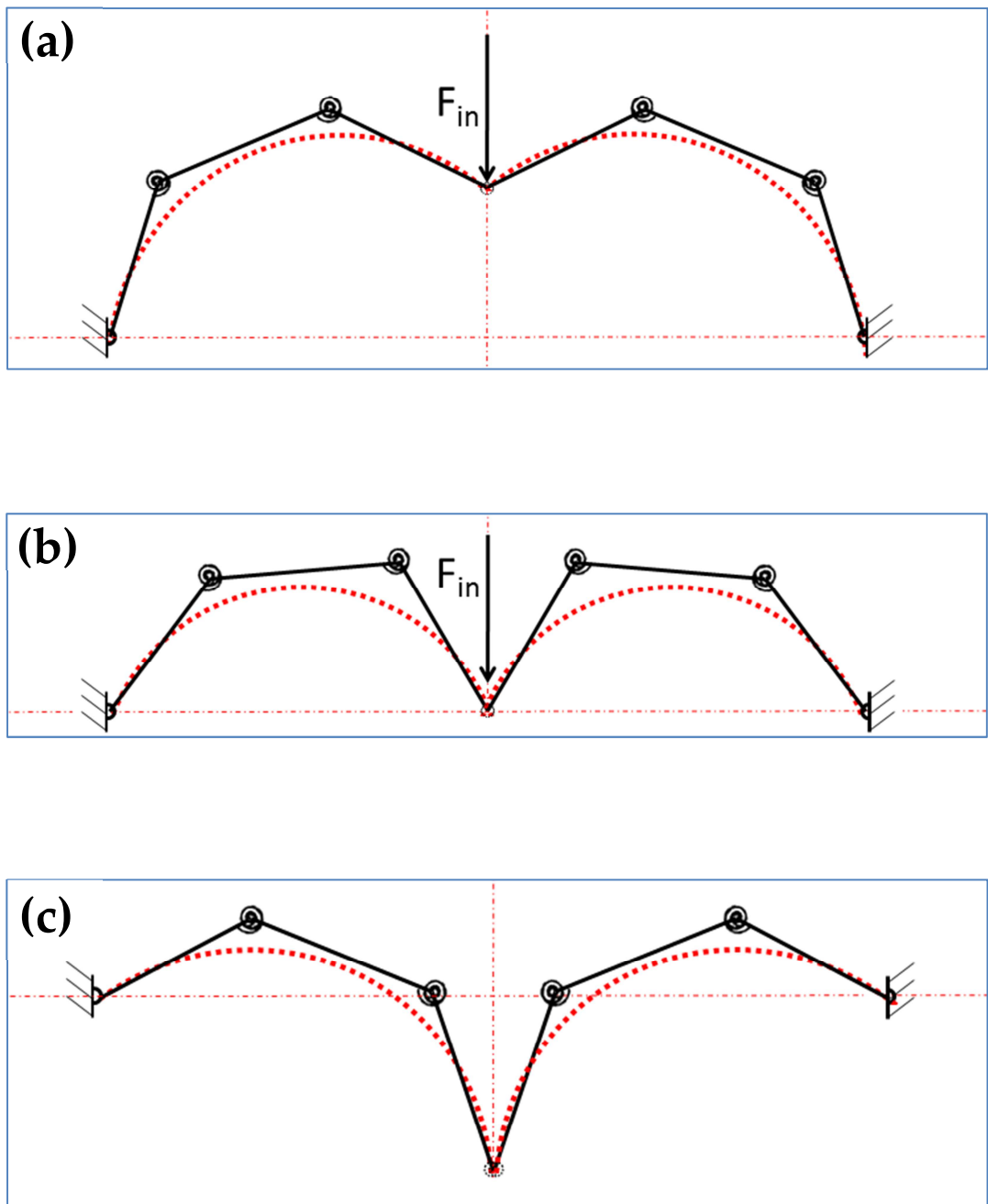


Figure 3-11: PRBM of the Whole System: (a) 1st Stable Position, (b) Unstable Position, (c) 2nd Stable Position

3.6 Conclusion

On the first subchapter, the definitions of functionally binary pinned-pinned (FBPP) segments and its functionally binary fixed-pinned (FBFP) half model were presented.

Starting with the Bernoulli-Euler equation one can carry out the calculation steps and finalize the exact solution by solving elliptic integrals for the determination of the deflection characteristics of the described FBPP segment. The process was presented on the second subchapter of this chapter. Nevertheless, the process is quite complicated and not suitable for trial and error manipulation. Rather if the PRBM is used as a middle step, the design stages can be made easily and parametrically. These steps were given on the third subchapter.

The proposed method (arc fitting) is a beneficial option for the PRBM construction if the rotation of the tip pin joint is predefined. The method reduces the error (deviation of the tip positions from the actual path) considerably and applicable to any rotation amount by fitting the “best arc” that can be fitted on the path. The disadvantage is that one must carry out the exact calculation steps at least once for a specific rotation amount. Comparison of the “golden section” and “arc fitting” methods for PRBM construction was provided on the fourth subchapter

After getting a suitable PRBM of the mechanism parametrically (link lengths and spring constants in terms of input parameters), one can easily move further calculation steps to achieve the final shape design. The design parameters will be used as constraints on the PRBM relations and the final model will be constructed based on manufacturing and physical limitations. The PRBM of the whole mechanism (presented on the 5th subchapter) can be used to analyze the designed mechanism to be certain.

CHAPTER 4

DESIGN OF THE LOCKING MECHANISM

4.1 Introduction

The aim of the design stages is generally to come up with a solution that safely accomplishes the design requirements. These requirements (technical specifications of the company) can be counted as follows:

- Locking and unlocking forces (50N [+20/-10]) are determined beforehand by the safety regulations and should not vary from the nominal value beyond tolerances.
- The solution must be feasible in order to be attainable in real life. For that reason the mechanism must be compact and for practical reasons it better be suitable for injection-molding.
- The safety of the lock mechanism is of high importance. It means that, life (50.000 cycles) and strength must be considered precisely.

4.2 Description of the Design Space and Physical Constraints

The design space that can be used to place the mechanism is shown in Figure 4-1. The off-plane distance (height of the mechanism, p) is 23mm. at maximum.

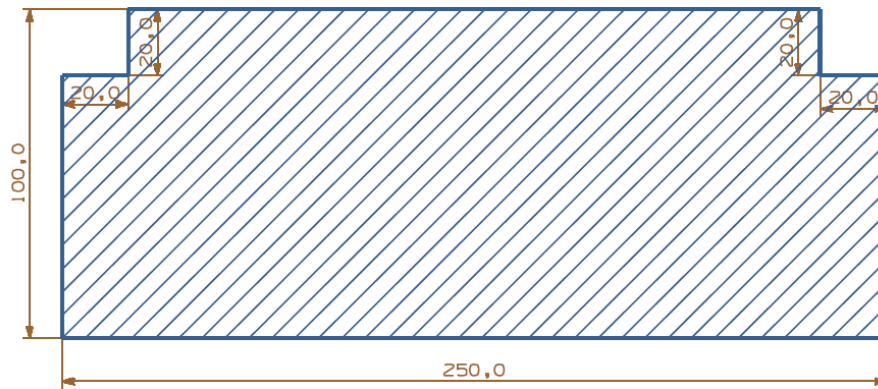


Figure 4-1: Design Space for Installation

Since the part will be injection molded, wall thickness (h) cannot exceed a maximum value (varies depending on the material) and it must be constant. Length of the mechanism must be of reasonable size for practical reasons such as transportation, handling and storing considerations.

Rotation of the pin joint ($\Delta\theta_0$) must be high enough to grasp the locking element and low enough to enable the releasing. It has been selected as 45° . This free parameter is picked as an application example but it can take other values that satisfy mentioned limitations.

4.3 Segment Profile Design

The aim of this subchapter is to give the procedure to determine the height of the segment (p) for the given forcing and physical constraints. First of all, general sketch of the mechanism is given on Figure 4-2. Estimated initial position of the segments (a) and an intermediate position of one segment (b) are illustrated parametrically. Final position is just the rotated shape of the initial position (they are both stable positions of the segment). The

length of each half-segment is called L and the full length of the mechanism (including both segments) refers to L' . Hence L' is 4 times L . ζ is the angle of connection (the value that defines the connection of the two segments), F_{in} is the input force and F_{each} is the force component that effects each one of the segments. As indicated in the figure, the angle ω that determines the rotation amount of the segment takes the value " $\Delta\theta_0/2$ " in the beginning. Then it decreases and at the unstable equilibrium position it becomes zero. Its final value is the negative of initial one, namely " $-\Delta\theta_0/2$ ".

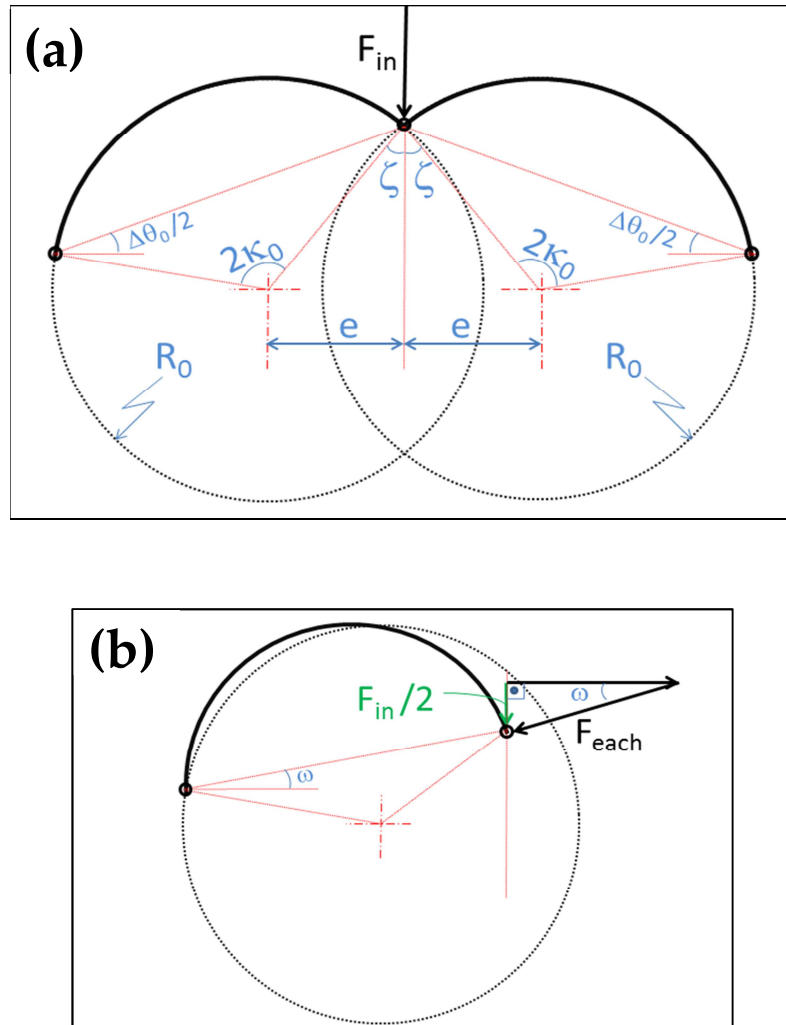


Figure 4-2: (a) Estimated Initial Position of Both Segments (Symmetrical),
 (b) Estimated Intermediate Position of the Left Segment

ζ and F_{each} that are seen on Figure 4-2 can be evaluated geometrically as:

$$\zeta = \kappa_0 - \frac{\Delta\Theta_0}{2} \quad (4.1)$$

$$F_{in} = \frac{2 F_{each}}{\sin(\omega)} \quad (4.2)$$

ζ only changes with the change of curvature. But F_{each} must be calculated throughout the deflection. To analyze the deflection characteristics, some more parameters are required which are illustrated on Figure 4-3. a' is the distance between two pin joints. The change in that value determines the deflection amount on the segment. d is the vertical displacement of the middle pin joint.

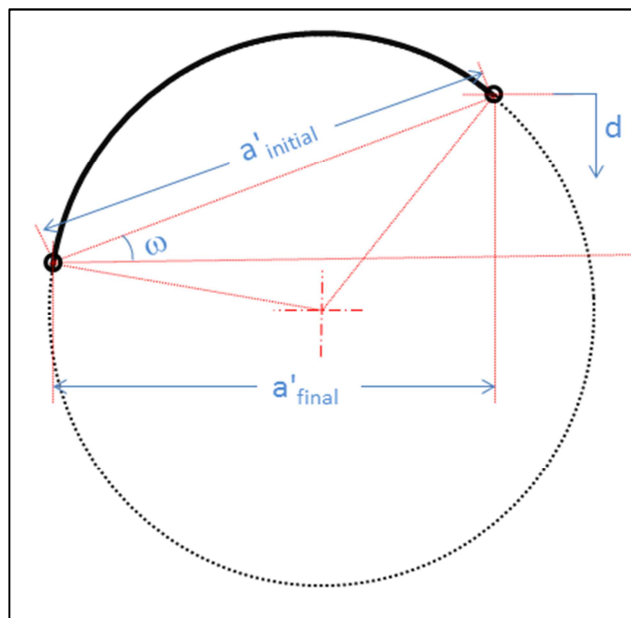


Figure 4-3: Illustration of the Parameters that Define Deflection Characteristics

Now, from the difference of the initial and final distances between pin joints, PRB angle difference ($\Delta\Theta$) must be calculated. The method will be based on geometry. The difference between the lengths a'_{initial} and a'_{final} is simply the total horizontal displacement of the tip. Hence the single half segment horizontal end displacement (Δx) is equal to the half of that distance. Accordingly, following relation can be obtained from the geometry on Figure 4-4.

$$\Theta = \cos^{-1} \left(\frac{r \cdot \cos \Theta_i - \Delta x}{r} \right) \quad (4.3)$$

$$\Theta = \cos^{-1} \left(\cos \Theta_i - \frac{1}{\rho} \cdot \frac{\Delta x}{L} \right) \quad (4.4)$$

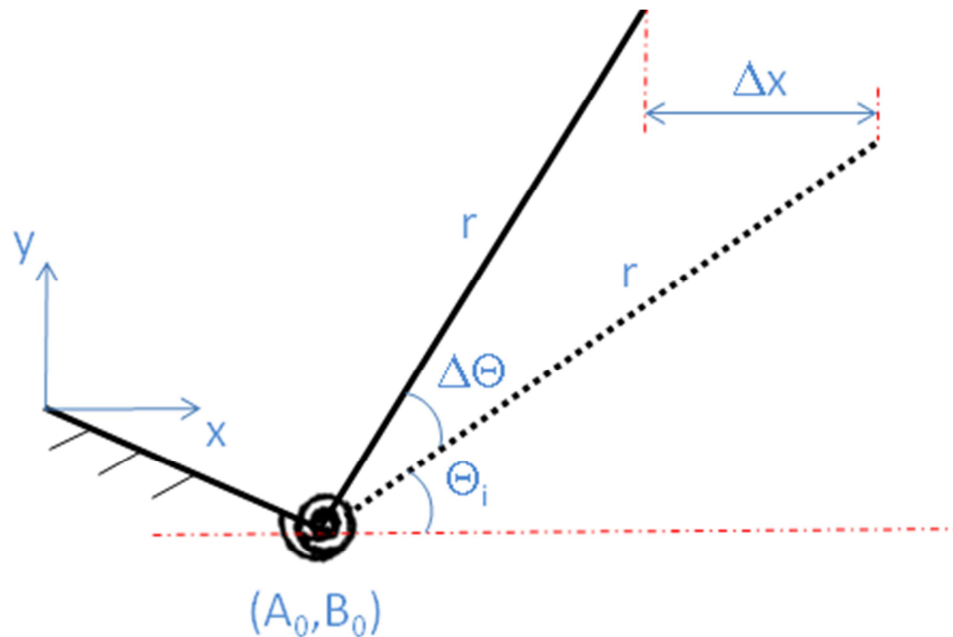


Figure 4-4: Initial and Final Positions of the PRBM of the Half-Segment

Finally, from the specified $\Delta\Theta$, thickness of the segments will be determined. Procedure is rather straightforward. Equation (3.40) gives Θ_i , summation of Θ_i and $\Delta\Theta$ gives Θ . Tangential non-dimensionalized load factor (α^2) can be calculated from calculated spring coefficients ($K_{\Theta 1}$ and $K_{\Theta 2}$) and PRB angle difference ($\Delta\Theta$) using equation (3.47). To sum up, following equations (4.5) and (4.6) are to be used;

$$\Theta = \Theta_i + \Delta\Theta \quad (4.5)$$

$$\alpha^2 = [K_{\Theta 1}\Delta\Theta + K_{\Theta 2}(\Delta\Theta)^2] \cdot \frac{1}{\sin \Theta} \quad (4.6)$$

Assuming a wall thickness of h and height p , the moment of inertia of the cross-sectional area (I) can be computed as:

$$I = \frac{1}{12}ph^3 \quad (4.7)$$

To get moment of inertia (I) from α^2 , equation (3.13) is rewritten as:

$$I = \frac{F_{each}L^2}{E\alpha^2} \quad (4.8)$$

Once I is known, height (p) can be evaluated for any thickness (h), from the following relation:

$$p = 12\frac{I}{h^3} \quad (4.9)$$

4.4 Replacement of the Pin Joints with Living Hinges [35]

The purpose is to discuss the replacement of the pin joints with living hinges; then the mechanism may be monolithic. The stress levels will be compared with the yield point. The replacement methods will be explained in detail and the possibility of constructing a reliable design will be left to the next sub-chapter at which the design parameters will be clarified.

Living hinges are designed basically by reducing the thickness of the cross section (Figure 4-5). There are many aspects to be taken care of. These will be explained further in this subsection. Since the most critical hinge is the one at the middle, only that one will be analyzed. Others can easily be designed with the same procedure.

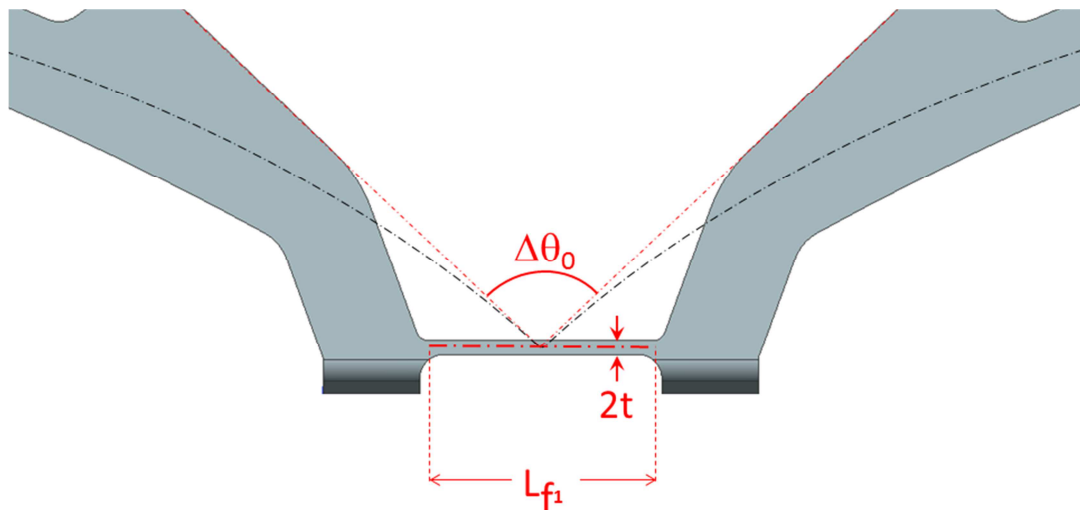


Figure 4-5: Undeflected Shape of the Living Hinge

First of all, the sharp edges must be removed to eliminate stress concentration effects. Larger radius must be used on the back side (opposite side of the rotation path) to let the material deflect without plastic deformation. Secondly, the recess left on the top of the hinge is critical. It is designed as such in order to give space between two sides at the folded position. Otherwise there would be a notch at the bottom tip that will create concentrated stress (Figure 4-6).

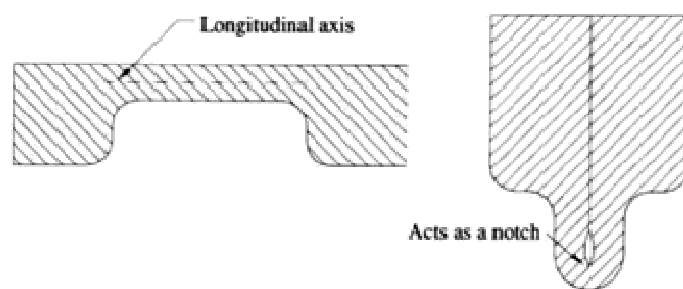


Figure 4-6: An Example of the Wrong Designed Living Hinge without Leaving Recess

The parameters as thickness ($2t$), recess or radii on different corners are provided roughly in literature [35]. The design parameter to be determined is the hinge length (L_{fi}). To evaluate this value some assumptions, that are proven to hold true, are used as:

- The hinge can be approximated by a circle at the folded position.
- The neutral axis of the hinge is assumed to be coincident with the middle section of the circle thickness. In other words, the neutral axis does not drift during deflection.

- Maximum tension occurs in the outermost fibers and the maximum compression occurs in the innermost fibers.
- Maximum tension must be compared with the yield strength of the material in order to get the safety factor of the hinge.

By using the predefined assumptions, one can sketch the deflected shape of the hinge basically as described on Figure 4-7.

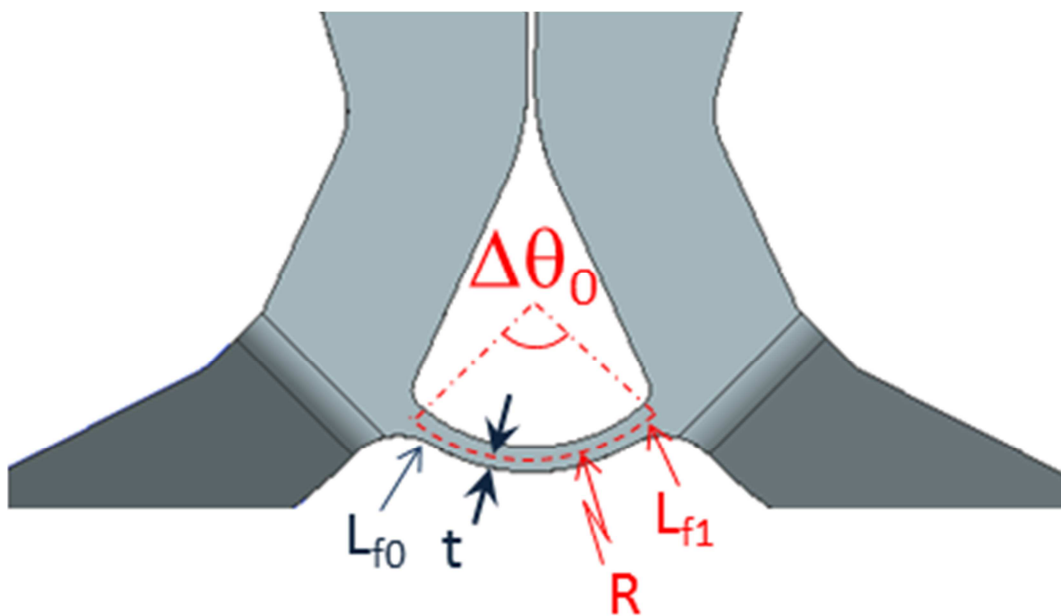


Figure 4-7: Deflected Shape of the Living Hinge

To determine the length of the hinge (L_{f1}), these steps will be carried out.

$$L_{f1} = \frac{\pi R}{2} \quad (4.10)$$

$$L_{f0} = \frac{\pi(R+t)}{2} \quad (4.11)$$

Bending strain on the outer fibers is as follows:

$$\varepsilon_{bending} = \frac{(L_{f0} - L_{f1})}{L_{f1}} \quad (4.12)$$

Using equations (4.10) and (4.11);

$$\varepsilon_{bending} = \frac{t}{R} \quad (4.13)$$

$$\sigma_{bending} = \frac{E_{sec} t}{R} \quad (4.14)$$

where E_{sec} is the secant modulus of elasticity of the material that is defined as the ratio of yield stress to yield strain. Now that bending stress ($\sigma_{bending}$) has been calculated, axial stress (σ_{axial}) will also be written as:

$$\sigma_{axial} = \frac{F_{each_max}}{2t p} \quad (4.15)$$

Inserting the relation for R, equation (4.10), and combining the previous two equations one can get;

$$\sigma_{total} = \frac{t \pi E_{sec}}{2 L_{f1}} + \frac{F_{each_max}}{2t p} \quad (4.16)$$

Comparing the total stress (σ_{total}) with yield stress of the material (σ_y), and plugging the safety factor (SF), following relation can be used to get the hinge length (L_{f1}):

$$\frac{\sigma_y}{SF} = \frac{t \pi E_{sec}}{2 L_{f1}} + \frac{F_{each_max}}{2t p} \quad (4.17)$$

To analyze the feasibility of flexural hinge replacement procedure, equation (4.17) must be investigated with the corresponding parameters. These parameters will be determined on further sub-chapters, so the decision will be made then.

4.5 Material Selection and Final Shape Design

The shape design of the mechanism will be covered in this subchapter. Starting with the material selection, determination of different parameters in design phases is presented.

Before proceeding with the design, material selection must be made. At least a first estimate must be done to carry on. Material properties to be taken into account in the selection process are elasticity, yield strength, fatigue strength, manufacturability, and cost. Considering these values, different materials are analyzed, some have high yield strength but too stiff, some are elastic but expensive. Final selection was made on the favor of POM (polyoxymethylene). It has high elasticity (low elastic modulus) compared to its yield strength (Appendix-F). It is known that POM has a high flexural fatigue and impact strength. As a first estimate, this relatively

expensive material is chosen due to its improved mechanical properties. In case of high factor of safety values, the material will be replaced with cheaper ones. Some of its mechanical properties are given below:

- Yield Strength: 73MPa
- Yield Strain: 0.12
- Modulus of Elasticity: 3400MPa
- Ultimate Tensile Strength: 80MPa

Further analyses are based on the provided values. $F_{in}=50N$ is provided by the technical specifications of the company and $\Delta\theta_0=45^\circ$ was assumed beforehand. By fixing the $\Delta\theta_0$ value, the shapes become fully defined for each different curvature (κ_0) value. Changing the length (L) only scales the mechanism. Those shapes are illustrated on Figure 4-8.

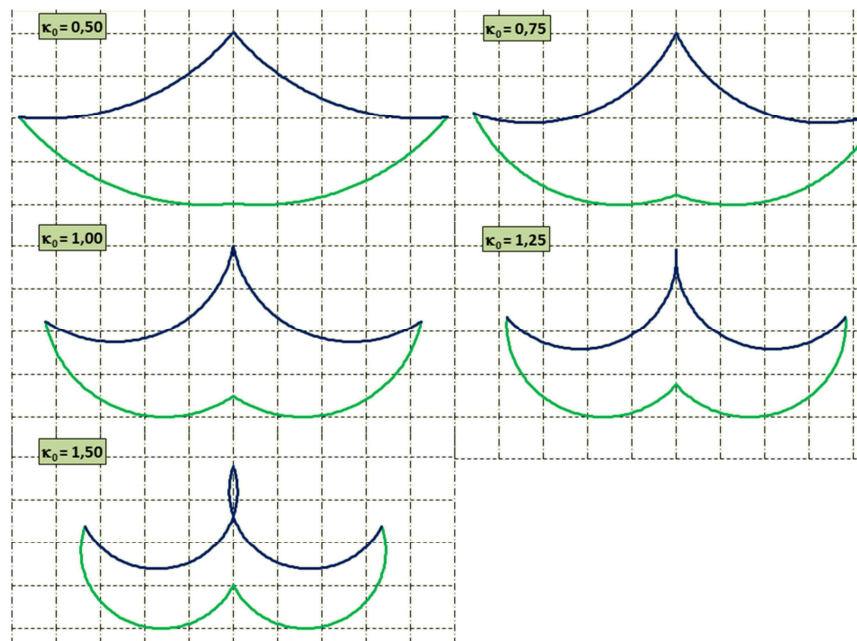


Figure 4-8: Locked (Green) and Unlocked (Blue) Positions of the Mechanism for $\Delta\theta_0=45^\circ$

As one can notice from Figure 4-8, for the curvature values of 1.25 and 1.50 the segment intersects itself in the unlocked position. That can also be seen from the angle of connection (ζ) values. Mechanisms with ζ larger than $\Delta\theta_0$ (45°) are self-intersecting (Table 4-1). Hence the larger curvature that can be selected is 1.

Table 4-1: Angle of Connection (ζ) Values for Each Curvature

κ_0	ζ (deg)
0.50	6.15
0.75	20.47
1.00	34.80
1.25	49.12
1.50	63.44

While choosing the curvature one must keep in mind that for the same thickness and height values, locking force increases with the decreasing curvature. Since the force requirement is quite high for the specific case and there is a limitation on the wall thickness of the material due to the injection molding criteria the curvature of 0.5 will be selected.

Length of the half segment (L) that determines the scale of the mechanism will be chosen as to fit in the design space. By making the mechanism shorter, a compact and stiff system will be obtained. On the other hand, the mechanism must grip the locking part that has a limitation in thickness too. Therefore it is appropriate to choose it as small as possible, considering a reasonable locking part thickness. It is selected as 40mm accordingly.

General wall thickness of the mechanism (h) is chosen considering moldability (for injection molding), elastic deformation capability and

durability. When that value increases elastic deformation becomes harder and moldability decreases. On the other hand, thickening the part stiffens and shortens the mechanism. There is also a height limitation on the design space, that the total height must be smaller than 23mm. By trial and error 3.1mm thickness (h) and 20.5mm height (p) are chosen to be convenient.

The variation of input force (F_{in}), the force on each segment (F_{each}) and potential energy (PE) are illustrated on Figure 4-9. One can easily notice the bistable behavior by inspecting the potential energy change characteristics.

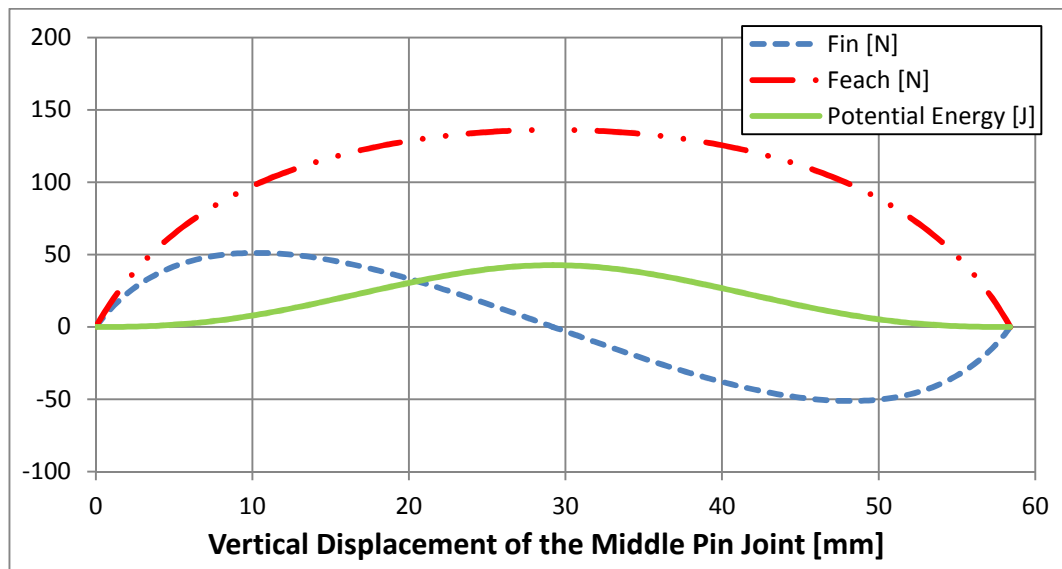


Figure 4-9: Input Force (F_{in}), Force on Each Segment (F_{each}) and Potential Energy Variation along Deflection Path of the 1st Mechanism (POM)

Now that the parameters that describe the shape of the mechanism are obtained (Table 4-2) flexure hinge replacement option will be analyzed.

Table 4-2: Design Parameters of the Mechanism (POM)

Angle of Rotation [deg]	$\Delta\theta_0$	45
Curvature	κ_0	0.50
Angle of Connection [deg]	ζ	6.15
Wall Thickness [mm]	h	3.1
Length of the Mechanism [mm]	L'	160
Total Height [mm]	p	20.5
Max. Force on Each Segment [N]	F_{each_max}	136.2
Locking Force [N]	F_{in_max}	50
Secant Modulus [MPa]	E_{sec}	608.3

Thickness of the living hinge is assumed as a minimum value considering moldability ($2t=0.4mm$) and the safety factor is taken to be small (1.5) to find any possible solution. Length of the living hinge is calculated accordingly using equation (4.10) as;

$$\frac{\sigma_y}{SF} = \frac{t \pi E_{sec}}{2 L_{f1}} + \frac{F_{each_max}}{2t p} \quad (4.18)$$

$$L_{f1} = \left[\left(\frac{\sigma_y}{SF} - \frac{F_{each_max}}{2t p} \right) \frac{2}{t \pi E_{sec}} \right]^{-1} \quad (4.19)$$

Inserting the necessary parameters, hinge length can be found as;

$$L_{f1} \cong 6.0mm \quad (4.20)$$

It must be kept in mind that 3 of these joints will be replaced, meaning that more than 10% of the mechanism will consist of hinge areas. That would distort the force and motion characteristics that was predicted. Considering that situation, length of the hinge is considerably high relative to the total length, although the inputs are chosen at the limits. Thinner hinge thickness, longer segments or lower safety factor values are not possible, because of moldability, force and life requirements respectively. Hence replacement of pin joints with living hinges is not possible for this specific application. However, for lower forces or other production techniques, replacement can be achieved.

One design example will be presented in order to verify the theory. Parameters will be altered for two intentions; decreasing the force requirements and choosing a material capable of rapid prototyping. The material is chosen among available materials considering its flexibility and strength. It is Innov'PA 1550 (Appendix-G). Considering the mechanical properties of this material and other corresponding inputs, design parameters are tabulated in Table 4-3.

Table 4-3: Design Parameters of the Mechanism (Innov'PA)

Angle of Rotation [deg]	$\Delta\theta_0$	45
Curvature	κ_0	1.00
Angle of Connection [deg]	ζ	34.8
Wall Thickness [mm]	h	2.6
Length of the Mechanism [mm]	L	240
Total Height [mm]	p	18.2
Max. Force on Each Segment [N]	$F_{\text{each_max}}$	10.7
Locking Force [N]	$F_{\text{in_max}}$	3.50
Secant Modulus [MPa]	E_{sec}	375

For the changed parameters, the variation of input force (F_{in}), the force on each segment (F_{each}) and the potential energy (PE) are illustrated on Figure 4-10.

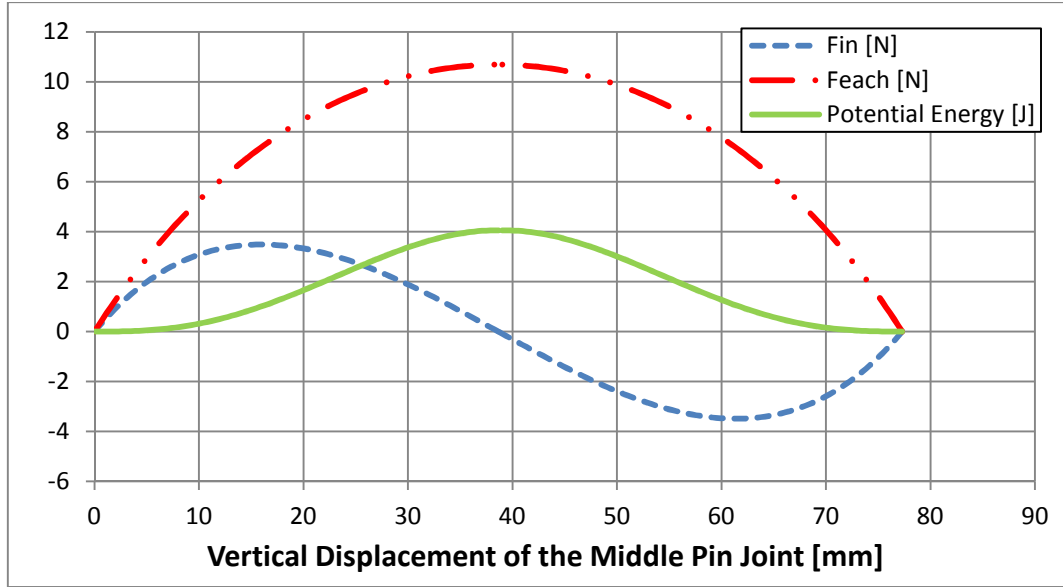


Figure 4-10: Input Force (F_{in}), Force on Each Segment (F_{each}) and Potential Energy Variation along Deflection Path of the 1st Mechanism (Innov'PA)

Inserting new parameters to equation (4.19) the living hinge length comes out to be 4.1mm.

$$L_{f2} \cong 4.1mm \quad (4.21)$$

By decreasing the locking force, the length of the living hinge is decreased. For this situation, total living hinge length is nearly 5% of the mechanism, which is considered acceptable. Hence modeling will be made with the joints replaced by living hinges, as described previously.

Finally the realization of the mechanisms is achievable. The 3-D modeling is made by NX UG 5.0 ® and the design is finalized by drafting the technical drawings. Top and isometric views of the finalized 3-D models (on the locked stable position) can be seen on Figure 4-11 and Figure 4-12.

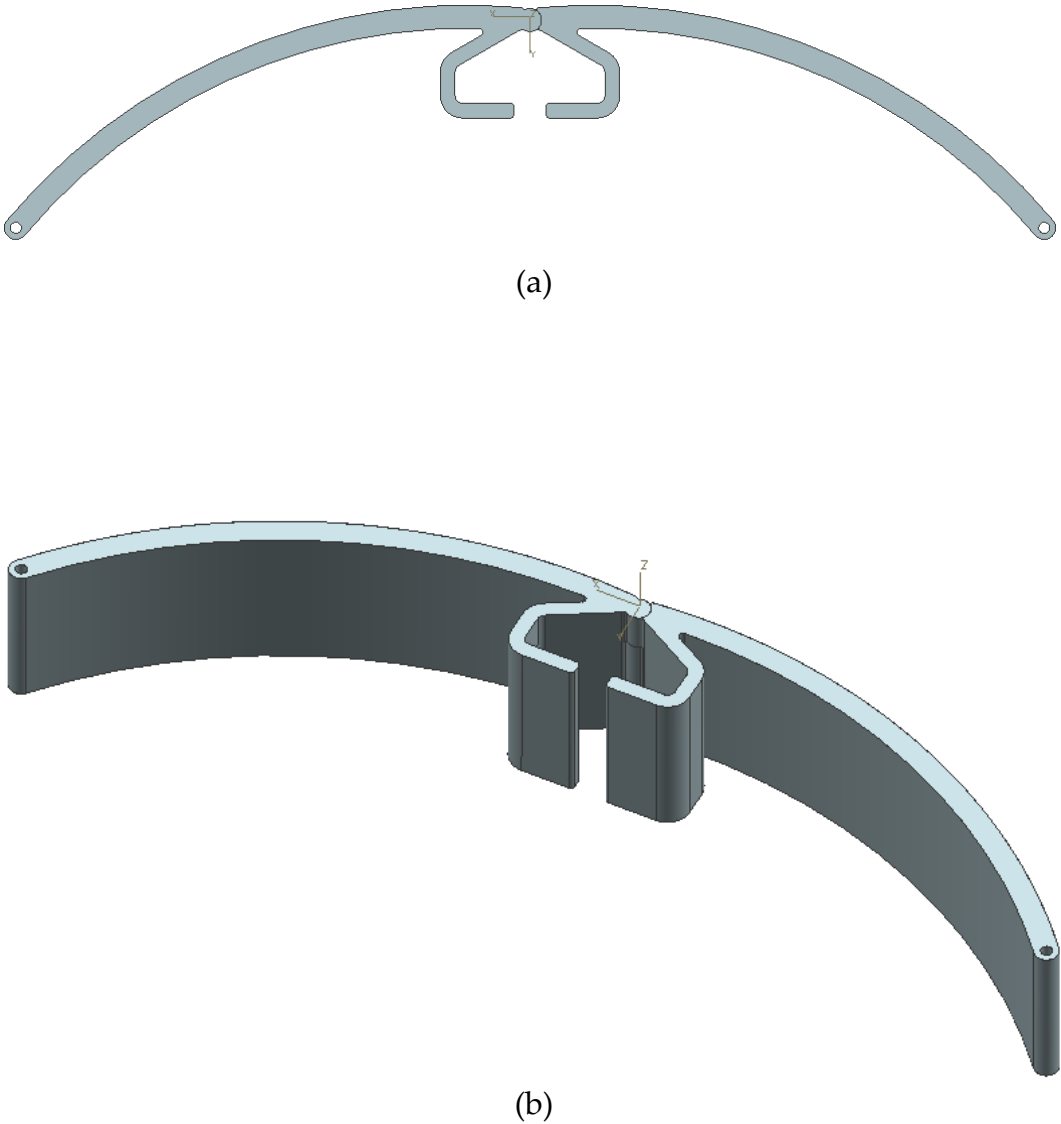
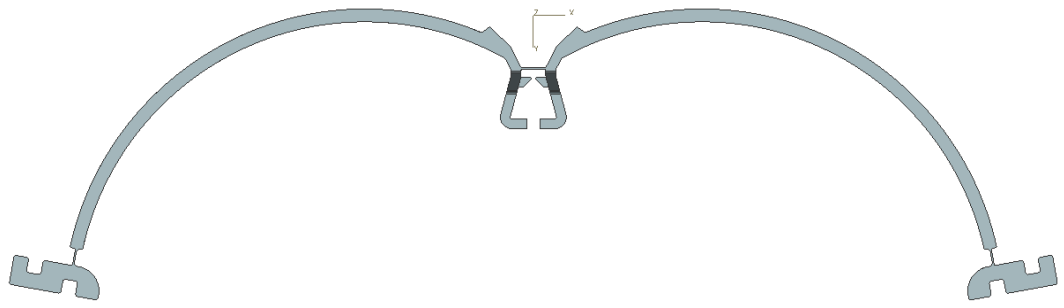
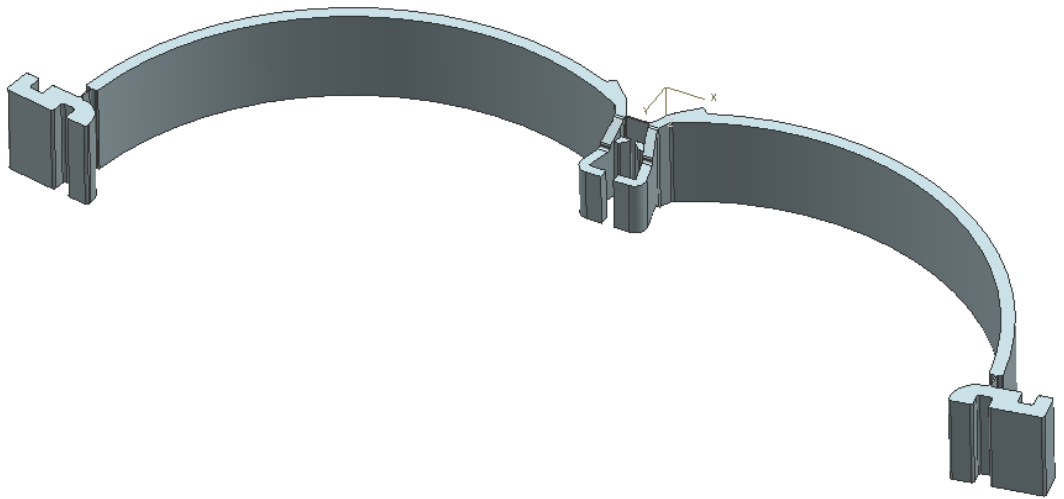


Figure 4-11: Top (a) and Isometric (b) Views of the 1st Mechanism (POM)



(a)



(b)

Figure 4-12: Top (a) and Isometric (b) Views of the 2nd Mechanism (Innov'PA)

4.6 Evaluation and Conclusion

In this chapter; first, the design limitations specified by the company regulations and design space constraints has been described. Then the segment design has developed parametrically as a sketch. The design calculations of the living hinge replacement of the pin joints have been presented next. After that the proper material has been chosen and according to its physical properties and obtained design calculations the final shape has been constructed. Finally the fatigue life estimation of the mechanism has been done.

As a result, the finalized shape of the locking mechanism is developed. It consists of two pieces and suitable for injection molding. It is shown that for this specific forcing, single piece construction (monolithic) is not possible. It is expected to have infinite life and accomplishes the force and strength requirements according to the theoretical calculations. On the next chapter, the validation of these expectations will be made.

CHAPTER 5

FINITE ELEMENT MODEL (FEM) ANALYSIS AND PHYSICAL PROTOTYPE TESTING

5.1 Introduction

So far all the calculations about forcing and deflection characteristics were theoretical. The validation of these calculations is critical before the design is put into practice. For that reason, in this chapter, finite element analysis and prototype testing procedures will be carried out. Both steps are important with their different outputs. For example, although stress states will not be an output of the prototype tests, their operation characteristics will provide information about the behavior of the living hinges. Stress output of the FEM analysis will be an input to the fatigue analysis and that is also critical to satisfy the life requirement.

5.2 Finite Element Model (FEM) and Fatigue Life Estimation

In order to confirm the results that are calculated theoretically FEM of the mechanism will be constructed and analysis based on the design criteria will be conducted. A commercial computer software for finite element analysis (Ansys ®) will be used. Since the mechanism is symmetrical about

vertical axis, only the right half (one segment) will be analyzed and the force values will be doubled. Material properties are entered accordingly and the FEM of the segment is shown in Figure 5-1.

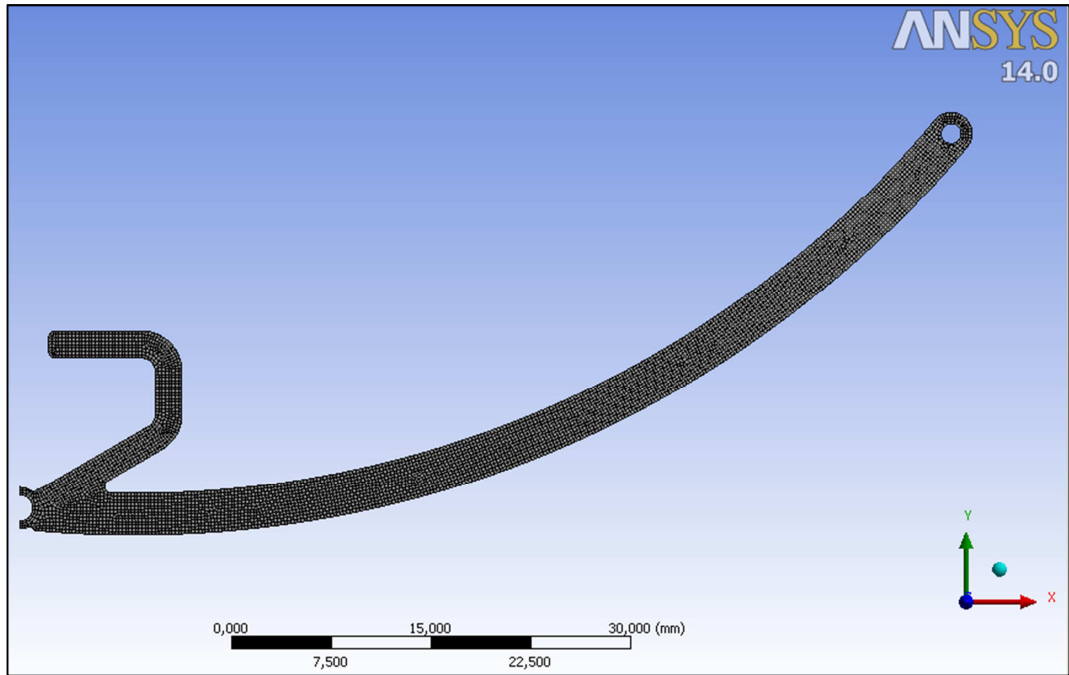


Figure 5-1: FEM Model of the Right Segment

The mesh construction of the model is analyzed and it is seen that 4920 mesh elements (most of them are quad) and 15616 nodes are created. The quality of the elements is also analyzed and average element quality comes out to be 0.991 on the scale of unity Figure 5-2.

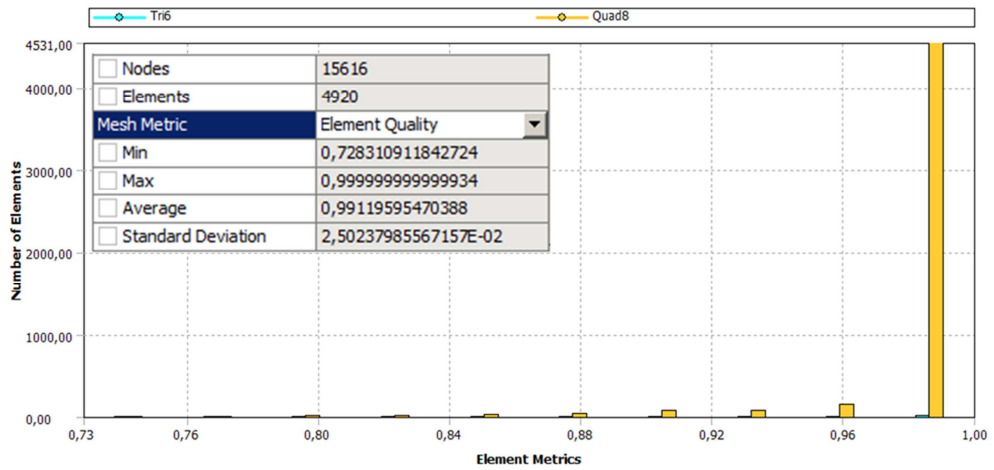


Figure 5-2: Information on Mesh Element of the FEM

Next step is to define the boundary conditions and forcing. The segment involves one cylindrical joint and one vertical force. The pin joint where the force is applied has degrees of freedom of translation at “y” and rotation at “z” Figure 5-3.

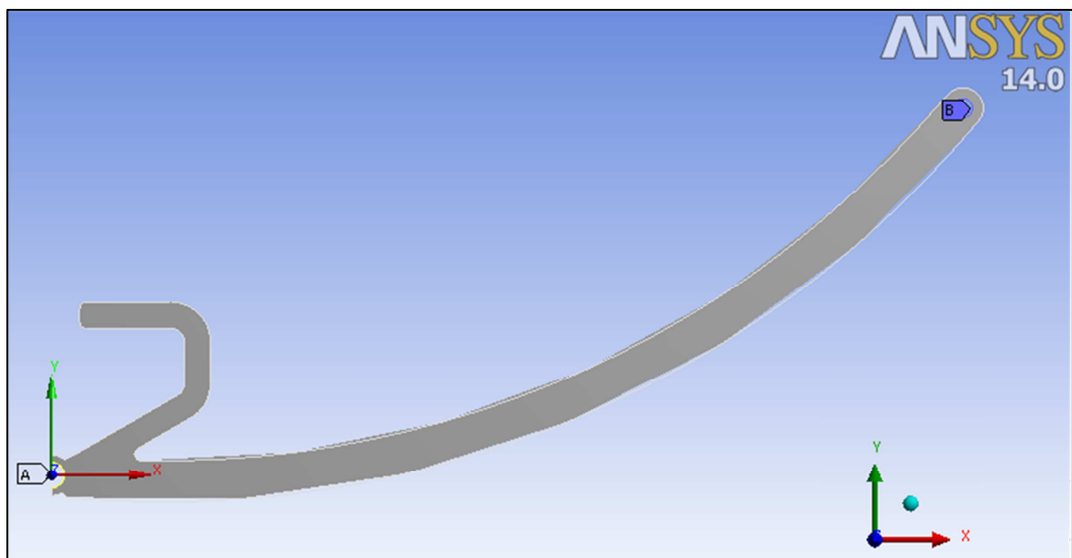


Figure 5-3: Boundary Conditions and Forcing

The outputs of the analysis are stress distribution and required force input. Maximum stress on the segment occurs in the middle areas of the segment and it is around 48.7MPa (Figure 5-4). Comparing with the yield strength of the material, safety factor for static failure comes out to be 1.5 that is acceptable. The fatigue life will be investigated based on this maximum stress value on the next subchapter.

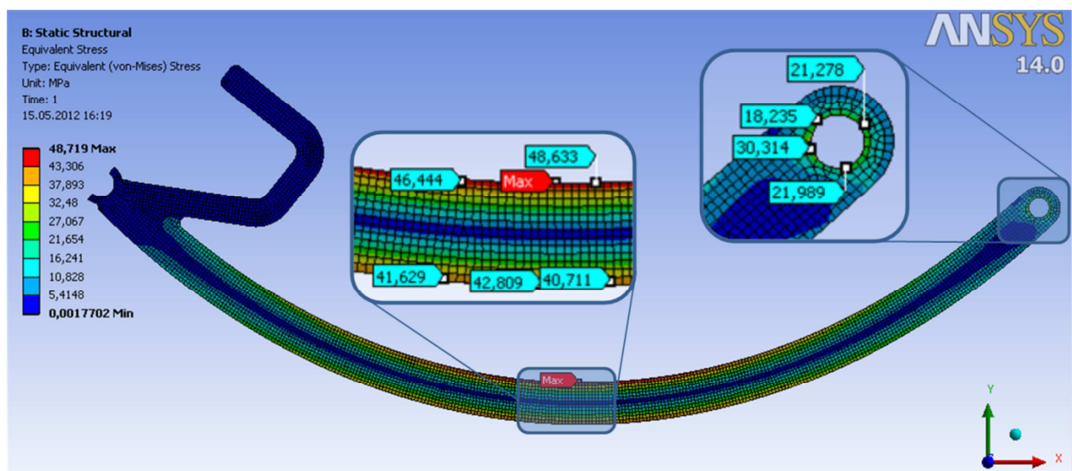


Figure 5-4: Stress Distribution of the Deformed Shape

The input force (F_{in}) and the force on each segment (F_{each}) which are acquired from FEM analysis and theoretical calculations are plotted on Figure 5-5.

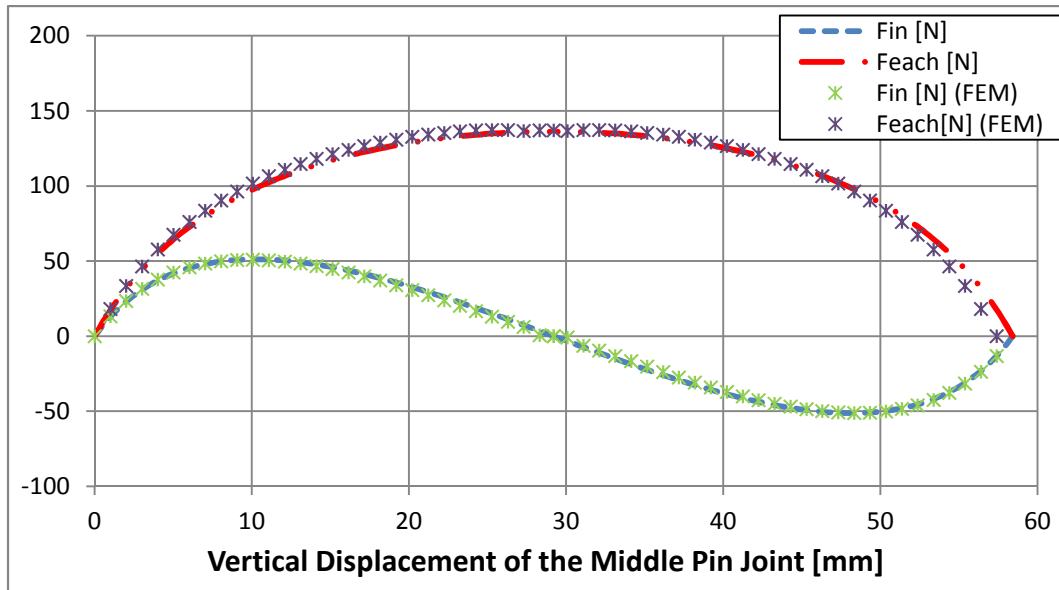


Figure 5-5: Variation of Input Force (F_{in}) and Force on Each Segment (F_{each}) along Deflection Path (Theoretical and FEM Results)

Analysis results are consistent with the theoretical calculations hence the forcing calculations can be said to be quite accurate. Since the validation of the calculations is done and the static failure risk is eliminated the FEM analysis is accomplished. On the next subchapter fatigue analysis will be carried out using the maximum stress level obtained from this analysis.

5.2.1 Life Estimation

The fatigue life of the mechanism is quite important for safety regulations as stated before. Therefore the calculations will be carried on properly as required. Maximum stress level that is obtained from the finite element analysis will be utilized. Since the mechanism will be locked during most of its life, it will be manufactured on that position. Thus stress relaxation and creep effects are aimed to be minimized. This fact leads to the conclusion

that the minimum stress occurred is zero. Using these values, alternating stress (σ_a) and mean stress (σ_m) can be evaluated from equations (2.7) and (2.8), as follows:

$$\sigma_m = \sigma_a = \frac{\sigma_{max}}{2} = \frac{48.7}{2} = 24.35MPa \quad (5.1)$$

Equation (2.8) can be rearranged to get the safety factor by taking the endurance limit (S_e) equals 0.3 times S_{UT} . That average value that is explained on equation (2.5) is considered to be safe since the fatigue strength of the material POM is known to be quite well. Also inserting other parameters it can be written that;

$$SF = \frac{6}{13} \frac{S_{UT}}{\sigma_{max}} \quad (5.2)$$

$$SF \cong 0,74 \quad (5.3)$$

Safety factor that is smaller than unity points out to finite life. Now the life must be checked whether it is safe for life requirements or not. The life of the mechanism can be found by analyzing the curve given on Figure 5-4. By matching the maximum stress amplitude with the number of cycles to failure, one can find out that the life will be almost 2×10^5 . That life is safe since the requirement dictates that this value must be larger than 5×10^4 .

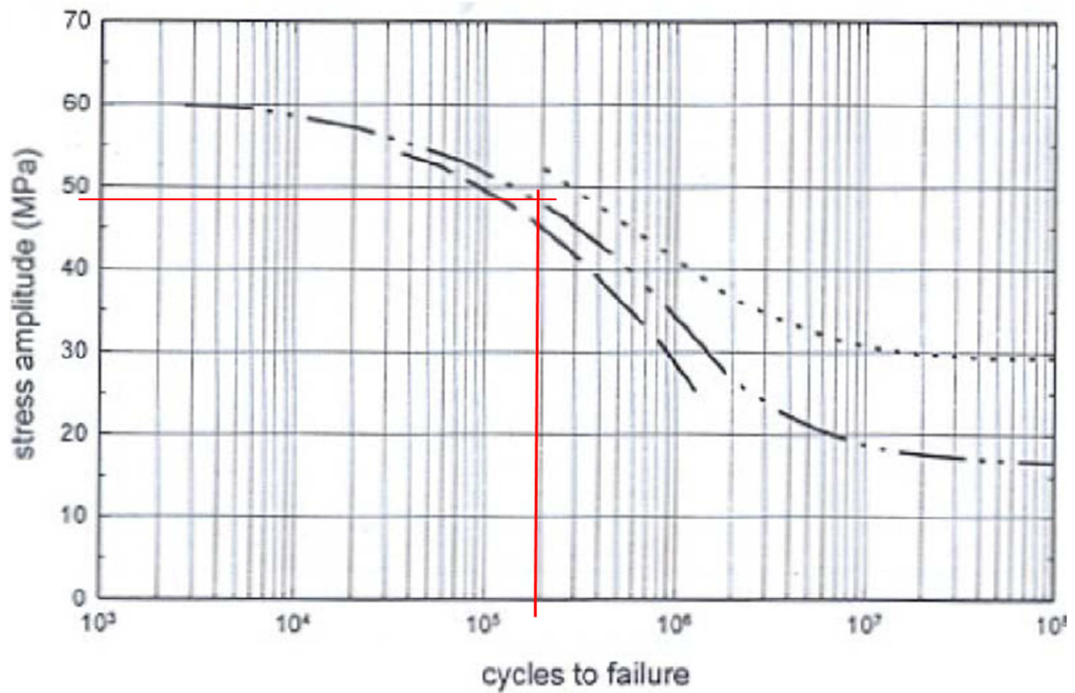


Figure 5-6: S-N Diagram of Extruded (Dashed) and Molded (Intermittent) POM (Delrin) [36]

5.3 Physical Model (Prototyping)

The validation of the theoretical calculations has been carried out one more time with the physical prototype. 3-D model described on the Figure 4-12 is produced by rapid prototyping. Selective laser sintering (SLS) method is utilized due its ability to cover wide range of materials. INNOV'PA 1550 is chosen because of flexibility and strength requirements.

The experiment setup (Figure 5-7) is basically prepared to measure the input force (F_{in}) that is required to deflect the mechanism for a specified amount. A dynamometer is placed at a mobile platform right at the middle of the mechanism.



Figure 5-7: Experimental Setup

With the movement of the dynamometer the mechanism deflects and the input force increases. The data are read for each 1mm increment. The data that are obtained are plotted with the theoretical expectations (Figure 5-8).

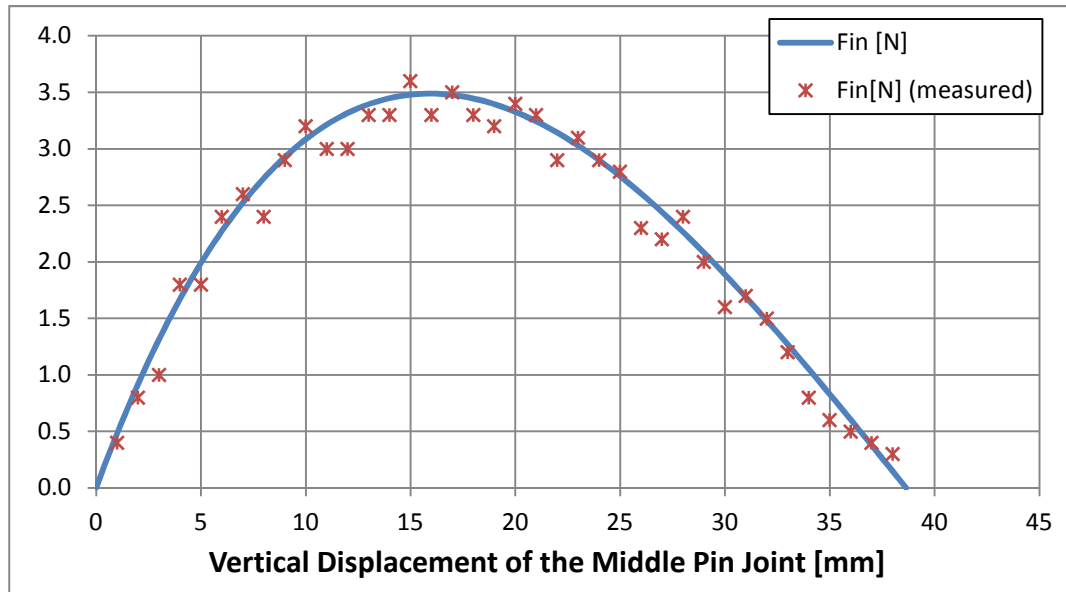


Figure 5-8: Variation of Input Force (F_{in}) along Deflection Path (Theoretical and Experimental Results)

Experimental results are in agreement with the calculations made from the theoretical derivations. Slight deviations from the theoretical results may be caused by the accuracy of the measurement device (dynamometer) and the setup construction.

Beyond numerical comparison, measurements indicated some non-numeric facts. One point is the performance of the living hinges. Although life expectancy from the prototypes is not possible, during experiments living hinges operated quite well for tens of times. The off plane or transverse deformations were not observed i.e. the middle hinge always translated linearly. Another point is the importance of mounting the mechanism. The force output can vary significantly by changing the position or the orientation of the fixed parts. Last issue that must be pointed out is the symmetrical deflection expectation that was successful during experiments.

CHAPTER 6

CONCLUSION & FUTURE WORK

6.1 Conclusion

Here on this study, one application of compliant mechanisms on functionally binary pinned-pinned (FBPP) segments has been presented. In order to get the deflection characteristics of the segment, it has been divided into two fixed-pinned parts and the exact solution is obtained. The half segment is modeled by pseudo-rigid-body model (PRBM) through a newly proposed method called “arc fitting”. Further calculations have been carried on accordingly in order to get a feasible and durable locking mechanism that will be utilized in dishwashers. Physical constraints such as space limitations, forcing requirements and material supply have been considered and the final model has been designed. It is composed of two segments connected to each other and to the ground by pin joints. Static and dynamic failure risks have been examined and ruled out. Finite element model (FEM) analysis and physical prototype measurements have been carried out in order to validate the theoretical results.

The results obtained from the calculations and measurements were in agreement. Starting with the PRBM construction to realizing the physical model, the errors introduced were seemed to be negligible. Hence the design method presented on this study has been shown its validity.

The application of bistable mechanisms as locking devices is common in the market but systematic synthesis of a compliant bistable locking mechanism is distinctive in literature. For different applications, one can carry out the presented steps to design locking devices in accordance with their specific requirements.

6.2 Future Work

As specified before only one application of FBPP segments is focused on this study as a locking mechanism. There can be other applications of these segments such as clutches, brakes, switches etc. One can chose a different application area to design for different mechanisms.

The method of constructing the PRBM proposed here was called “arc fitting” and basically depends on fitting a circular arc on the deflection path of the pin joint. Among this and other current methods one can develop a different method by choosing any parameter as the input parameter. Different modeling methods will obviously provide different advantages.

The final mechanism is designed to be lumped compliant (like rigid body joints equivalent but the joints are living hinges) but that is apparently not a necessity. The design can be non-monolithic (joints are indeed rigid pin joints) as well. For further applications, this can be considered as an option.

REFERENCES

- [1] Howell, L. L., "Compliant Mechanisms," Wiley, 2001.
- [2] Söylemez, E., "Mechanisms," 3rd ed. 64. Middle East Technical University, 1999.
- [3] <http://www.mlahanas.de/Greeks/war/CatapultTypes.htm>, Last accessed on 19.04.2012.
- [4] Besselink, P. A., "Bistable spring construction for a stent and other medical apparatus," *United States Patent 6,488,702, (9/012,843)*, 2002.
- [5] Sridhar, K., et al., "Design of Compliant Mechanisms: Applications to MEMS," *Analog Integr. Circuits Signal Process.*, vol. 29, no. 1-2, pp. 7-15, 2001.
- [6] Sigmund, O., "On the Design of Compliant Mechanisms Using Topology Optimization," *Mechanics of Structures and Machines*, vol. 25, no. 4, pp. 493-524, 1997.
- [7] Halg, B., "On a nonvolatile memory cell based on micro-electro-mechanics," *Proceedings of Micro Electro Mechanical Systems, 1990. Proceedings, An Investigation of Micro Structures, Sensors, Actuators, Machines and Robots. IEEE*, pp. 172-176, 1990.
- [8] Matoba, H., Ishikawa, T., Kim, C. J., and Muller, R. S., "A Bistable Snapping Microactuator," *Proceedings of Micro Electro Mechanical Systems, 1994, MEMS '94, Proceedings, IEEE Workshop on*, pp. 45-50, 1994.
- [9] Wagner, B., et al., "Bistable Microvalve with Pneumatically Coupled Membranes," *Proceedings of Micro Electro Mechanical Systems, An Investigation of Micro Structures, Sensors, Actuators, Machines and Systems*, pp. 384-388, 1996.
- [10] Lu, K. J., "Synthesis of Shape Morphing Compliant Mechanisms," University of Michigan., 2004.

- [11] Midha, A., Norton, T. W., and Howell, L. L., "On the Nomenclature, Classification, and Abstractions of Compliant Mechanisms," *Journal of Mechanical Design*, vol. 116, no. 1, pp. 270-279, 1994.
- [12] Miller, E., "Plastics Products Design Handbook," New York: M. Dekker, 1981.
- [13] Murphy, M. D., Midha, A., and Howell, L. L., "The Topological Synthesis of Compliant Mechanisms," *Mechanism and Machine Theory*, vol. 31, no. 2, pp. 185-199, 1996.
- [14] Mettlach, G. A., Midha, A., "Using Burmester Theory in the Design of Compliant Mechanisms," *Proceedings of ASME Design Engineering Technical Conferences, 96-DETC/MECH-118*, 1996.
- [15] Howell, L. L., "A Generalized Loop-Closure Theory for the Analysis and Synthesis of Compliant Mechanisms," UMI, 1993.
- [16] Jensen, B. D., and Howell, L. L., "Bistable Configurations of Compliant Mechanisms Modeled Using Four Links and Translational Joints," *Journal of Mechanical Design*, vol. 126, no. 4, pp. 657-666, 2004.
- [17] Shigley, J. E., Mischke, C. R., and Budynas, R. G., "Mechanical Engineering Design," McGraw-Hill, 2004.
- [18] Nielsen, L. E., and Landel, R. F., "Mechanical Properties of Polymers and Composites," M. Dekker, 1994.
- [19] Lingaiah, K., "Machine Design Databook," 2nd ed. McGraw-Hill, 2003.
- [20] Timoshenko, S., "Theory of Elastic Stability," McGraw-Hill, 1961.
- [21] Leipholz, H. H. E., "Stability Theory: An Introduction to the Stability of Dynamic Systems and Rigid Bodies," Academic Press, 1970.
- [22] Lagrange, J. L., "Mecanique Analytique," L'Academie Royal des Sciences, 1788.
- [23] Oh, Y., and University of, M., "Synthesis of Multistable Equilibrium Compliant Mechanisms," University of Michigan, 2008.

- [24] Pendleton, T. M., Jensen, B. D., "Development of a Tristable Compliant Mechanism," *Proceedings of 12th IFToMM World Congress*, 2007. Besançon, France.
- [25] Jensen, B. D., Howell, L. L., and Salmon, L. G., "Design of Two-Link, In-Plane, Bistable Compliant Micro-Mechanisms," *Journal of Mechanical Design*, vol. 121, no. 3, pp. 416-423, 1999.
- [26] Noveanu, S., and Mandru, D., "Locking Systems Based on Compliant Mechanisms," *Proceedings of Acta Technica Napocensis*, pp. 857-862, 2008.
- [27] Edwards, B. T., "Functionally Binary Pinned-pinned Segments," Brigham Young University. Department of Mechanical Engineering., 1996.
- [28] Edwards, B. T., Jensen, B. D., and Howell, L. L., "A Pseudo-Rigid-Body Model for Functionally Binary Pinned-Pinned Segments Used in Compliant Mechanisms," *Proceedings of ASME Design Engineering Technical Conferences*, 1999. Las Vegas, Nevada.
- [29] Chernov, N., "Circular and Linear Regression: Fitting Circles and Lines by Least Squares," CRC Press/Taylor & Francis, 2011.
- [30] Chernov, N., and Lesort, C., "Least Squares Fitting of Circles," *Journal of Mathematical Imaging and Vision*, vol. 23, no. 3, pp. 239-252, 2005.
- [31] Shakarji, C. M., "Least-Squares Fitting Algorithms of the NIST Algorithm Testing System," *Journal of Research of the National Institute of Standards and Technology*, vol. 103, no. 6, pp. 633-641, 1998.
- [32] Landau, U. M., "Estimation of a Circular Arc Center and Its Radius," *Computer Vision, Graphics, and Image Processing*, vol. 38, no. 3, pp. 317-326, 1987.
- [33] Späth, H., "Least-squares fitting by circles," *Computing*, vol. 57, no. 2, pp. 179-185, 1996.
- [34] Späth, H., "Orthogonal Least Squares Fitting by Conic Sections," *Proceedings of 2nd International Workshop on Recent Advances in Total Least Squares Techniques and Errors-in-Variables Modeling*, 1997. Leuven, Belgium.
- [35] Tres, P. A., "Designing Plastic Parts for Assembly," 2nd ed. Hanser, 2006.

[36] Plastics Design Library Staff, *Fatigue and Tribological Properties of Plastics and Elastomers*. 1995, William Andrew Publishing/Plastics Design Library.

[37] King, L. V., "On the Direct Numerical Calculation of Elliptic Functions and Integrals," Cambridge University Press, 1924.

APPENDICES

APPENDIX A: ELLIPTIC INTEGRAL SOLUTION METHODOLOGY

Incomplete elliptic integral of the first and second kinds are defined by the following two equations respectively:

$$F(\varphi, k) = \int_0^\varphi \frac{d\theta}{\sqrt{1-k^2 \sin^2 \theta}}$$

$$E(\varphi, k) = \int_0^\varphi \sqrt{1 - k^2 \sin^2 \theta}$$

There are no known elementary solutions to these kinds of equations but the numerical calculation process is straightforward. The method is described by King [37]. He has also shown that the method converges to the solution rapidly and as precise as desired by setting the calculation error beforehand.

The numerical process takes the variables modulus (k) and amplitude (φ) as the inputs and manipulates until the error reduced to the predefined level.

The iterations are carried out according to recurrence formula defined by the Landen's scale of increasing amplitudes as such:

$$\tan(\varphi_{i+1} - \varphi_i) = \frac{b_i}{a_i} \tan(\varphi_i) \quad \varphi_{i+1} > \varphi_i$$

$$a_{i+1} = \frac{1}{2}(a_i + b_i)$$

$$b_{i+1} = \sqrt{a_i b_i}$$

$$c_{i+1} = \frac{1}{2}(a_i - b_i)$$

The initial values of these coefficients are given as:

$$a_0 = 1$$

$$b_0 = \sqrt{1 - k^2}$$

$$c_0 = k$$

The iterations are carried out (n times) until c_n becomes as less as desired. During iterations to ensure that the correct φ_{n+1} is evaluated considering the related constraints, a correcting procedure must be applied as such:

$$(\varphi_{i+1})_{corr} = \varphi_{i+1} + m\pi$$

Where;

$$m = \text{rounding of } \frac{2\varphi_i - \varphi_{i+1}}{\pi} \text{ to nearest whole number}$$

Then using the final coefficients, elliptic integrals are evaluated from the following relations:

$$F(\varphi, k) = \frac{\varphi_n}{a_n 2^n}$$

$$E(\varphi, k) = \frac{\pi}{2a^n} \left(1 - \frac{1}{2} \sum_{i=0}^n 2^i c_i^2\right)$$

APPENDIX B: VBA CODE ON ELLIPTIC INTEGRAL SOLUTION

The VBA codes written to evaluate elliptic integrals in MS EXCEL® are presented below.

1. VBA CODE TO EVALUATE INCOMPLETE ELLIPTIC INTEGRAL OF THE FIRST KIND

```
Function incomp_ell_int_second_kind_evaluate(modul, amp, Optional error As  
Double = 10 ^ (-16))
```

*'Function that takes the module and the amplitude (and also calculation error if desired) as
the input and returns the incomplete elliptic integral of the second kind*

```
Dim sum1, sum2, check_old, check, a(), b(), c(), fi(), m(), fi_corr(), r As Double
```

```
Dim i, u, j, k As Integer
```

```
Dim comp_frst, incmp_frst, incmp_frst_corr, incmp_scnd_corr As Double
```

```
u = 20
```

```
ReDim a(u), b(u), c(u), fi(u), m(u), fi_corr(u)
```

```
r = 1
If modul > 1 Then
amp = WorksheetFunction.Asin(modul * Sin(amp))
modul = 1 / modul
r = modul
End If
```

```
j = 0
k = 1
```

```
If amp > (WorksheetFunction.Pi / 2) Then
Do Until amp <= (WorksheetFunction.Pi / 2)
amp = amp - WorksheetFunction.Pi
j = j + 1
Loop
End If
```

```
If amp < 0 Then

Do Until (-WorksheetFunction.Pi / 2) <= amp
amp = amp + WorksheetFunction.Pi
j = j - 1
Loop
```

```
If amp < 0 Then
amp = -amp
k = -1
End If
```

```
End If
```

$$a(0) = 1$$

$$b(0) = \text{Sqr}(1 - \text{modul}^2)$$

$$fi(0) = \text{amp}$$

$$fi_corr(0) = \text{amp}$$

$$m(0) = 0$$

$$\text{sum1} = \text{modul}^2$$

$$\text{sum2} = 0$$

$$\text{check_old} = \text{amp}$$

$$c(0) = \text{modul}$$

$$i = 1$$

Do While $c(i - 1) > \text{error}$

$$a(i) = (a(i - 1) + b(i - 1)) / 2$$

$$b(i) = \text{Sqr}(a(i - 1) * b(i - 1))$$

$$c(i) = (a(i - 1) - b(i - 1)) / 2$$

$$fi(i) = \text{Atn}(\text{Tan}(fi_corr(i - 1)) * b(i - 1) / a(i - 1)) + fi_corr(i - 1)$$

$$m(i) = \text{Round}((2 * fi_corr(i - 1) - fi(i)) / \text{WorksheetFunction.Pi}, 0)$$

$$fi_corr(i) = fi(i) + \text{WorksheetFunction.Pi} * m(i)$$

$$\text{sum1} = \text{sum1} + 2^i * c(i)^2$$

$$\text{sum2} = \text{sum2} + c(i) * \text{Sin}(fi_corr(i))$$

$$\text{check} = fi_corr(i) / 2^i / a(i)$$

If $\text{check} - \text{check_old} < -(10^{(-16)})$ Then

Exit Function

End If

check_old = check

i = i + 1

Loop

comp_frst = WorksheetFunction.Pi / (2 * a(i - 1))

comp_scnd = comp_frst * (1 - sum1 / 2)

incmp_frst = fi_corr(i - 1) / (a(i - 1) * 2 ^ (i - 1))

incmp_scnd = incmp_frst + sum2 - sum1 / 2 * incmp_frst

incmp_frst_corr = r * (2 * j * comp_frst + k * incmp_frst)

incmp_scnd_corr = 2 * j * comp_scnd + k * incmp_scnd

If r = 1 Then

incomp_ell_int_second_kind_evaluate = incmp_scnd_corr

ElseIf r = modul Then

incomp_ell_int_second_kind_evaluate = (1 / modul) * (incmp_frst_corr +
incmp_scnd_corr)

End If

End Function

2. VBA CODE TO EVALUATE INCOMPLETE ELLIPTIC INTEGRAL OF THE SECOND KIND

Function incomp_ell_int_first_kind_evaluate(modul, amp, Optional error As Double = 10 ^ (-16))

'Function that takes the module and the amplitude (and also calculation error if desired) as the input and returns the incomplete elliptic integral of the first kind

Dim sum1, sum2, check_old, check, a(), b(), c(), fi(), m(), fi_corr(), r As Double

Dim i, u, j, k As Integer

Dim comp_frst, incmp_frst As Double

u = 20

ReDim a(u), b(u), c(u), fi(u), m(u), fi_corr(u)

r = 1

If modul > 1 Then

amp = WorksheetFunction.Asin(modul * Sin(amp))

modul = 1 / modul

r = modul

End If

j = 0

k = 1

If amp > (WorksheetFunction.Pi / 2) Then

Do Until amp <= (WorksheetFunction.Pi / 2)

```

amp = amp - WorksheetFunction.Pi
j = j + 1
Loop
End If

If amp < 0 Then

    Do Until (-WorksheetFunction.Pi / 2) <= amp
    amp = amp + WorksheetFunction.Pi
    j = j - 1
    Loop

    If amp < 0 Then
    amp = -amp
    k = -1
    End If

End If

a(0) = 1
b(0) = Sqr(1 - modul ^ 2)
fi(0) = amp
fi_corr(0) = amp
m(0) = 0
sum1 = modul ^ 2
sum2 = 0
check_old = amp
c(0) = modul

i = 1

```

```

Do While c(i - 1) > error
a(i) = (a(i - 1) + b(i - 1)) / 2
b(i) = Sqr(a(i - 1) * b(i - 1))
c(i) = (a(i - 1) - b(i - 1)) / 2

fi(i) = Atn(Tan(fi_corr(i - 1)) * b(i - 1) / a(i - 1)) + fi_corr(i - 1)

m(i) = Round((2 * fi_corr(i - 1) - fi(i)) / WorksheetFunction.Pi, 0)

fi_corr(i) = fi(i) + WorksheetFunction.Pi * m(i)

sum1 = sum1 + 2 ^ i * c(i) ^ 2
sum2 = sum2 + c(i) * Sin(fi_corr(i))

check = fi_corr(i) / 2 ^ i / a(i)

If check - check_old < -(10 ^ (-16)) Then
Exit Function
End If
check_old = check

i = i + 1

Loop

incmp_frst = fi_corr(i - 1) / (a(i - 1) * 2 ^ (i - 1))
comp_frst = WorksheetFunction.Pi / (2 * a(i - 1))

incomp_ell_int_first_kind_evaluate = r * (2 * j * comp_frst + k * incmp_frst)

End Function

```

APPENDIX C: SNAPSHOT OF NUMERICAL CALCULATIONS

x :=		1
	1	0.837
	2	0.83
	3	0.824
	4	...

y :=		1
	1	0.466
	2	0.474
	3	0.483
	4	...

--> Set of Data Points

n := 95 --> Number of Data Points

$x_{0_i} := 0.2$ $y_{0_i} := 0.05$ --> Initial Guesses

"Given-Find" routine to evaluate the equations numerically:
(** Nonlinear Levenberg-Marquardt method is utilized.)

Given

$$\frac{d}{dx_{0_i}} \left[\sum_{i=1}^n \left[\sqrt{(x_i - x_{0_i})^2 + (y_i - y_{0_i})^2} - \frac{1}{n} \sum_{j=1}^n \sqrt{(x_j - x_{0_i})^2 + (y_j - y_{0_i})^2} \right]^2 \right] = 0$$

$$\frac{d}{dy_{0_j}} \left[\sum_{i=1}^n \left[\sqrt{(x_i - x_{0_i})^2 + (y_i - y_{0_i})^2} - \frac{1}{n} \sum_{j=1}^n \sqrt{(x_j - x_{0_i})^2 + (y_j - y_{0_i})^2} \right]^2 \right] = 0$$

$$\begin{pmatrix} x_0 \\ y_0 \end{pmatrix} := \text{Find}(x_{0_i}, y_{0_i}) = \begin{pmatrix} 0.211205 \\ -0.010153 \end{pmatrix}$$

$$r := \frac{1}{n} \cdot \sum_{i=1}^n \sqrt{(x_i - x_0)^2 + (y_i - y_0)^2} = 0.786387$$

$$y_p := \sqrt{r^2 - (x - x_0)^2} + y_0$$

APPENDIX D: α_t^2 vs. $\Delta\theta$ PLOTS FOR DIFFERENT CURVATURE VALUES (κ_0)

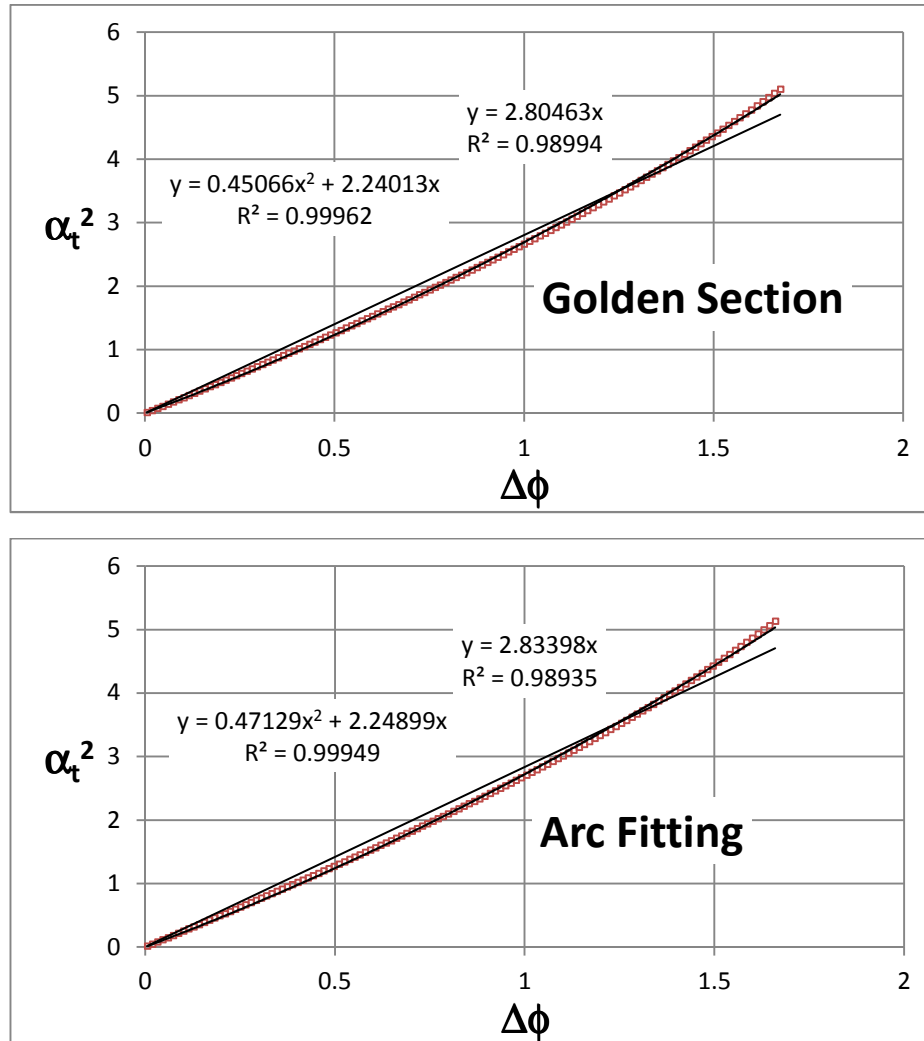


Figure D-6-1: Force (Non-dimensionalized Load Factor [α_t^2]) – Deflection (Pseudo-Rigid-Body Angle Difference [$\Delta\theta$]) Characteristics for $\kappa_0=0.50$ Obtained by Golden Section and Arc Fitting Methods Respectively

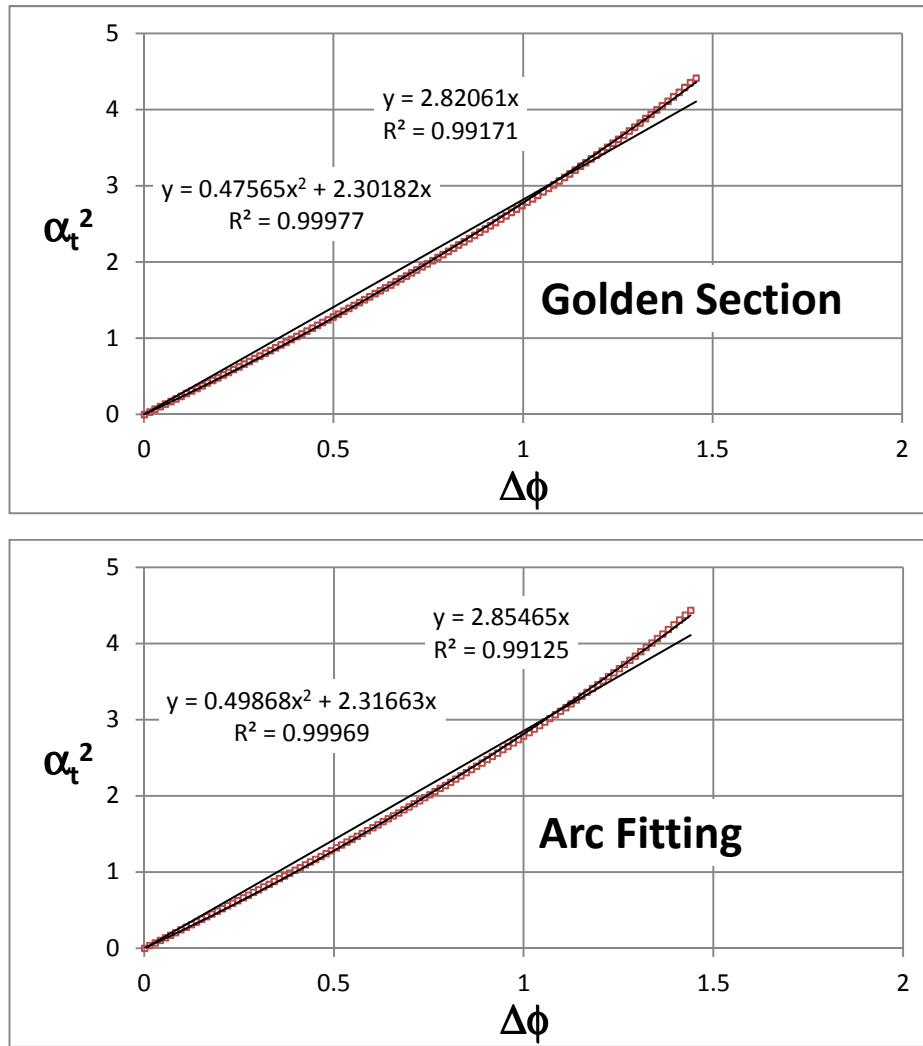


Figure D-6-2: Force (Non-dimensionalized Load Factor [α_t^2]) – Deflection (Pseudo-Rigid-Body Angle Difference [$\Delta\theta$]) Characteristics for $\kappa_0=0.75$ Obtained by Golden Section and Arc Fitting Methods Respectively

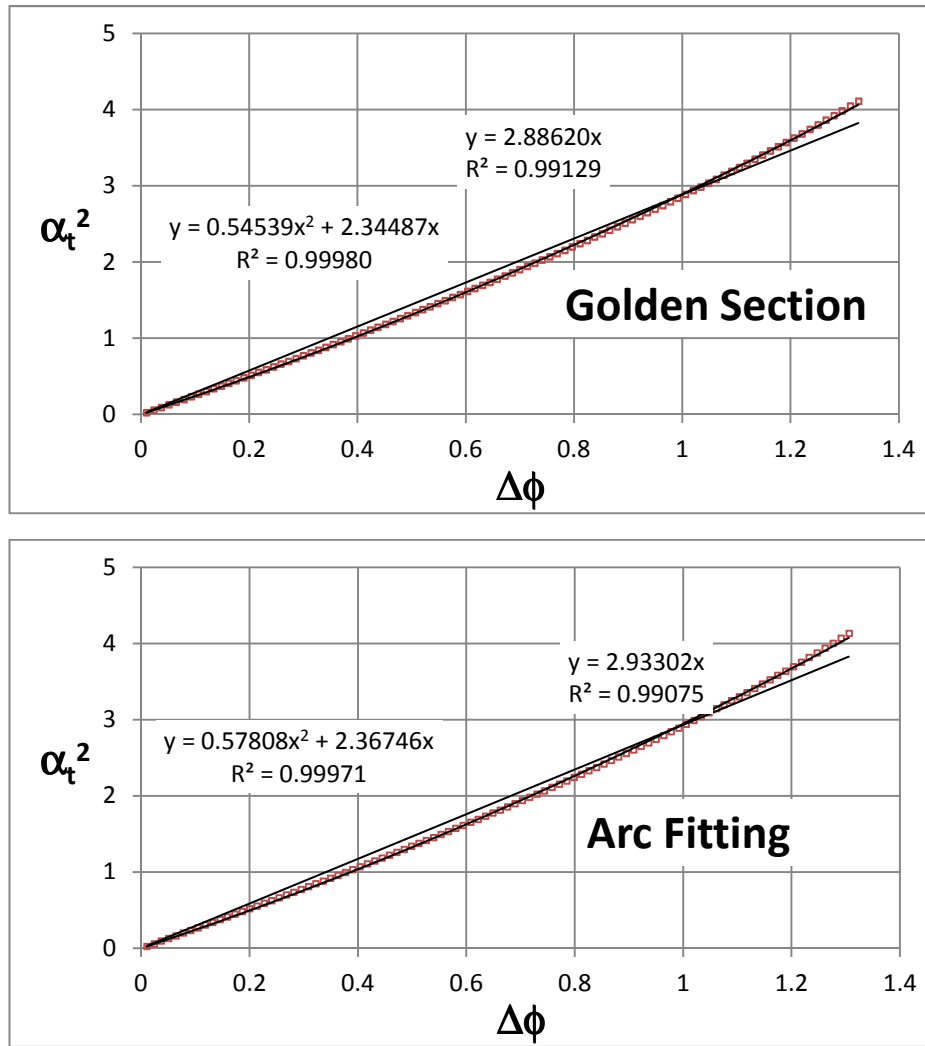


Figure D-6-3: Force (Non-dimensionalized Load Factor [α_t^2]) – Deflection (Pseudo-Rigid-Body Angle Difference [$\Delta\theta$]) Characteristics for $\kappa_0=1.00$ Obtained by Golden Section and Arc Fitting Methods Respectively

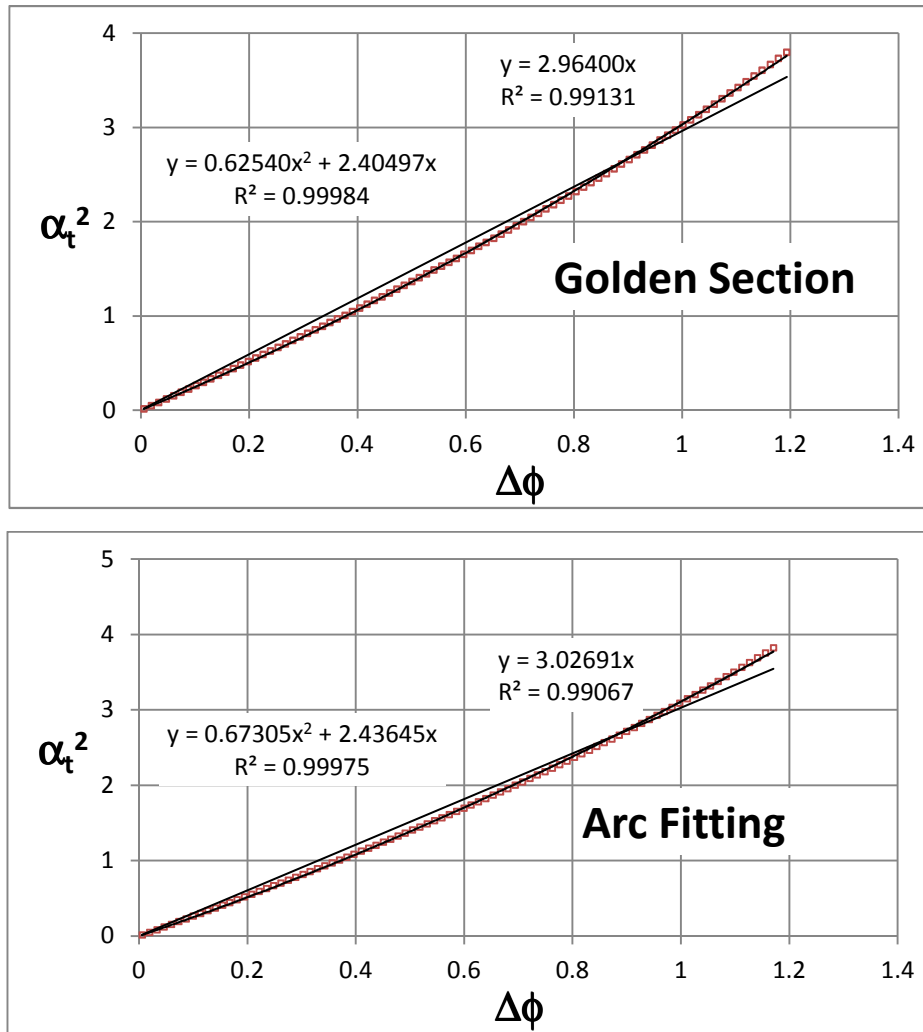


Figure D-6-4: Force (Non-dimensionalized Load Factor [α_t^2]) – Deflection (Pseudo-Rigid-Body Angle Difference [$\Delta\theta$]) Characteristics for $\kappa_0=1.25$ Obtained by Golden Section and Arc Fitting Methods Respectively

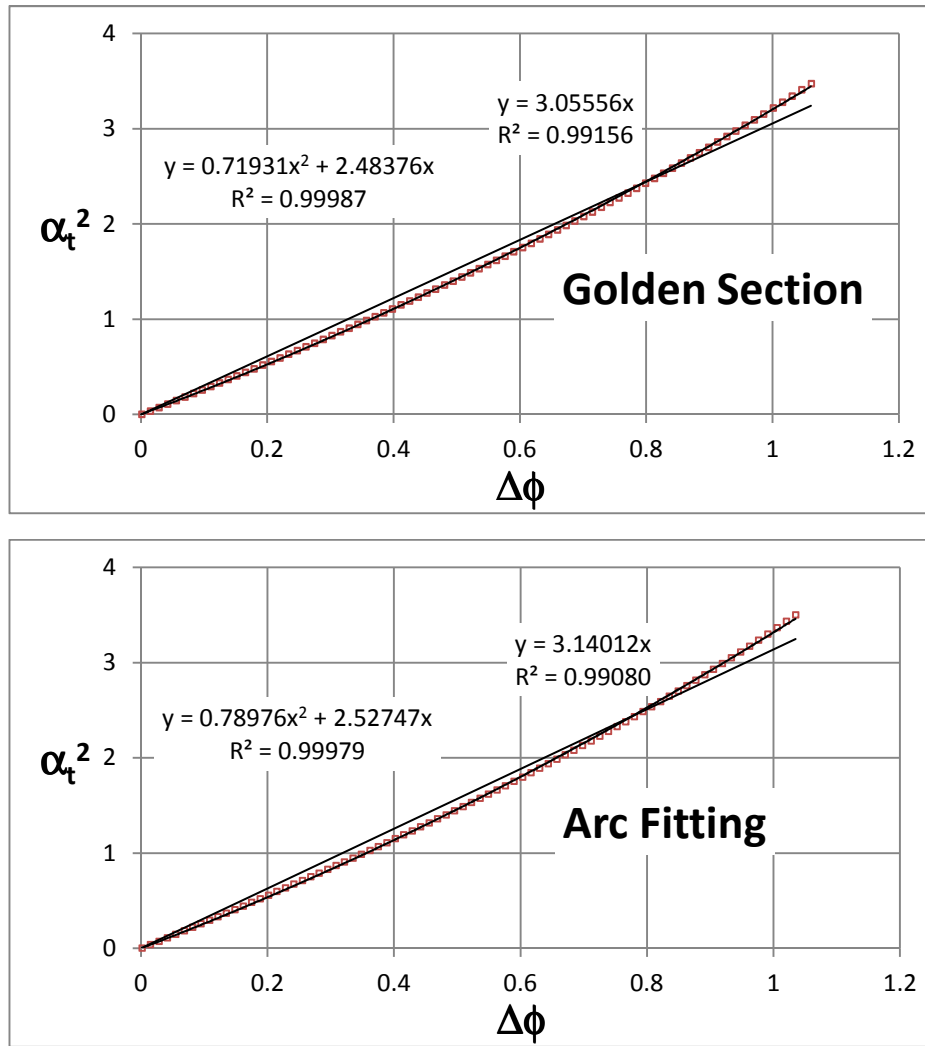


Figure D-6-5: Force (Non-dimensionalized Load Factor [α_t^2]) – Deflection (Pseudo-Rigid-Body Angle Difference [$\Delta\theta$]) Characteristics for $\kappa_0=1.50$ Obtained by Golden Section and Arc Fitting Methods Respectively

**APPENDIX E: ERROR VALUES FOR VARIOUS
CURVATURES (κ_0) AND FIXED PIN JOINT
ROTATION ($\Delta\theta_0=45^\circ$)**

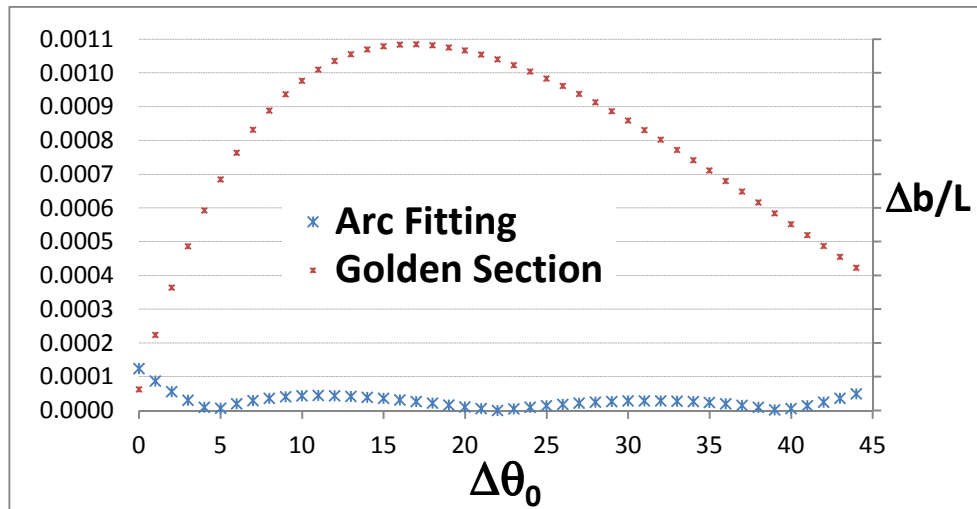


Figure E-1: Error Comparison for $\Delta\theta_0=45^\circ$ and $\kappa_0=0.50$

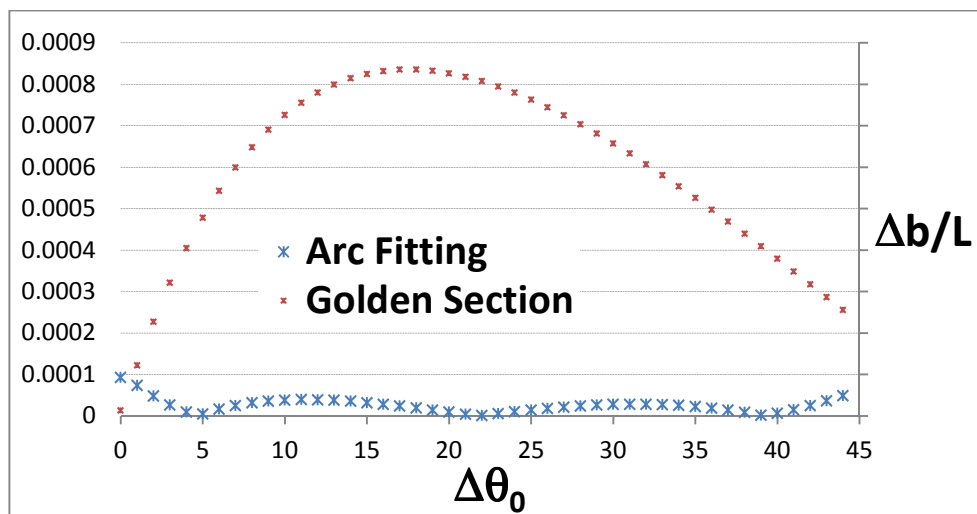


Figure E-2: Error Comparison for $\Delta\theta_0=45^\circ$ and $\kappa_0=0.75$

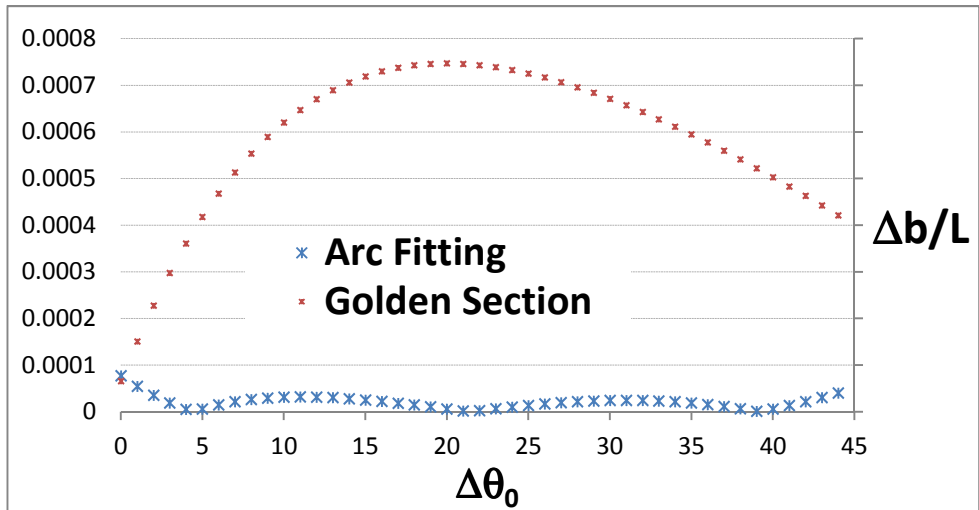


Figure E-3: Error Comparison for $\Delta\theta_0=45^\circ$ and $\kappa_0=1.00$

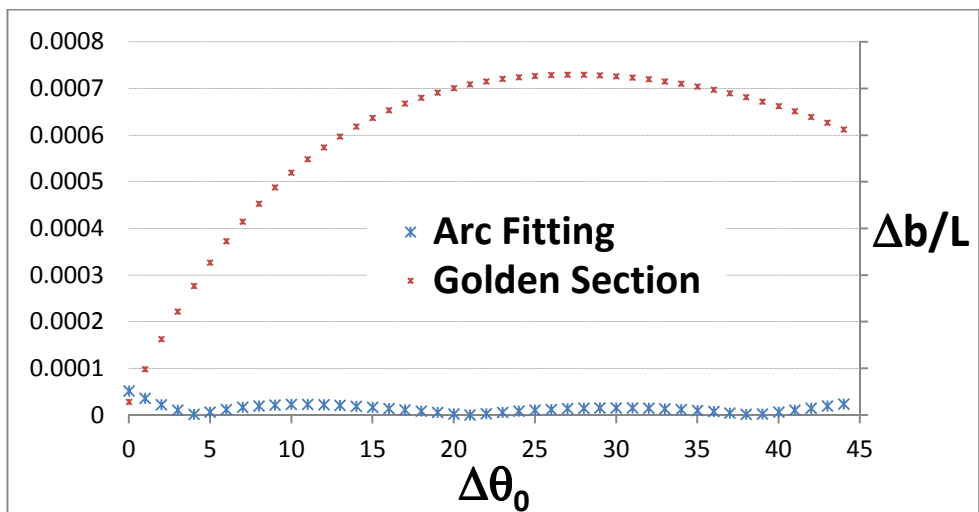


Figure E-4: Error Comparison for $\Delta\theta_0=45^\circ$ and $\kappa_0=1.25$

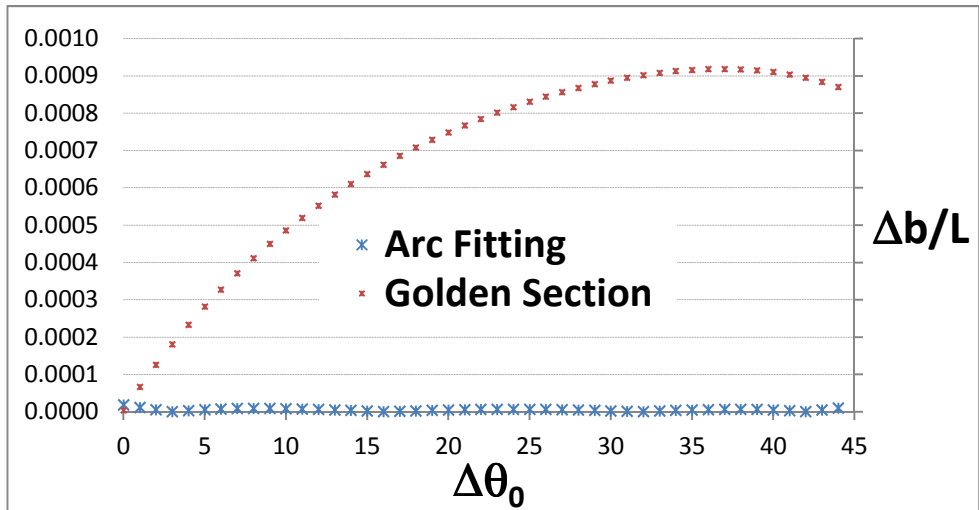


Figure E-5: Error Comparison for $\Delta\theta_0=45^\circ$ and $\kappa_0=1.50$

APPENDIX F: MATERIAL SPECIFICATIONS OF POLYOXYMETHYLENE (POM)

Product Information



Delrin®

acetal resin

PRELIMINARY DATA

Delrin® DE7057 NC010

Delrin® DE7057 NC010 is a modified medium viscosity resin for general purpose use.

Property	Test Method	Units	Value
Mechanical			
Yield Stress	ISO 527-1/-2	MPa	
50mm/min			73
Yield Strain	ISO 527-1/-2	%	
50mm/min			12
Nominal Strain at Break	ISO 527-1/-2	%	
50mm/min			25
Strain at Break	ISO 527-1/-2	%	
50mm/min			40
Tensile Modulus	ISO 527-1/-2	MPa	
1mm/min			3400
Notched Izod Impact	ISO 180/1A	kJ/m ²	8
Thermal			
Melting Temperature	ISO 3146C	°C	178
Flow			
Melt Flow Rate	ISO 1133	g/10 min	14
Other			
Density	ISO 1183	kg/m ³	1420
Processing			
Melt Temperature Range	ISO 294	°C	210-220
Processing Moisture Content		%	<0.2
Hold Pressure Range		MPa	80-100

Contact DuPont for MSDS, general guides and/or additional information about ventilation, handling, purging, drying, etc.
Mechanical properties measured at 23°C (73°F) unless otherwise stated.

The above data are preliminary and are subject to change as additional data are developed on subsequent lots.

Delrin® is a DuPont registered trademark.

030729/991117

The information provided in this data sheet corresponds to our knowledge on the subject at the date of its publication. This information may be subject to revision as new knowledge and experience becomes available. The data provided fall within the normal range of product properties and relate only to the specific material designated; these data may not be valid for such material used in combination with any other materials or additives or in any process, unless expressly indicated otherwise. The data provided should not be used to establish specification limits or used alone as the basis of design; they are not intended to substitute for any testing you may need to conduct to determine for yourself the suitability of a specific material for your particular purposes. Since DuPont cannot anticipate all variations in actual end-use conditions DuPont makes no warranties and assumes no liability in connection with any use of this information. Nothing in this publication is to be considered as a license to operate under or a recommendation to infringe any patent rights. Caution: Do not use this product in medical applications involving permanent implantation in the human body. For other medical applications see "DuPont Medical Caution Statement", H-51459 or H-50102.

APPENDIX G: MATERIAL SPECIFICATIONS OF INNOV'PA 1550



Material Data Sheet

Polyamide fine composite powder PFP03: Innov'PA 1550 for systems of Rapid Prototyping

Description, Applications :

Innov'PA 1550 is a fine powder based on polyamide 12 (thermoplastic) especially formulated to function on rapid prototyping systems by laser sintering or radiation. It enables to obtain productions of models and functional parts in "plastic engineering" with long cycle of life and excellent chemical resistance.

This polyamide powder gives final productions in natural color (white-cream towards the yellow in mass).

Innov'PA 1550 is based on a new formulation with improved mechanical characteristics. The whole of the improvements of the mechanical properties gives a better cohesion of the layers involving a more plastic behavior and responsive mechanics of the parts manufactured approaching the injected one. A simple blasting of the part obtain is enough, these parts can be finished and painted if needed. A refined specifies granulometry, precise and very tightened allows to obtain an excellent resolution of contour and surface.

These innovative properties make possible to consider **Rapid Manufacturing**.

The process ability of the powder on the rapid prototyping systems is optimized; thus all the powder of a building can be re-used after sifting. The refreshing factor for regeneration, because of the adapted formulation of **Innov'PA 1550**, is lower than the usual rates used on the various systems of rapid prototyping.

The typical applications of Innov'PA 1550 are parts and models of design, functional, precise, requested mechanically, chemically and in temperature.

- **Granulometry refined around 45 µm**
- **Excellent resolution of contour and surface for Rapid Manufacturing**
- **Mechanical properties and mechanical behavior such as injected parts**
- **Exploitable on any type of system of prototyping: Pluri-manufacturers**
- **Use continues powder cycles sifting-regenerating**
- **Regeneration factor lowered**
- **Aspect and natural coloring of the product, cohesion of layer**
- **Chemical resistance of Polyamide 12**
- **Economic cost of exploitation (ratio Q Powder/ Number of building)**
- **Provisioning independent of the manufacturers**



Date sheet Innov'PA 1550 ENG Sept07

1 / 2

www.exceltec.eu

EXCELTEC Sarl
Espace Hi-plaine, 30 avenue Montpoulier
F-69680 Chassieu France
Fax : +33 (0)472 936 671

1. General Properties :

Measurement	Method & Condition	Metric Value
Average particle size	Diffraction laser	40 < ___ < 50 μm
powder packed Density 23°C	Method ExcelTec	0.5 ± 0.05 g/cm ³
Part density 23°C	Method ExcelTec	0.98 ± 0.05 g/cm ³
Moisture absorption 24 hrs, 50% HR, 23°C	ASTM D570	0.30 ± 0.05 %

2. Thermal Properties :

Measurement	Method & Condition	Metric Value
T ^o f Melting point	DSC	181 < ___ < 185 °C
T ^o g Glazing point	DSC	34 ± 2 °C
Heat Deflection Temperature at 1.82 MPa	ASTM D648	86 ± 1 °C
T ^o Process <small>* according to machine reading</small>	Glazing method	- 14 ± 2 °C (ex : 174 °C ± 2)*

3. Mechanical Properties :

Measurement	Method & Condition	Metric Value
Tensile strength	ISO 527	45 ± 1 MPa *
Young Modulus	ISO 827	1 550 ± 150 MPa *
Elongation at break	ISO 527	16 ± 2 % *
Flexural Modulus	ISO 178	1 350 ± 25 MPa *
Charpy - Impact strength	ISO 179	80 dry / ± 2 KJ/m ² *
		50 cond. 24 hrs
Charpy - Notched impact strength	ISO 179	6 ± 0.5 KJ/m ² *
Shore Test (Shore D) <small>* statistics after several cycles >10 refresh</small>	ISO R 868	68 ± 3 Shore D

4. Chemical Resistances :

Matrix in Polyamide 12 with a good chemical resistance to alkaline, hydrocarbons, oils, gasoline's, gas oil and solvents. Attack by the acids. Sealing of wall starting from 1.6 mm thickness.

5. Electrical Properties :

Measurement	Method & Condition	Metric Value
Volume resistivity 50% HR, 23°C	CEI 93	1.4 E ⁺¹³ Ohms/m
Horizontal and Vertical Surface Volume resistivity	CEI 93	1.7 E ⁺¹⁸ Ohms

Isolant	Anti Statique	Dissipateur	Conducteur
1E ⁺¹⁵	1E ⁺¹⁴	1E ⁺¹³	1E ⁺¹²
1E ⁺¹¹	1E ⁺¹⁰	1E ⁺⁹	1E ⁺⁸
1E ⁺⁷	1E ⁺⁶	1E ⁺⁵	1E ⁺⁴
1E ⁺³	1E ⁺²	1E ⁺¹	1E ⁺⁰

Ohms/m

6. Surface Finish :

Measurement	Method & Condition	Metric Value
natural Coloration	Visual	White creams to yellow in mass
Upper Facing processed & blasting, Surface Ra 5 Ra	ISO 4287	9 ± 1 μm
Upper Facing after Finishing, Surface Ra 5 Ra	ISO 4287	< 1 ± 0.5 μm

The mechanical properties can vary according to the positioning of the tensile bars, operating conditions and exposure parameters of the systems used. These data rest on the current state of our knowledge. They do not give the exact characteristics of material and does not represent a guarantee.